DEPARTMENT OF THE AIR FORCE

AIR UNIVERSITY

AIR FORCE INSTITUTE OF TECHNOLOGY

Wright-Patterson Air Force Base, Ohio

19980312 096

TIME RESOLVED PHOTOLUMINESCENCE SPECTRA OF A MID-INFRARED MULTIPLE QUANTUM WELL SEMICONDUCTOR LASER

THESIS

Anthony L. Franz, Captain, USAF

AFIT/GAP/ENP/97D-04

[DTIC QUALITY INSPECTED 2.

AFIT/GAP/ENP/97D-04

TIME RESOLVED PHOTOLUMINESCENCE SPECTRA OF A MID-INFRARED

MULTIPLE QUANTUM WELL SEMICONDUCTOR LASER

THESIS

Presented to the Faculty of the Graduate School of Engineering of the

Air Force Institute of Technology

Air University

Air Education and Training Command

In Partial Fulfillment of the Requirements for the

Degree of Master of Science in Engineering Physics

Anthony L. Franz

Captain, USAF

December, 1997

TIME RESOLVED PHOTOLUMINESCENCE SPECTRA OF A MID-INFRARED

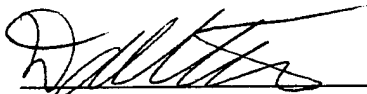# MULTIPLE QUANTUM WELL SEMICONDUCTOR LASER
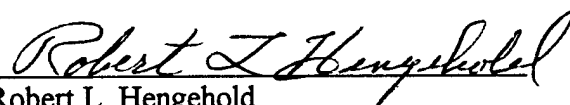
Anthony L. Franz

Captain, USAF

Approved:

Craig C. Largent (Chairman)

24 Nov 97
Date

David E. Weeks

24 Nov 97
Date

Robert L. Hengehold

24 Nov 97
Date

Acknowledgments

As with most things in life this thesis was not accomplished without a great deal of assistance. At the top of the list is my advisor, Capt. Craig Largent, who provided time and instruction before and during the thesis quarter. I would like to thank Dr. David Weeks for his many questions and discussions. I would also like to thank Dr. Robert Hengehold for his guidance in deciding on the scope of the effort. Rick Patton thoughtfully supplied me with a spacious work area and Kathy Potter and Cindy Wyckoff quickly found any obscure reference work I asked for. Finally thanks go to Theresa for her patience and understanding. I appreciate everything you do.

Table of Contents

List of Figures

List of Tables

Abstract

Recombination mechanisms in mid-IR semiconductor lasers are strongly dependent on the carrier density of the active region. Therefore, in order to determine the importance of different recombination mechanisms, an accurate knowledge of the carrier density is important. The objective of this research is to improve previous carrier density estimates through the incorporation of spectral information. In the long run, this will help researchers to more accurately characterize the recombination mechanisms and improve the efficiency of the lasers at these wavelengths.

One hundred photoluminescence (PL) spectra were calculated for a variety of carrier densities. Calculations were made for an InAsSb/InAlAsSb multiple quantum well laser sample assuming parabolic bands. In order to compare the results with experiment, the calculated spectra were convolved with the measured pump beam spectrum to account for broadening in the measurement process. The widths of the convolved calculated spectral profiles were tabulated as a function of carrier density.

Actual spectra were measured using the Ultrafast Mid-Infrared Photoluminesce System, which uses upconversion to measure the PL intensity in time steps smaller than 1 ps. PL spectra were obtained at 30 times, ranging from 100 ps to 3 ns. Spectral widths were measured and tabulated as a function of time.

Combining the plot of convolved calculated spectral width vs. carrier density with the plot of measured spectral width vs. time, we were able to describe the variation of carrier density with time. The carrier density vs. time plot thus generated agreed with

earlier measurements by Cooley for low carrier densities. The discrepancy at higher carrier densities could be due to changing experimental conditions or the break down of the parabolic band approximation at higher carrier densities.

TIME RESOLVED PHOTOLUMINESCENCE SPECTRA OF A MID-INFRARED MULTIPLE QUANTUM WELL SEMICONDUCTOR LASER

1. Introduction

Background

Mid-infrared semiconductor lasers are being developed for infrared (IR) countermeasures and chemical analysis. These lasers take advantage of the 2-5 μm transparency window in the atmosphere and have applications in remote sensing and environmental monitoring. Past research has analyzed the nonradiative recombination mechanisms in these structures in an attempt to minimize them. Auger recombination can be a major contributor to loss of efficiency in these devices resulting in increased lasing threshold currents at higher temperatures (Agrawal, 1993: 98-100). Techniques to study the carrier dynamics of these devices will help find solutions to the Auger problem.

Capt William Cooley constructed the Ultrafast Mid-Infrared Photoluminescence System (UMIPS) as part of his dissertation research. UMIPS uses sum frequency generation (SFG), or upconversion, to examine the photoluminescence (PL) lifetime of lasers emitting in the mid-IR (Cooley, 1996). We have extended his technique to measure PL spectra at 0.1 picosecond intervals. Analysis of the resulting spectra can provide insight into the carrier density at each time the PL is measured.

After the sample is optically pumped with a pulse the carrier density will decrease over time as electrons and holes recombine. The typical model used to describe this decrease for situations below threshold is a rate equation

$$-\frac{\partial n}{\partial t} = An + Bn^2 + Cn^3 \qquad (1)$$

where A, B, and C are the Shockley-Read-Hall, radiative, and Auger coefficients, respectively and n is the carrier density (Agrawal, 1993: 38). It is assumed that the number of electrons equals the number of holes. Each coefficient describes a type of recombination where the power of n in each term depends on the number of electrons and holes required for the type of recombination.

The types of recombination considered are illustrated in Figure 1. Shockley-Read-Hall recombination occurs when a defect is present in the lattice. This defect has a localized continuous density of states and the electron returns to the valence band through these states (Agrawal, 1993: 119). Radiative recombination occurs when an electron transitions to an empty state (a hole) in the valence band. The excess energy is released as a photon which has a frequency equal to the energy difference between the two states. Band-to-band Auger recombination occurs when the excess energy from a downward transition is used to shift another electron into a higher energy state (Agrawal, 1993: 99). In direct gap semiconductors there are three types of Auger recombination processes which are differentiated by the bands involved (Agrawal, 1993: 99). These processes are shown in Figure 2. We are primarily interested in the CCCH Auger process.

Figure 1: Types of recombination in semiconductors.

Figure 2: Types of Auger recombination for direct gap semiconductors (after Figure 3.3 in Agrawal, 1993: 99).
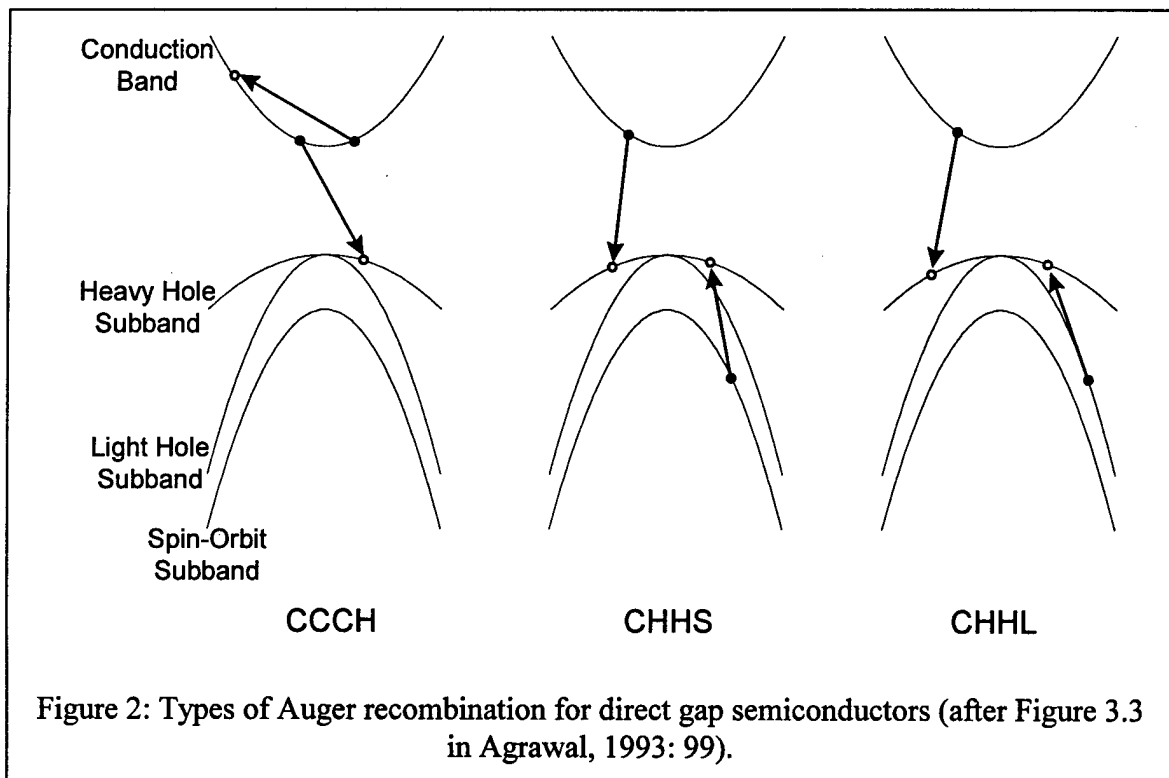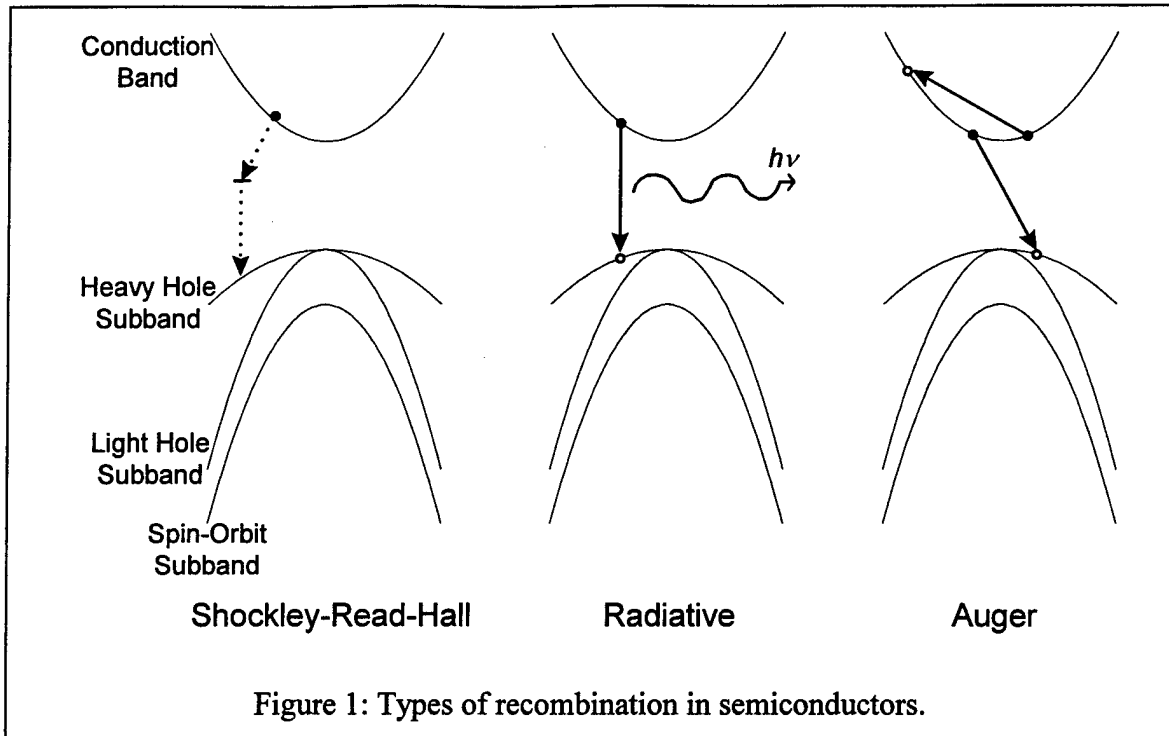
Approach

This effort used calculated and measured spectral data to find an estimate of the carrier density as a function of time. PL spectra were calculated based on a given carrier density. As the number of available carriers and holes decrease, fewer energy levels in the quantum wells will be occupied and the width of the PL spectra becomes narrower. The peak may also shift to slightly lower energies, depending on the range of carrier densities observed, as more radiative recombination occurs between lower energy levels. These calculated spectra had to be corrected for broadening that occurs in the experiment. To correct the calculated data for this effect, the spectrum of the upconversion pump beam used in the experiment was measured and convolved with the calculated PL spectra. The widths of the resulting convolved calculated spectra were obtained as a function of carrier density as illustrated in Figure 3a.

The measured spectral data were provided by Capt Craig Largent of the Engineering Physics Department at AFIT. He used the UMIPS to measure time-resolved spectra from the sample at different delay times after the excitation of the sample. The widths of these measured PL spectra were obtained as a function of time as illustrated in Figure 3b.

In order to determine carrier density as a function of time, the measured widths and convolved calculated widths were compared. This process is illustrated in Figure 3. Each delay time has a measured width associated with it. This measured width can be compared to the convolved calculated widths to find the one that matches it. The matching convolved calculated width is associated with a carrier density. This process

Figure 3: Schematic showing how carrier density was linked to time. The plots are illustrative and do not represent real data. (a) is a plot of the convolved calculated spectral widths vs. carrier density, and (b) is a plot of the measured widths vs. time. First a width w_1 is found for a given time t_1 using (b). Then w_1 is associated with a carrier density n_1 using (a). The result of this is a pair of values (t_1, n_1).

was repeated for each time to find the carrier density as a function of time. This relation was then plotted and compared to Cooley's results.

Overview

Chapter 2 will address the theoretical calculation of PL spectra for different carrier densities. Chapter 3 will discuss the UMIPS and the measured data obtained by Capt Largent. Chapter 4 will present the results of the spectral width calculation and discuss the convolution of the calculated spectra with the measured pump beam. The carrier density as a function of time results and conclusions from the analysis will be presented. Chapter 5 is a summary of the research and recommendations for future research in this area.

2. Theory

Overview

This chapter will address the theoretical aspects of the research. The goal of the theoretical calculations is to determine the width of the PL spectra that are expected for different carrier densities. The first step is to calculate the energy levels in the quantum wells. This is the topic of the second section. The third section discusses how the spontaneous emission spectra are calculated, and the fourth section discusses the convolution of these spectra performed to account for intraband relaxation. The last section is a summary of the calculation process.

It should be noted that a key assumption made in the calculations is that the band structure of the sample is parabolic so that

$$E_e(k_e) = E_c + \frac{\hbar^2 k_e^2}{2m_e}, \quad E_h(k_h) = E_v - \frac{\hbar^2 k_h^2}{2m_h} \tag{2}$$

where E_e and E_h are the energies of an electron and hole, k_e and k_h are the wave vectors for the electron and hole, E_c and E_v are the conduction and valence band edges, and m_e and m_h are the effective masses of the electrons and holes. The quality of the calculated spectra will depend on the quality of this assumption.

Energy Levels in the Quantum Wells

The first step in the calculation is to find the energy levels for electrons in the conduction band and for heavy and light holes in the valence band. The model used to calculate the energy levels is a single finite potential well. This is a standard problem in quantum mechanics texts and the results are well documented (Liboff, 1989: 256-65;

6

Figure 4: Finite square well model of the quantum well used in energy level calculations.
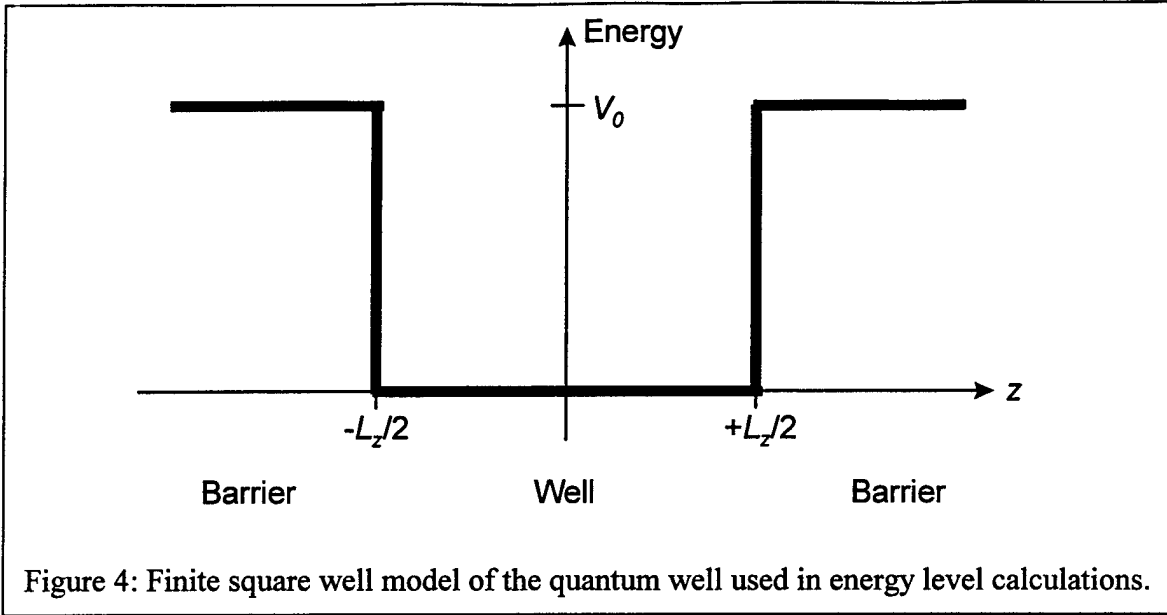
Cohen-Tannoudji, 1977: 74-7). In this model the potential energy surface is modeled as a square well in the z direction as shown in Figure 4. This model assumes a parabolic band structure and, by applying it to the multiple quantum well structure, that each well is isolated from neighboring wells.

The energy levels must be calculated for each band separately. Using the envelope functions as the wavefunctions and setting the electron momentum to zero the Schrödinger equation becomes

$$-\frac{\hbar^2}{2m}\frac{d^2}{dz^2}+VF_z = EF_z \tag{3}$$

where m is the effective mass, V is the potential, F_z is the envelope function in the z direction, and E is the energy of the band. It should be noted that both m and V have different values in the well and barrier regions. The effective mass for electrons, heavy holes, or light holes in each region is used when calculating the energy levels for the conduction, heavy hole, or light hole band respectively. Also, for reasons to be described

7

later, the value for V_0 in Figure 4 will be different for the conduction, heavy hole, and light hole bands. Plane wave solutions are assumed for the envelope functions and the following boundary conditions are applied at the interfaces (Corzine, 1993: 59-60):

$$F_{z,well} = F_{z,barrier} \quad \text{and} \quad \frac{1}{m_{well}}\frac{dF_{z,well}}{dz} = \frac{1}{m_{barrier}}\frac{dF_{z,barrier}}{dz} \tag{4}$$

There are two classes of solutions for the envelope functions: even and odd. The even solutions are cosines in the well and decay exponentially in the barrier; the odd solutions are sines in the well and also decay exponentially in the barrier (Liboff, 1989: 260). Using $k_z^2 = 2m_{well}E/\hbar^2$ and $\alpha_z^2 = \left(2m_{barrier}/\hbar^2\right)\left(V_0 - E\right)$, the characteristic equations for energy for even and odd solutions are

$$\tan\left(k_z\frac{L_z}{2}\right) = \frac{m_{well}}{m_{barrier}}\frac{\alpha_z}{k_z} \qquad \text{for even solutions}$$

$$\cot\left(k_z\frac{L_z}{2}\right) = -\frac{m_{well}}{m_{barrier}}\frac{\alpha_z}{k_z} \qquad \text{for odd solutions} \tag{5}$$

where L_z is the width of the quantum well and V_0 is the depth of the well. These characteristic equations can only be solved for discrete values of energy, E_n (Corzine, 1993a: 60-1). The energy levels for the conduction, heavy hole, and light hole bands, E_{cn}, E_{hhn}, and E_{lhn} respectively, are determined in this manner using the appropriate effective masses and well depths.

The depth of the well is determined by the energy gaps of the well and barrier and the band offsets. The offsets are a property of the material, but several factors can change the gap for a given material. A major factor is the temperature of the system. The temperature dependence will be assumed to follow the Varshni relation

$$E_g(T) = E_g(0) - \frac{\alpha T^2}{\beta + T} \qquad (6)$$

where $E_g(0)$ is the gap at $T = 0$ and α (in eV/K) and β (in K) are constant parameters fit

to experimental data (Varshni, 1967: 149).

In addition to temperature, the energy gap for the well will be affected by strain.

Stress in quantum well structures occurs when the lattice parameter of the well material is

different than the lattice parameter of the substrate and the well layer is thinner than a

critical thickness. If the well is thicker than the critical thickness then the lattice will

crack to relieve the strain. If the well is thinner then the lattice will not crack and will be

under compressive or tensile strain as shown in Figure 5 (O'Reilly, 1989:122-4). Figure 6

shows the effect of compressive strain on the band structure of the well. There is little

affect on the conduction band, but the valence band changes drastically. The gap between

the conduction band and valence band increases and the degeneracy of the heavy and light

holes is removed. Assuming parabolic bands at zone center, for III-V compound

semiconductors under a strain given by

$$\varepsilon_s = \frac{a_{0,\,substrate} - a_{0,\,well}}{a_{0,\,well}} \qquad (7)$$

the energy band shifts are given by

$$\Delta E_{hh} = -2a\varepsilon_s \frac{C_{11} - C_{12}}{C_{11}} + b\varepsilon_s \frac{C_{11} + C_{12}}{C_{11}}$$

$$\Delta E_{lh} = -2a\varepsilon_s \frac{C_{11} - C_{12}}{C_{11}} - b\varepsilon_s \frac{C_{11} + 2C_{12}}{C_{11}} \qquad (8)$$

Figure 5: Strain in semiconductor layers. (a) Three unstrained layers where the middle layer has a larger lattice parameter. (b) The middle layer distorts and is under compressive strain when placed between the two outer layers.

Figure 6: Effect of compressive strain on the band structure of a quantum well (after Figure 6 in Coleman, 1993: 375).
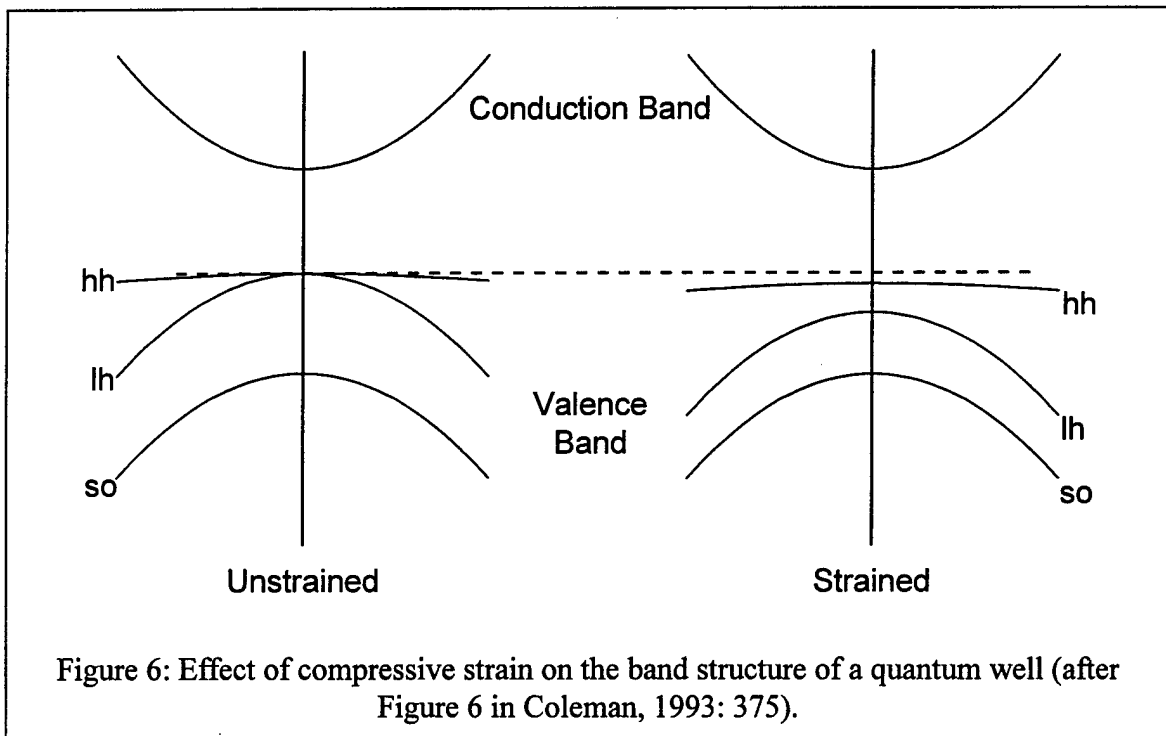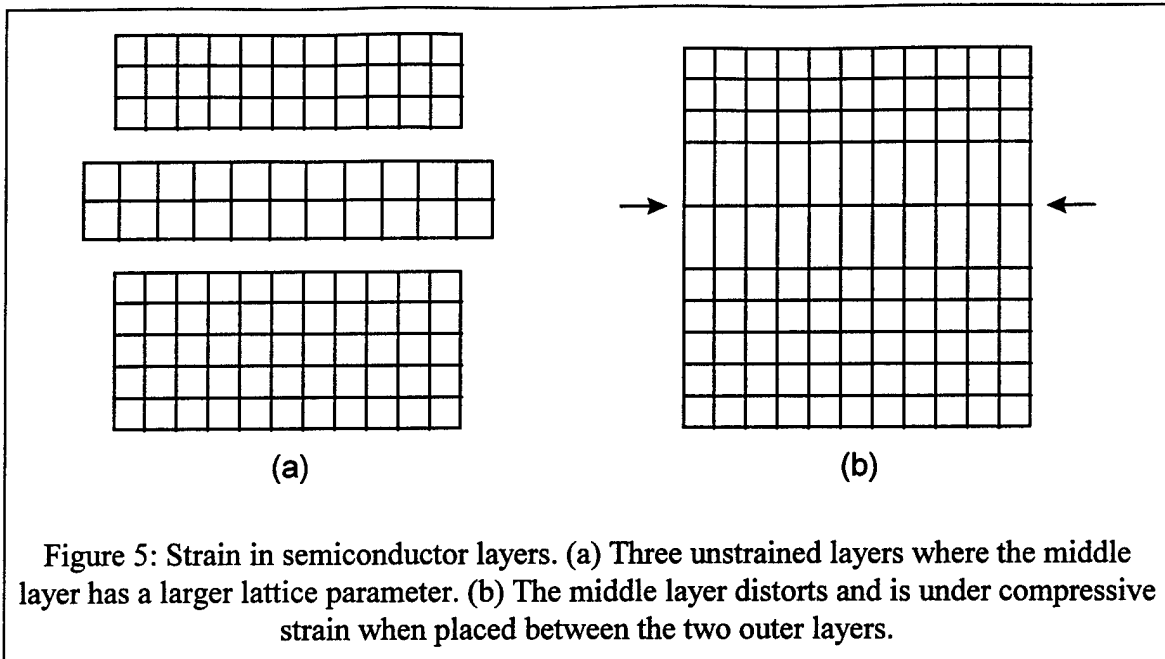
where a is the hydrostatic deformation potential, b is the shear deformation potential, and the Cs are elastic stiffness coefficients (Coleman, 1993: 377). For a well under compressive strain the energy gap is given by $E_g(T) + \Delta E_{hh}$.

Thus when strain is present and the conduction band offset does not equal ½, three separate well depths must be considered: one each for electrons (conduction band), heavy holes, and light holes. Equation (5) must be applied to each band with the appropriate effective masses and well depth, V_0. For a layer under compressive strain the well depths are given by

$$
\begin{aligned}
V_{cb} &= \Delta E_{cb} \left[E_{g,barrier}(T) - E_{g,well}(T) - \Delta E_{hh} \right] \\
V_{hh} &= \left[1 - \Delta E_{cb} \right] \left[E_{g,barrier}(T) - E_{g,well}(T) - \Delta E_{hh} \right] \\
V_{lh} &= \left[1 - \Delta E_{cb} \right] \left[E_{g,barrier}(T) - E_{g,well}(T) - \Delta E_{hh} \right] - \Delta E_{lh}
\end{aligned}
\tag{9}
$$

where ΔE_{cb} is the conduction band offset expressed as a fraction of one. A comparison of a strained and an unstrained well is shown in Figure 7.

Figure 7: Effect of compressive strain on the well depths.
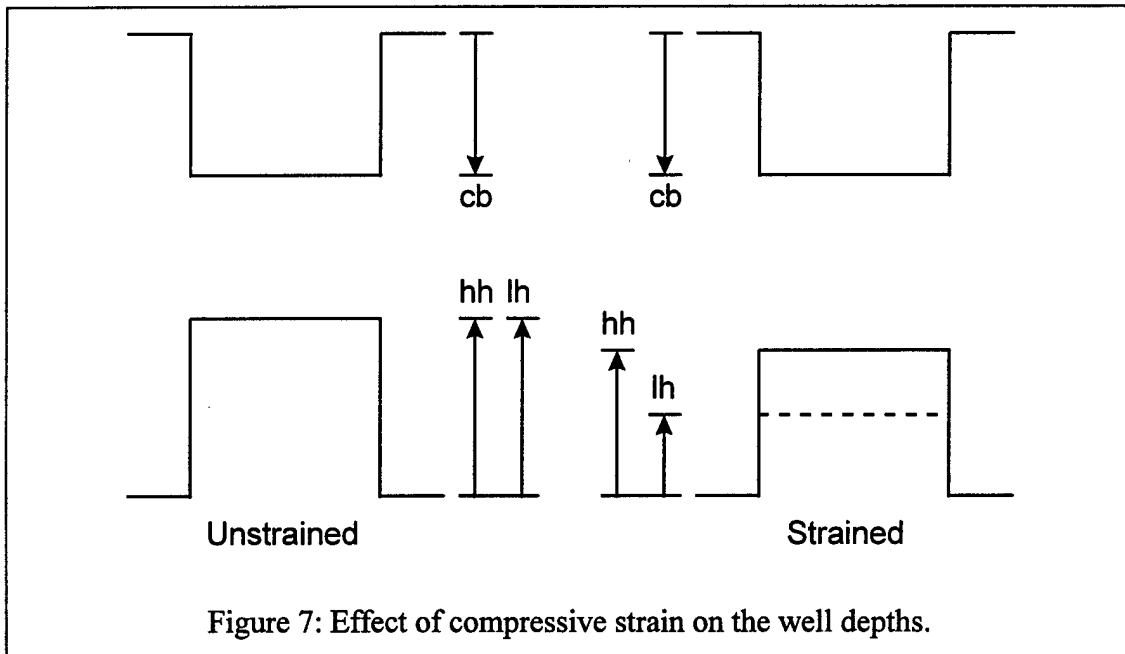
Spontaneous Emission Spectrum

The total spontaneous emission rate per unit volume over a given energy range is found by multiplying the transition rate per unit volume times the number of optical modes in the energy range:

$$R_{sp}(\hbar\omega)\, d(\hbar\omega) = W_{c\to v}\left[V\rho_{opt}(\hbar\omega)\, d(\hbar\omega)\right] \tag{10}$$

where $W_{c\to v}$ is the transition rate from the conduction band to the valence band, V is the volume of the active region, and ρ_{opt} is the optical density of states (Corzine, 1993:42).

The transition rate is found using Fermi's Golden Rule, which is derived using time-dependent perturbation theory to solve Schrödinger's equation when the Hamiltonian has the form $H = H_0 + \lambda H'(t)$. In general the transition rate, W, from state a to state b is given by

$$W_{a\to b} = \frac{2\pi}{\hbar}\left|H'_{ab}\right|^2 \rho(E) \tag{11}$$

where $H'_{ab} = \langle b|H'|a\rangle$, H' is the perturbation term in the Hamiltonian and $\rho(E)$ is the density of states as a function of energy (Bransden, 1983: 111-6 and Liboff, 1989: 576-84). Spontaneous emission involves the interaction of the electron in the conduction band with an electromagnetic wave. The wave interaction term is treated as a perturbation to the system so that

$$H'(\mathbf{r}) \equiv \frac{e}{2m_0}A(\mathbf{r})\hat{\mathbf{e}}\cdot\mathbf{p} \quad\text{and}\quad H'_{eh} \equiv \langle\psi_h|H'(\mathbf{r})|\psi_e\rangle \tag{12}$$

where e and m_0 are the charge and mass of an electron, A is the vector potential of the spontaneous emission wave, $\hat{\mathbf{e}}$ is the polarization unit vector of the wave, and $\mathbf{p}$ is the

momentum operator (Corzine, 1993: 28-9). ψ_i are the wavefunctions of the electrons and holes and are solutions to the Schrödinger equation when $H = H_0$. Using the envelope function approximation,

$$\psi_i \equiv F_i(\mathbf{r})\, u_i(\mathbf{r}) \tag{13}$$

where F_i is the envelope function and u_i is the Bloch function. The key assumption is that the Bloch functions are not a strong function of $\mathbf{k}$ (Corzine, 1993: 19). The Bloch functions are periodic with the crystal lattice (McKelvey, 1993: 319) and the envelope functions are normalized plane waves for unconfined directions in the crystal. The envelope functions for the confined direction of the well were discussed on page 8 (Corzine, 1993: 20,59).

For momentum to be conserved in the transition, $\mathbf{k}_h = \mathbf{k}_e + \mathbf{k}_{photon}$ must be valid. Typically the wavelength of the light is much greater than the De Broglie wavelength of the electron. If this is true then $\mathbf{k}_h = \mathbf{k}_e$ and the transitions are said to obey $\mathbf{k}$-selection rules. This applies to band-to-band transitions, not localized transitions, where the envelope functions of the initial and final states are plane waves (Corzine, 1993: 30).

For a quantum well the electrons and holes are confined along the growth direction so the z direction envelope functions must be included in the wavefunctions. If the wavelength of the light is much larger than the width of the well then the vector potential is can be considered to be a constant, A_0, in the region of the well. Using these assumptions and substituting Equation (13) into Equation (12) gives

$$|H'_{eh}|^2 = \left(\frac{eA_0}{2m_0}\right)^2 |M_T|^2, \quad |M_T|^2 \equiv \left|\langle u_v |\hat{\mathbf{e}}\cdot\mathbf{p}| u_c \rangle\right|^2 \left|\langle F_h | F_e \rangle\right|^2 \tag{14}$$

13

where $|M_T|^2$ are the transition matrix elements which will be described below (Corzine, 1993: 30-1).

Equation (14) is substituted into Fermi's Golden Rule (Equation (11)). The transition rate per unit volume can be expressed as

$$W_{c \to v} = \frac{2\pi}{\hbar} \left(\frac{eA_0}{2m_0} \right)^2 |M_T|^2 \rho_{red} \left(E_{eh} - E_g' \right) f_c \left(1 - f_v \right) \tag{15}$$

where ρ_{red} is the reduced density of states, E_{eh} is the transition energy $\hbar\omega$, E_g' is the gap between the subbands of the transition, and f_c and f_v are the Fermi-Dirac distributions for electrons in the conduction and valence bands respectively (Corzine, 1993; 33-5). These terms are discussed individually in the following sections.

Density of States

Fermi's Golden Rule has the density of states as a factor. The density of states for a quantum well is different than for a bulk semiconductor. A bulk crystal with dimensions L_x, L_y, and L_z is modeled as a square well with infinitely high walls in each dimension (the electrons are confined to the crystal). Requiring the wavefunctions to be zero at the boundaries gives standing waves for the wavefunctions of the form

$$\varphi(x,y,z) = \left(\frac{8}{L_x L_y L_z} \right)^{\frac{1}{2}} \sin\left(\frac{n_x \pi x}{L_x} \right) \sin\left(\frac{n_y \pi y}{L_y} \right) \sin\left(\frac{n_z \pi z}{L_z} \right) \tag{16}$$

where n_i are the quantum numbers in each direction (Cohen-Tannoudji, 1977: 199).

The wave vector has the form $\mathbf{k} = k_x + k_y + k_z$ where $k_i = n_i \pi / L_i$. The $\mathbf{k}$ vector sweeps out a sphere of volume $V_k = \frac{4}{3}\pi k^3$ which contains a number of states, N_s, given by

$$N_s = V_k \frac{L_x L_y L_z}{(2\pi)^3} \qquad (17)$$

where spin has been neglected. Spin will be addressed with the transition matrix

elements. In general, if $\rho(k)$ is the density of states then

$$\int \rho(k)dk = N_s/V \qquad (18)$$

when integrating over V_k, so that

$$\rho(k) \equiv \frac{1}{V} \frac{dN_s}{dk} \qquad (19)$$

where V is the total volume of the crystal (Corzine, 1993: 23-4). We are interested in the

energy of the electron, not its wave vector. The density of states as a function of energy

can be found through the relation

$$\rho(E)dE = \rho(k)dk \rightarrow \rho(E) = \frac{\rho(k)}{dE/dk} \qquad (20)$$

which requires a knowledge of how the energy depends on the wave vector (Corzine,

1993: 24). For the parabolic band approximation dE/dk can be found easily from

Equation (2):

$$E(k) = \frac{\hbar^2 k^2}{2m} \rightarrow \frac{dE}{dk} = \frac{\hbar^2}{m} k \qquad (21)$$

This relationship applies to the conduction and valence bands when the appropriate

effective masses are used.

For a bulk semiconductor V_k is a sphere as shown in Figure 8 and the density of

states is found by plugging Equation (17) into Equation (19)
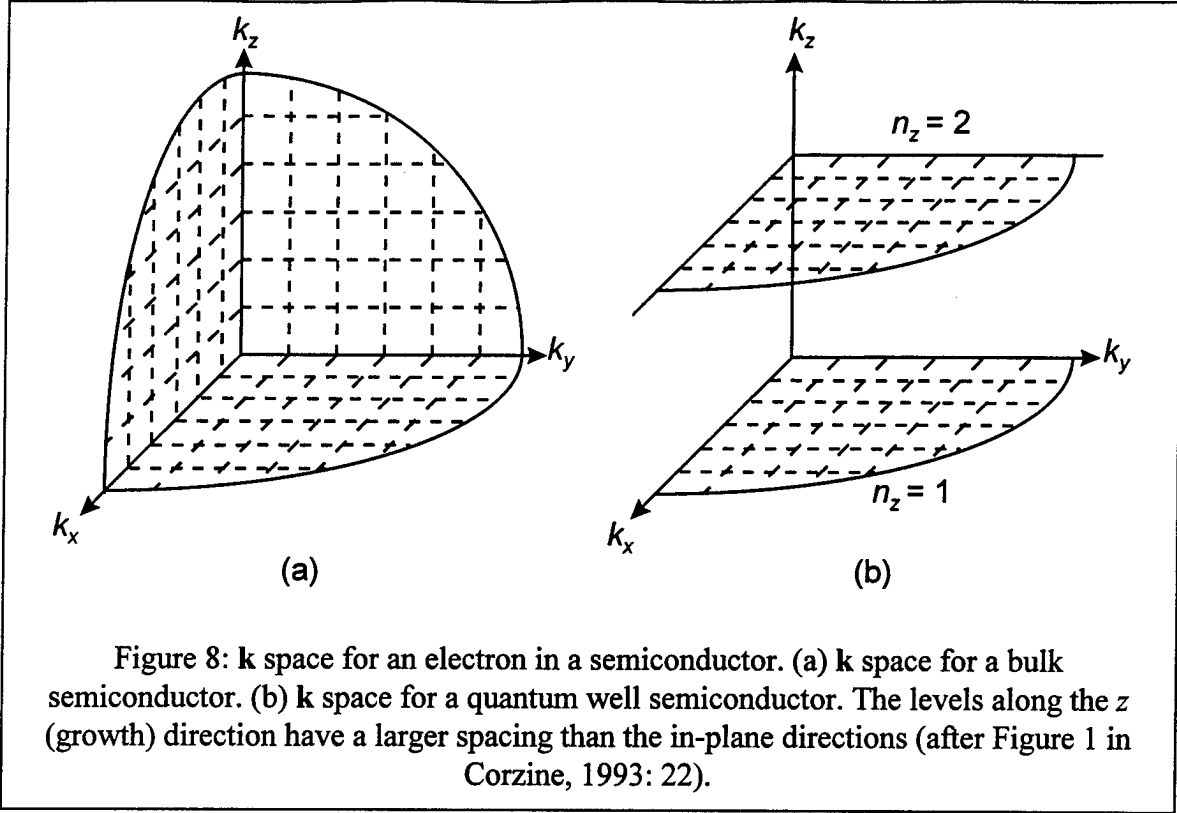
Figure 8: **k** space for an electron in a semiconductor. (a) **k** space for a bulk semiconductor. (b) **k** space for a quantum well semiconductor. The levels along the z (growth) direction have a larger spacing than the in-plane directions (after Figure 1 in Corzine, 1993: 22).

$$\rho(k) = \frac{1}{V}\frac{dN_s}{dk} = \frac{1}{V}\frac{d}{dk}\left(\frac{\frac{4}{3}\pi k^3}{(2\pi)^3 / (L_x L_y L_z)}\right) = \frac{1}{(2\pi)^3}\frac{L_x L_y L_z}{V}\frac{4}{3}3\pi k^2 = \frac{k^2}{2\pi^2} \qquad (22)$$

Substituting Equations (21) and (22) into Equation (20) gives

$$\rho(E) = \frac{\sqrt{E}}{4\pi^2}\left(\frac{2m}{\hbar^2}\right)^{\frac{3}{2}} \qquad (23)$$

for a bulk semiconductor with parabolic bands, ignoring spin degeneracy (Corzine, 1993: 23-5).

For a quantum well with $L_z \ll L_x$ and L_y, $k_z \gg k_x$ and k_y and the distance between consecutive levels of k_z will be very large compared to the spacing between consecutive levels of k_x and k_y as shown in Figure 8. The **k** vector will sweep out circles in each k_z

level so that $V_k = \pi k^2$ and one state occupies an area of $(2\pi)^2/(L_xL_y)$. N_s will equal V_k divided by this area so the density of states is

$$\rho(k) = \frac{1}{V}\frac{dN_s}{dk} = \frac{1}{V}\frac{d}{dk}\left(\frac{2\pi k^2}{(2\pi)^2/(L_xL_y)}\right) = \frac{1}{(2\pi)^2}\frac{L_xL_y}{V}2\pi k = \frac{k}{2\pi L_z} \qquad (24)$$

for a quantum well. Substituting Equations (21) and (24) into Equation (20) gives

$$\rho(E) = \frac{m}{2\pi\hbar^2 L_z} \qquad (25)$$

for each plane of k states in a two dimensional quantum well semiconductor with parabolic bands, ignoring spin degeneracy. This form of the density of states is a step function with the step size given in Equation (25). A new step occurs at each energy level of the quantum well (Corzine, 1993: 23-5). The density of states functions for a bulk (3D) and quantum well (2D) semiconductor are compared in Figure 9.

Figure 9: Comparison of the density of states, $\rho(E)$, for a quantum well and a bulk semiconductor. As the width of the quantum well increases the step size decreases and the quantum well case will approach the bulk case (after Figure 2 in Corzine, 1993: 25).

17
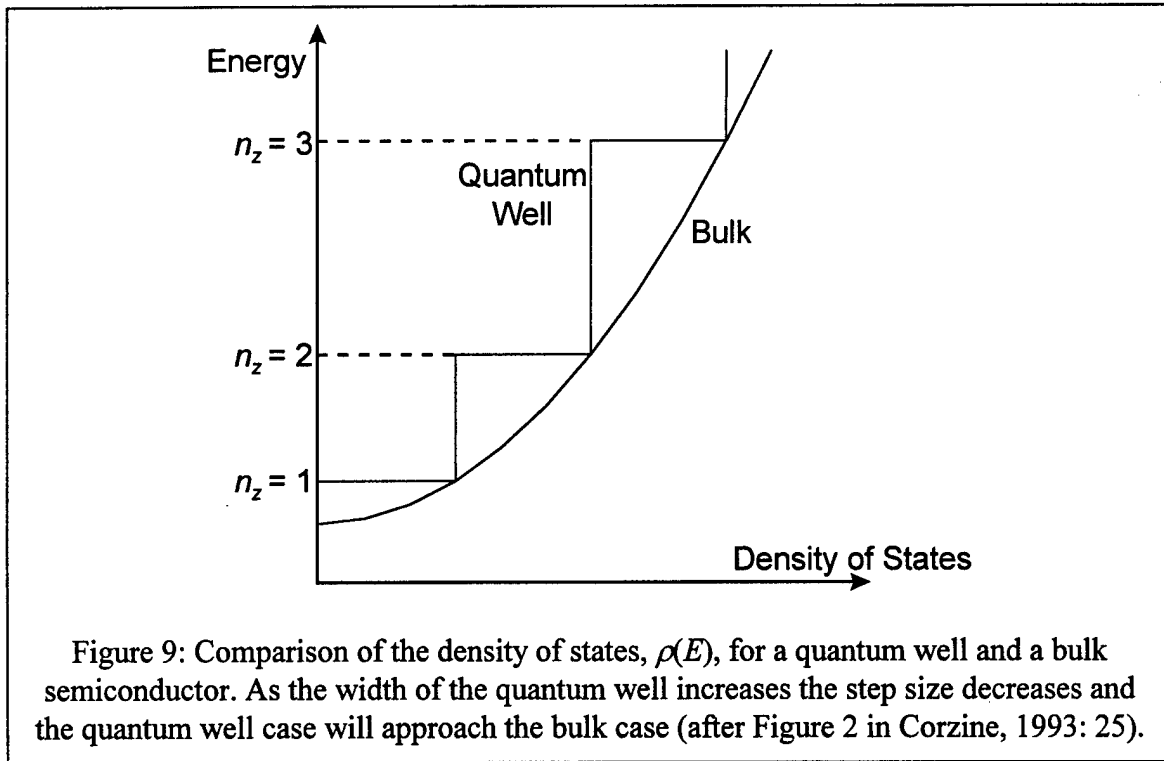
The reduced density of states is defined as (Corzine, 1993: 34)

$$\rho_{red} \equiv \frac{\rho(k)}{dE_{eh}/dk} \qquad (26)$$

where E_{eh} is the transition energy, $\hbar\omega$, given by

$$E_{eh} \equiv E_e - E_h = E_g' + \frac{\hbar^2 k^2}{2m_c} + \frac{\hbar^2 k^2}{2m_v} \qquad (27)$$

for the parabolic bands, where E_g' is the gap between the subbands of the transition.

Taking the derivative of this results in

$$\frac{dE_{eh}}{dk} = \frac{\hbar^2 k}{m_r}, \text{ where } \frac{1}{m_r} = \frac{1}{m_c} + \frac{1}{m_v} \qquad (28)$$

with m_r defined as the reduced mass. The reduced density of states, ρ_{red}, has the form of

Equation (25) with the mass replaced by the reduced mass and E by E_{eh} - E_g' (Corzine,

1993: 34).

Quasi-Fermi Functions

The transition rate given by Fermi's Golden Rule is for a transition from one state

in the conduction band to one state in the valence band. The possibility that some states

may be occupied must be taken into account. The transition rate is multiplied by the

probability of having an electron present in the conduction band state and not having an

electron present in the corresponding valence band state (presence of having a hole).

When the laser impinges on the sample, electrons from the valence band are

excited into the conduction band. Intraband relaxation occurs on the order of picoseconds

while recombination takes tens of picoseconds or more. After intraband relaxation and

before the start of recombination, the electrons occupy the lowest energy states available

18

Figure 10: Electron distributions after intraband relaxation has occurred. The electron distribution, n, is equal to the product of the density of states, ρ, and the Fermi function, f, with the appropriate quasi-Fermi level for each band.
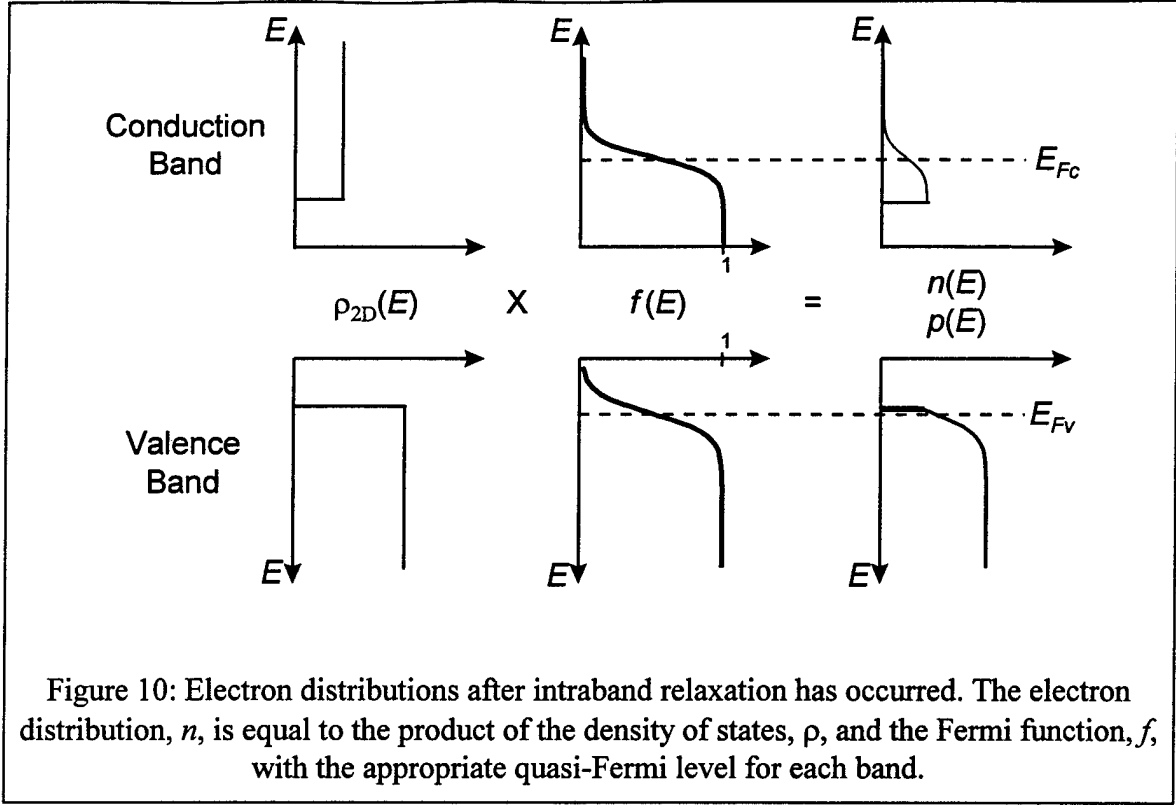
according to the Fermi-Dirac distribution with an appropriate quasi-Fermi level. This quasi-equilibrium condition is illustrated in Figure 10. The Fermi-Dirac distribution with a corresponding quasi-Fermi level is

$$f_c = \left[1 + \exp\left(\frac{E_e - E_{Fc}}{k_B T}\right)\right]^{-1} \quad \text{for the conduction band}$$

$$f_v = \left[1 + \exp\left(\frac{E_h - E_{Fv}}{k_B T}\right)\right]^{-1} \quad \text{for the valence band}$$

(29)

where E_e is the electron energy, E_h is the hole energy, k_B is Boltzmann's constant, and T is the temperature of the carriers. The quasi-Fermi levels, E_{Fc} and E_{Fv}, are the energies at which the probability of an electron occupying a state in the band is ½ (Verdeyen, 1995: 450 and Kittel, 1980: 379).

The total carrier density, N for the conduction band and P for the valence band, can be calculated by integrating the product of the density of states (times two to account for spin) and the quasi-Fermi function over the entire band. For parabolic bands this is

$$N = 2\int_{Ec}^{\infty} \rho^{2D}\left(E - E_c\right)f_c\,dE$$
$$P = 2\int_{-\infty}^{Ev} \rho^{2D}\left(E_v - E\right)\left(1 - f_v\right)dE$$

(30)

where E_c and E_v are the conduction and valence band edges and ρ^{2D} is the two dimensional density of states. Plugging Equations (25) and (29) into Equation (30) and integrating gives, for the conduction band,

$$N = \frac{m_c k_B T}{\pi \hbar^2 L_z} \sum_n \ln\left[1 + \exp\left(-\frac{E_{cn} - E_{Fc}}{k_B T}\right)\right]$$

(31)

where the summation is over the energy levels in the conduction band. For a given total carrier density a quasi-Fermi level can be calculated numerically (Corzine, 1993: 44). The quasi-Fermi level for the valence band is found by replacing N with P and summing over the energy levels in the heavy and light hole subbands.

Transition Matrix Elements

The transition matrix elements are defined in Equation (14). The envelope function term will be close to unity when the conduction band and the valence band state have the same quantum numbers and close to zero when they have different quantum numbers (Corzine, 1993: 31-2). It is assumed that $\left|\left\langle F_h \middle| F_e \right\rangle\right|^2$ is unity for these allowed transitions ($n_c = n_v$) and zero for other transitions ($n_c \neq n_v$). This reduces $\left|M_T\right|^2$ to

20

$$|M_T|^2 = \left| \left\langle u_v \left| \hat{\mathbf{e}} \cdot \mathbf{p} \right| u_c \right\rangle \right|^2 \qquad (32)$$

and the Bloch functions must be now be considered.

Semiconductor band structure is frequently modeled as shown in Figure 11. These bands can be thought of as originating from atomic orbitals where the conduction band corresponds to as s orbital and the valence bands correspond to the p_x, p_y, and p_z orbitals (McKelvey, 1993: 365-6). The Bloch functions for these orbitals are labeled u_s, u_x, u_y, and u_z, respectively, and have the same symmetry properties of the corresponding atomic orbitals. These symmetry relations combined with the momentum operator give the following relations:

$$\left\langle u_s \left| p_i \right| u_j \right\rangle = 0, \text{ for } i \neq j$$
$$\left\langle u_s \left| \mathbf{p} \right| u_i \right\rangle = \left\langle u_s \left| p_i \right| u_i \right\rangle \equiv M \qquad (33)$$
$$\left\langle u_s \left| \mathbf{p} \right| \bar{u}_i \right\rangle = 0$$

Figure 11: Subband structure for an unstrained semiconductor. The subbands are parabolic as represented by each bands' effective mass. E_g is the energy gap between the conduction and valence bands. Δ_{so} is the gap between the spin-orbit subband and the heavy and light hole subbands (after Figure 7 in Corzine, 1993: 49)
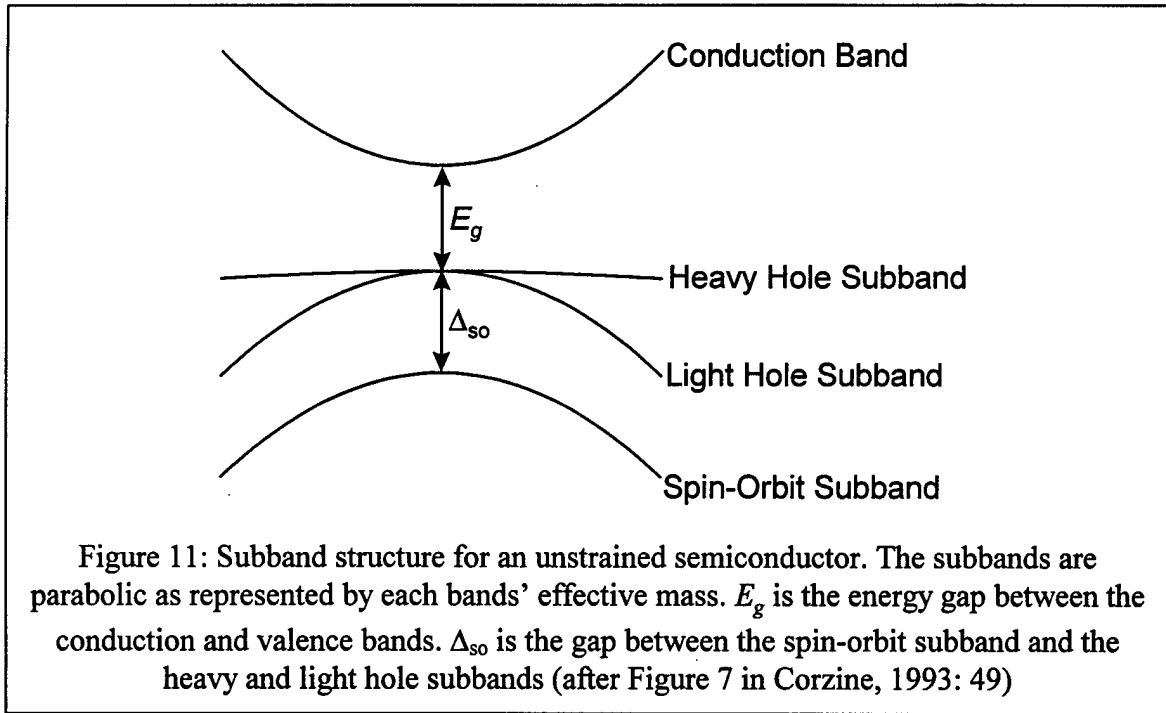
where $i = x, y, z$ and u_i, $\overline{u}_i$ indicate spin-up and spin-down functions (Corzine, 1993: 45-6). M is the orbital momentum matrix element and is a property of the material. The valence band Bloch functions u_{hh}, u_{lh}, and u_{so} can be written as linear combinations of the orbital Bloch functions. For electron **k** vectors directed along the z direction

$$
\begin{aligned}
u_{hh} &= -\frac{1}{\sqrt{2}}\left(u_x + iu_y\right), & \overline{u}_{hh} &= \frac{1}{\sqrt{2}}\left(\overline{u}_x + i\overline{u}_y\right) \\
u_{lh} &= -\frac{1}{\sqrt{6}}\left(\overline{u}_x + i\overline{u}_y - 2u_z\right), & \overline{u}_{lh} &= \frac{1}{\sqrt{6}}\left(u_x - iu_y + 2\overline{u}_z\right) \\
u_{so} &= -\frac{1}{\sqrt{3}}\left(\overline{u}_x + i\overline{u}_y + u_z\right), & \overline{u}_{so} &= \frac{1}{\sqrt{3}}\left(u_x - iu_y - \overline{u}_z\right)
\end{aligned}
\tag{34}
$$

where six equations are used to account for the spin-up and spin-down states (Corzine, 1993: 47). Including these spin states there are four possible transitions from the conduction band to each valence band. Setting the overlap integral to unity as described on page 20 gives

$$
\left|M_T\right|_v^2 = \sum_{u_c, \overline{u}_c} \sum_{u_v, \overline{u}_v} \left|\left\langle u_v \left| \hat{\mathbf{e}} \cdot \mathbf{p} \right| u_c \right\rangle\right|^2
\tag{35}
$$

Expanding the dot product into its components, replacing u_v in Equation (35) with the appropriate relations for each band from (34) and using the selection rules in (33) gives the relative transition strength with respect to $|M|^2$ for transitions to each valence band as

$$
\frac{\left|M_T\right|_v^2}{\left|M\right|^2} = \begin{cases} 1 - \left|\hat{\mathbf{k}} \cdot \hat{\mathbf{e}}\right|^2 & \text{for the heavy hole band} \\ \frac{1}{3} + \left|\hat{\mathbf{k}} \cdot \hat{\mathbf{e}}\right|^2 & \text{for the light hole band} \\ \frac{2}{3} & \text{for the spin - orbit band} \end{cases}
\tag{36}
$$

where $\hat{\mathbf{k}}$ is the unit vector of the electron wave vector which was set to the z direction (Corzine, 1993: 50-1).

22

Figure 12: Dependence of the transition strength on the angle, θ, between the electron's **k** vector and the wave's polarization vector, **e**, for transitions to the heavy and light hole subbands. The strengths labeled are in units of $|M|^2$ (after Figure 9 in Corzine, 1993: 53).
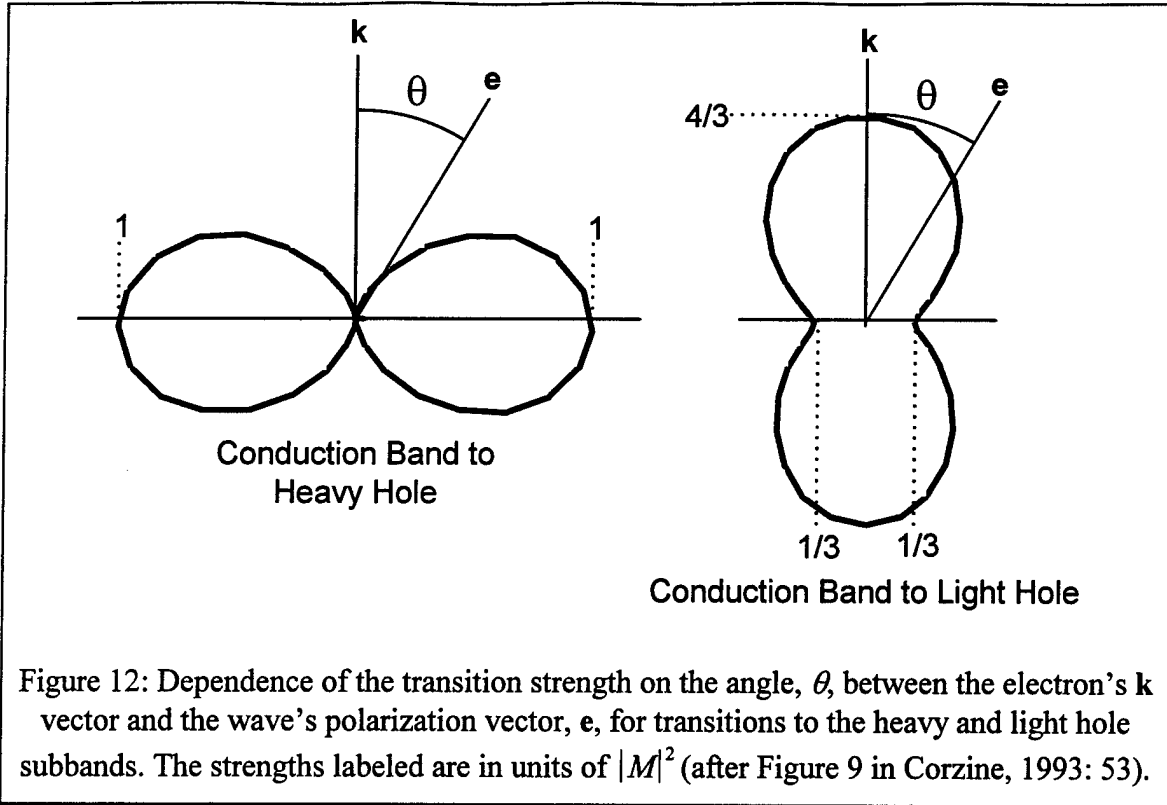
By averaging over all of the possible directions of the **k** vector in the first quadrant of **k** space it is seen that for a quantum well the average direction is the growth or z direction. Because of the dot product in Equation (36), the transition strength is a function of the angle between $\hat{k}$ and $\hat{e}$. This angular dependence is plotted in Figure 12 for the heavy and light hole subbands. Setting $\hat{k}$ equal to $\hat{k}_{ave}$ allows the transition strengths to be found for three orthogonal $\hat{e}$ set in directions relative to the quantum well as shown in Figure 13 (Corzine, 1993: 52-5). We are interested in all spontaneous emission regardless of polarization so the $|M_T|^2$ term in Equation (15) needs to be replaced with an average over the three polarization directions, $|M_{ave}|^2$, defined as (Corzine, 1993: 43)

Figure 13: Relative band edge transition strengths (Figure 11b, Corzine, 1993: 55).
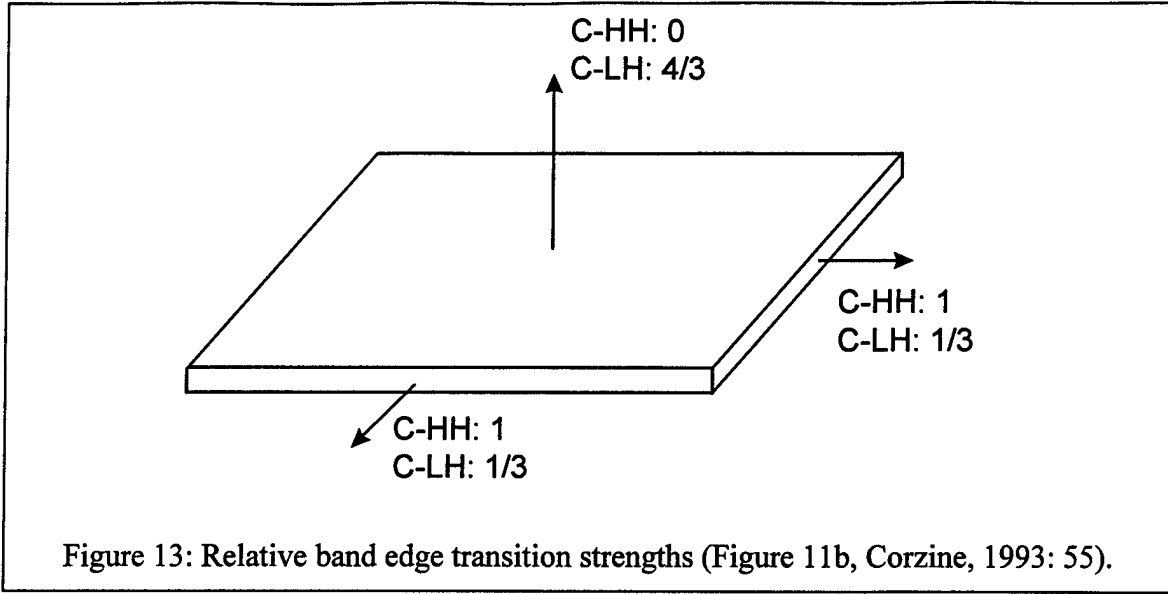
$$|M_{ave}|^2 \equiv \frac{1}{3} \sum_{\substack{\text{all three} \\ \text{polarizations}}} |M_T|^2 \qquad (37)$$

For the transitions in a quantum well, substituting Equation (36) into Equation (37) gives

$$|M_{ave}|^2 = \left\{ \begin{array}{c} \frac{1}{3}(0+1+1)|M|^2 \\ \frac{1}{3}\left(\frac{4}{3}+\frac{1}{3}+\frac{1}{3}\right)|M|^2 \\ \frac{1}{3}\left(\frac{2}{3}+\frac{2}{3}+\frac{2}{3}\right)|M|^2 \end{array} \right\} = \frac{2}{3}|M|^2 \qquad (38)$$

for transitions to all bands. The values for the heavy hole and light hole transitions came

from Figure 13. Equation (38) is used in Equation (15) in place of the $|M_T|^2$ term.

$|M|^2$ must be determined for the sample to quantify the spontaneous emission

rate. Using the **k·p** technique for the four bands in Figure 11 an equation for the

approximate conduction band effective mass, m^*, can be rearranged to solve for $|M|^2$

(Corzine, 1993: 48-9)

$$\qquad (39)$$

24

$$|M|^2 = \left(\frac{m_0}{m*} - 1\right) \frac{E_g + \Delta_{so}}{2\left(E_g + \frac{2}{3}\Delta_{so}\right)} m_0 E_g$$

It should be noted that $m*$ is not the true effective mass because contributions from higher and lower level bands will make the true effective mass heavier and lighter respectively. The inaccuracy in Equation (39) depends on how large an effect these unaccounted for bands have on the true effective mass (Corzine, 1993: 48-9 and Yan, 1990: 214-5).

Optical Density of States

The optical density of states in an energy range is found by using the 3D density of states, $\rho(k)$, found in Equation (22). For photons

$$k_{opt} = n_r \frac{2\pi}{\lambda} = n_r \frac{\omega}{c} = \frac{n_r}{\hbar c}(\hbar\omega), \quad \frac{dk_{opt}}{d(\hbar\omega)} = \frac{n_g}{\hbar c} \tag{40}$$

where n_r and n_g are the index of refraction and the group index of refraction. Substituting these relations into Equation (20) yields

$$\rho_{opt}(\hbar\omega) = \frac{1}{\pi^2} \frac{n_r n_g}{(\hbar c)^3}(\hbar\omega)^2 \tag{41}$$

in units of energy^{-1} cm^{-3}, where a factor of two has been multiplied to account for the two polarization states (Corzine, 1993: 42).

Vector Potential

The vector potential is found by relating the energy in the field to the energy of a photon. Solving for the vector potential gives

$$A_0^2 = \frac{2\hbar\omega}{n_r n_g \varepsilon_0 \omega^2 V} \tag{42}$$

Substituting Equations, (15), (38), (41), and (42) into Equation (10) gives

$$R_{sp}(\hbar\omega) = \frac{1}{\hbar\omega} \frac{\pi e^2 \hbar}{n_r n_g \varepsilon_0 m_0^2} \frac{2}{3} |M|^2 \rho_{red}\left(E_{eh} - E_g'\right) \rho_{opt}(\hbar\omega) f_c \left(1 - f_v\right) \qquad (43)$$

in units of transitions per (s cm³ energy) (Corzine, 1993: 42-3). This is the equation used to calculate the spontaneous emission spectrum.

Intraband Relaxation

The spectrum calculated by Equation (43) will have sharp peaks resulting from the discrete density of states. In reality intraband relaxation will cause the peaks to broaden. This is due to carrier-carrier scattering and carrier-phonon scattering. This process can be described by convolving the spectrum calculated with Equation (43) with a broadening function B:

$$r_{sp}(\hbar\omega) = \int_{E_g'}^{\infty} R_{sp}\left(E_{eh}\right) B\left(\hbar\omega - E_{eh}\right) dE_{eh} \qquad (44)$$

where $r_{sp}(\hbar\omega)$ is the convolved spontaneous emission as a function of the photon energy, $\hbar\omega$ and $R_{sp}(E_{eh})$ is the unconvolved spontaneous emission as a function of the energy difference between the electron and hole states (Asada, 1993: 99). The broadening function used is derived in Asada, 1993. The lineshape used is non-Lorentzian and comes from the Fourier transform of the response of the polarization to an impulse electric field (Asada, 1993: 98).

It should be noted here that the intraband relaxation convolution is not the convolution mentioned in the Introduction. The intraband relaxation convolution takes into account a phenomenon that is inherent to the semiconductor structure. The

convolution mentioned in the Introduction is performed to take into account a phenomenon that is introduced in the measurement process. This phenomenon will be described in the next Chapter. The terms "calculated spectrum" and "calculated widths" used in this thesis refer to spectra calculated with Equation (44) and the width of these spectra. The terms "convolved calculated spectra" and "convolved calculated widths" refer to the spectra that have been corrected for the experimental broadening mentioned in the Introduction and the widths of these spectra.

Summary of Calculation Procedure

The goal of the theoretical calculations is to determine the width of the PL spectra that are expected for different carrier densities. The calculation involves several steps. First the energy levels of the well region are calculated using Equations (5). Then spontaneous emission spectra are calculated for a range of carrier densities using Equation (43). The spectra are then convolved according to Equation (44) to account for intraband relaxation. Plots of some of these spectra will be presented in Chapter 4.

As explained in the next chapter, these spectra have to be convolved again to account for broadening that occurs in the experimental measurements before the widths can be determined. Then the widths of the spectra can be plotted as a function of the carrier density used to calculate each PL spectrum.

3. Experiment

Overview

Capt Craig Largent of the Department of Engineering Physics at AFIT took the experimental data used in this thesis using the UMIPS constructed by Capt Cooley. This chapter will describe the experiment so the reader will understand what was measured and how the data was taken. The goal of the measurements is to obtain the width of the PL spectra at different delay times. The next section describes the configuration of the UMIPS and the technique. The third section describes the upconversion process and the fourth section describes efficiency and tuning considerations. The fifth section describes the method used to measure the spectra and presents the results as a plot of measured width as a function of delay time. The last section discusses the physical source of the convolution discussed in the Introduction.

UMIPS Experiment

The quantum well sample is optically pumped by a pulse of laser light. Figure 14 shows a schematic of the UMIPS. Using a mode locked laser, short pulses can be produced at high repetition rates (Verdeyen, 1995: 296-7). The pump beam is split so that only one leg reaches the sample. The sample is excited and spontaneous emission occurs. The emission is recombined with the second leg of the pump beam in a Potassium Titanyl Arsenate (KTA) crystal. Sum frequency generation (SFG), or upconversion, occurs producing a third wave at a different wavelength, which is measured by a spectrometer.

Figure 14: Ultrafast Mid-Infrared Photoluminescence System (Cooley, 1996: 4-6).
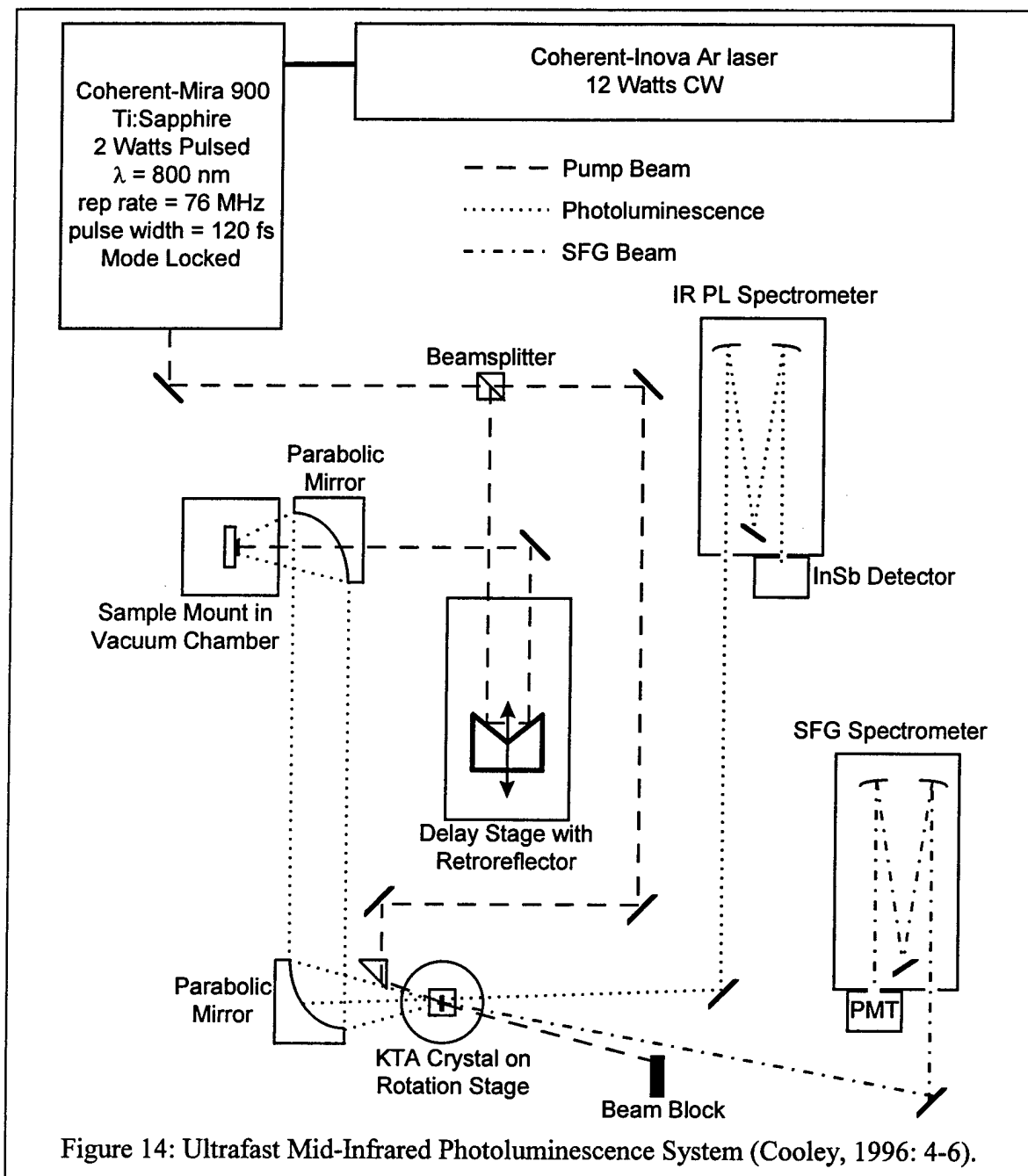
Upconversion will take place in the crystal and produce a third beam of

upconverted photons such that

$$\omega_p + \omega_{PL} = \omega_{up} \qquad (45)$$

Figure 15: Schematic of the light gate. SFG photons are only emitted when the delayed pulse overlaps the PL (after Figure1b in Shah, 1988: 277).
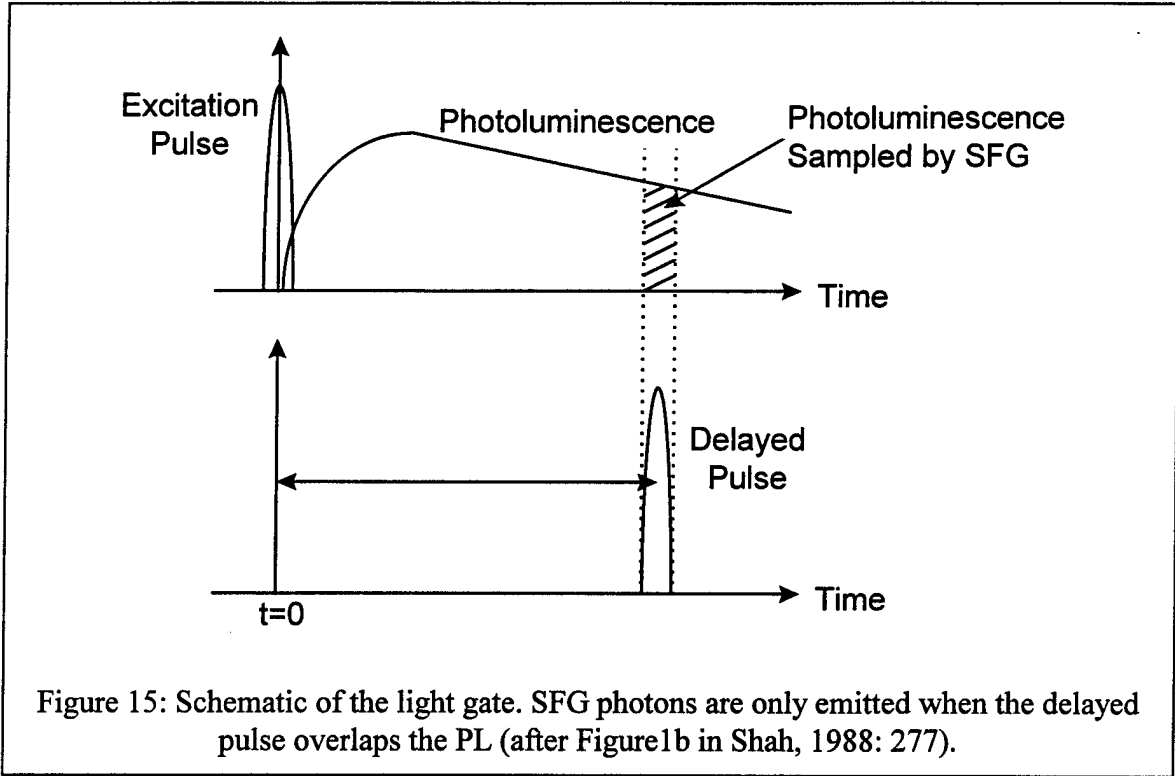
where ω_p, ω_{PL}, and ω_{up} are the frequencies of the pump beam, the PL wave, and the upconverted wave, respectively. Upconversion will only take place when the pump and PL waves overlap in space and time in the nonlinear optical crystal. As shown in Figure 15, the pump beam acts as a light gate. By varying the distance the upconversion pump beam has to travel, the PL can be sampled at different delay times after the sample has been pumped (Shah, 1988: 277).

Upconversion

Upconversion is a nonlinear optical phenomena. When an electromagnetic wave interacts with a medium, the polarization induced in the medium can be expressed as a series expansion

$$P_i = \varepsilon_0 \chi_{ij} E_j + 2 d_{ijk} E_j E_k + \cdots \qquad (46)$$

30

where P_i is the induced polarization vector, E_i is the induced electric field, ε_0 is the permeability of free space, χ_{ij} is the linear susceptibility, and d_{ijk} is the second-order susceptibility (Yariv, 1984: 504). Higher order terms in Equation (46) have been dropped.

Upconversion occurs when two waves mix in a crystal for which $d_{ijk} \neq 0$. The waves are modeled as plane waves with frequencies ω_1 and ω_2. Plugging these waves into the second term on the right hand side of Equation (46) gives rise to a cross term with a frequency ω_3, where $\omega_3 = \omega_1 + \omega_2$. The crystal is assumed to be homogeneous, nonabsorbing, and magnetically isotropic (Yariv, 1984: 70). The crystal must be transparent to the three frequencies of interest. The polarization of this new wave is given by

$$P_i^{\omega_3} = 2 d_{ijk} E_j^{\omega_1} E_k^{\omega_2} \tag{47}$$

The exact form of the susceptibility tensor, d_{ijk}, depends on the crystal symmetry (Yariv, 1984: 506-7).

Efficiency

The efficiency of the upconversion process affects the strength of the upconverted signal. For the case of negligible pump depletion this is given as

$$\eta(0) = \frac{2 \pi^2 d_{eff}^2 L^2 (P_p / A)}{c \varepsilon_0^3 \lambda_{PL} \lambda_{up} n_p n_{PL} n_{up}} \tag{48}$$

where $\eta(0)$ is the quantum efficiency, d_{eff} is the effective nonlinear coefficient of the crystal, L is the length of the interaction in the crystal, P_p and A are the power and area of the pump beam on the crystal, and n_p, n_{PL}, and n_{up} are the indexes of refraction for the pump, PL, and upconverted beams respectively (Shah, 1988: 278). The waves must be in

31

phase with each other or they will interfere and the efficiency will be reduced. The wave

vectors are governed by

$$\mathbf{k}_{up} = \mathbf{k}_p + \mathbf{k}_{PL} - \Delta\mathbf{k} \qquad (49)$$

where phase matching is achieved when $\Delta\mathbf{k} = 0$ and Equation (45) is valid (Midwinter,

1965: 1135). The quantum efficiency will decrease with increasing $\Delta\mathbf{k}$ as

$$\eta(\Delta\mathbf{k}) = \eta(0)\frac{\sin^2(L\,\Delta\mathbf{k})}{(L\,\Delta\mathbf{k})^2} \qquad (50)$$

where $\eta(0)$ is the efficiency for the phase matched case and is defined in Equation (48)

(Shah, 1988: 278). The phase matching angle can be calculated for this interaction by

adding the pump and PL wave vectors according to Equation (49) as shown in Figure 16.

Using the law of cosines and $k = 2\pi n/\lambda$ gives

$$\frac{n_{up}^2}{\lambda_{up}^2} = \frac{n_{PL}^2}{\lambda_{PL}^2} + \frac{n_p^2}{\lambda_p^2} - 2\frac{n_{PL}}{\lambda_{PL}}\frac{n_p}{\lambda_p}\cos(\pi - \psi) \qquad (51)$$

where ψ is the angle between the pump and PL wave vectors in the crystal in radians

(Cooley, 1996: 2-22).

The KTA crystal is biaxial and is oriented so that phase matching will occur when

the ordinary polarization of the PL mixes with the extraordinary polarization of the pump

beam to produce an upconversion wave that is polarized in the ordinary direction. This is

Figure 16: Applying the law of cosines with the wave vectors.

32
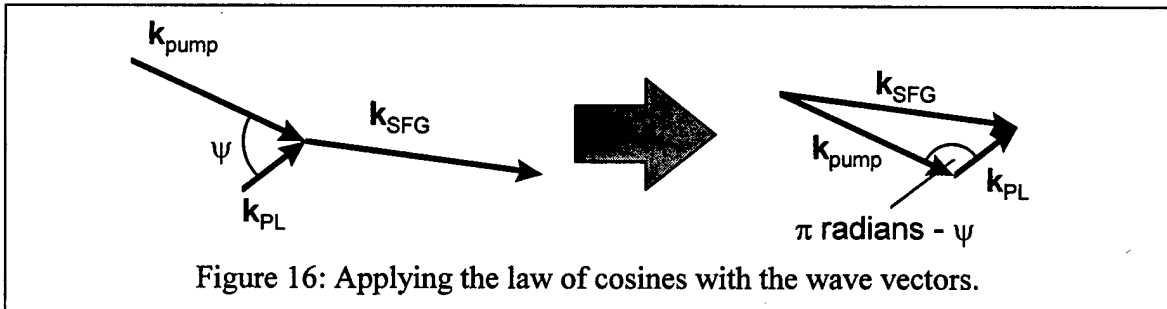
called an "oeo" interaction and the index of refraction for the pump depends on the angle between the pump beam and the optic axis. Since n_p is a function of θ, this equation can be solved for the angle that the pump beam will make with the optic axis so that Δk is zero. This angle is the phase matching angle and will change as the wavelengths of the pump and PL change. Thus by turning the crystal the upconversion can be tuned to a specific wavelength. Also, for the oeo interaction $d_{eff} = d_{32} \sin\theta_{up}$, where θ_{up} is the angle between the upconverted wave vector and the optic axis and d_{32} comes from the nonlinear susceptibility tensor (Dmitriev, 1991: 24).
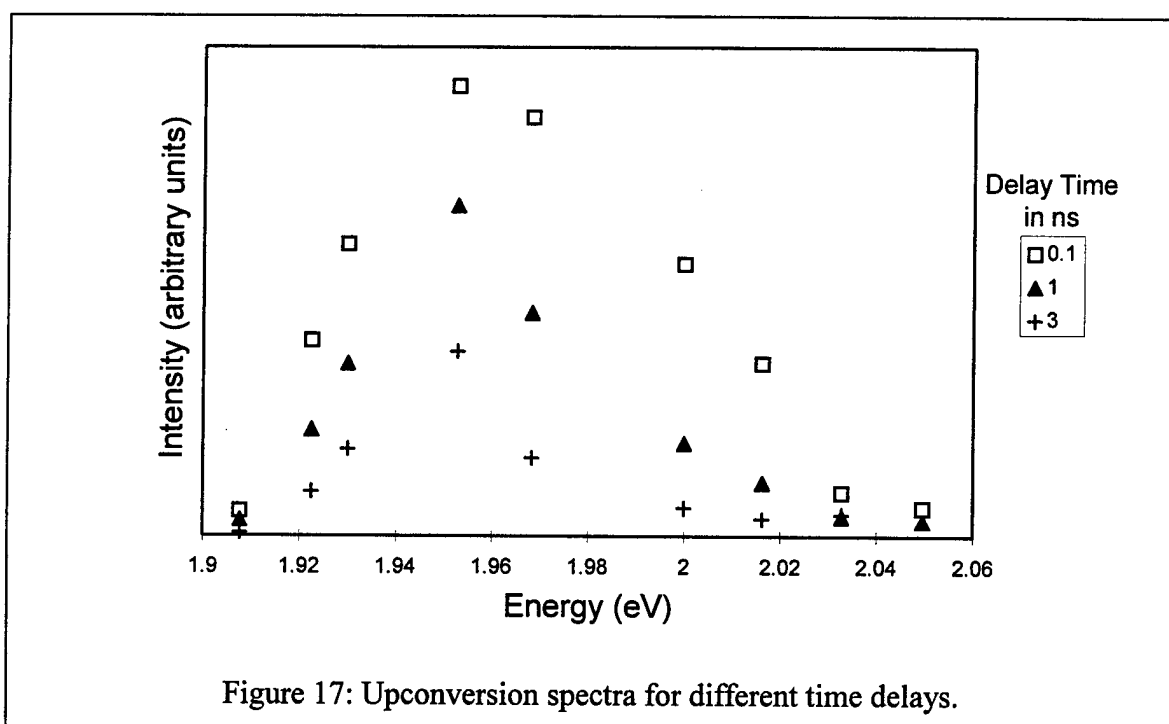
Measured Spectral Widths

Capt Largent used the UMIPS to measure the upconversion spectra as a function of delay time. Data can be taken by scanning in either wavelength or time. The spectrometer can be scanned over a range of wavelengths for a set delay time. Then the delay time is adjusted and the spectrometer scans over the wavelength range at the new time delay. PL spectra can be measured at each time delay this way. As was mentioned earlier in the Chapter, the crystal is tuned to a wavelength of interest by turning it to a phase matching angle. If the spectrometer is scanned and the crystal is not tuned to the wavelength the spectrometer is set for, the intensity of the signal will decrease for wavelengths that are not near the wavelength the crystal is tuned to. Since the UMIPS does not have a rotation stage that can turn in step with the spectrometer, the spectra were measured by setting the spectrometer to a wavelength of interest, tuning the crystal to that wavelength, and scanning the delay stage over a range of time. By repeating this for several wavelengths at the same delay times, a PL spectrum can be found by taking all of the data for a particular delay time and plotting it as a function of wavelength.

Data was taken at 77 K by setting the spectrometer to a set wavelength and turning the KTA crystal to achieve the maximum signal. Thirty spectra were measured at delay times ranging from 100 ps to 3 ns in steps of 100 ps. Some of the spectra for different delay times are plotted in Figure 17.

To find the width of the spectra, each point was converted from wavelength to energy space. Capt Largent fit the data in each time slice with a sixth order polynomial and the FWHM of the fit was calculated. The results are shown in Figure 18. As expected the widths decrease with time. This indicates the carrier density is dropping due to recombination as time passes.

Broadening Due To Upconversion

When the pump and PL waves mix in the KTA crystal, no broadening of the upconversion wave will occur if the pump beam is a delta function. By design the pump laser has been set up to emit short pulses to maintain the temporal resolution of the

Figure 17: Upconversion spectra for different time delays.
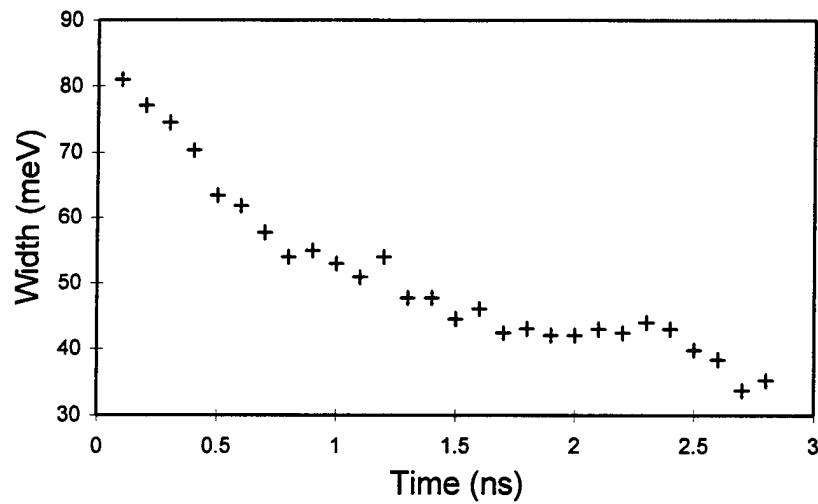
Figure 18: Measured widths as a function of time.

upconversion spectra. This means that the spectrum in frequency space is large and the

upconversion spectrum will be the convolution of the pump and PL spectra. This is

because the entire pump spectrum can add with the first energy of the PL spectrum and

with the second energy in the pump spectrum and so on. To account for this effect, the

calculated spectra were convolved with a measured spectrum of the pump beam so that an

accurate comparison of the calculated and measured widths could be performed.

4. Results

Overview

This chapter presents the results of the calculations and compares them to previously measured data. First the sample is described and the material parameters for the well and barrier discussed. The third section discusses the calculation of the spontaneous emission spectral widths as a function of total carrier density. The fourth section explains the convolution procedure used to adjust the calculated spectral widths for broadening that occurs in the measurement process. The last section shows the carrier density as a function of time and compares this result to Cooley's result.

Sample Description

The sample was a multiple quantum well structure consisting of ten $InAs_{0.935}Sb_{0.065}$ well layers ten nm thick interspersed between 11 $In_{0.85}Al_{0.15}As_{0.9}Sb_{0.1}$ barrier layers that are 20 nm thick. The sample was grown by Molecular Beam Epitaxy on an InAs substrate at the Massachusetts Institute of Technology/Lincoln Laboratory (MIT/LL). The sample has been thoroughly described in a previous publication (wafer B in Choi, 1996). Details of the growth process have also been published previously (Turner, 1995). Figure 19 shows an energy diagram of the laser structure. A conduction band offset of 0.75 was used in the calculations. This number came from Cooley who got it from Turner.

Several parameters are needed for the calculations that depend on the type of materials used in the laser structure. The well material is the most important in terms of its effect on the calculations. This sample has a ternary structure of the form $InAs_{1-x}Sb_x$

Figure 19: Quantum well structure for Laser B (after Figure 4-1 in Cooley, 1996: 4-2).
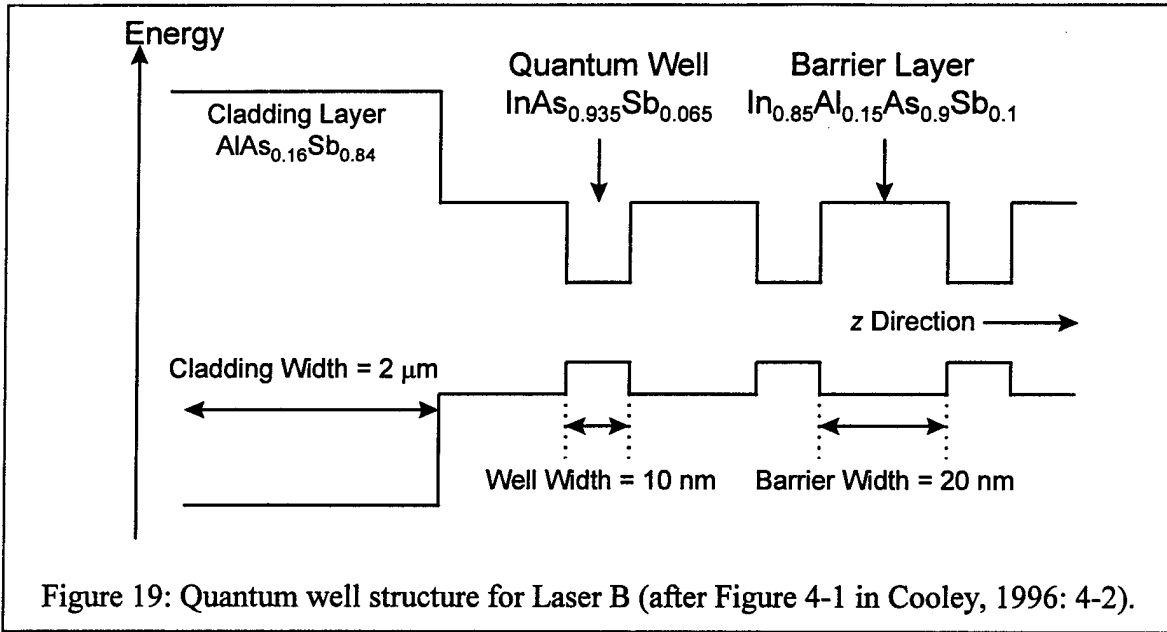
which has not been thoroughly characterized. Where values for the ternary have not been published, linear interpolation between the values for InAs and InSb was used to find a value for the sample. Table 1 lists the parameters for the binary compounds used and the interpolated values found for the well.

Several sources listed empirical relations or data for the energy gap of $InAs_{1-x}Sb_x$ as a function of antimony mole fraction for a given temperature (Woolley, 1964: 1883; Stringfellow, 1971: 805; Osbourn, 1984: 176; Yen, 1987: 928; Fang, 1990: 7038). A relationship for the energy gap as a function of antimony mole fraction and temperature initially published by Wieder and Clawson (Wieder, 1973: 220) and reprinted in Rogalski, 1989: 37, that fits these empirical relations well is

$$E_g(x,T) = 0.411 - \frac{3.4 \times 10^{-4} T^2}{210 + T} - 0.876x + 0.70x^2 + 3.4 \times 10^{-4} xT(1-x) \qquad (52)$$

Table 1: Material parameters for binary compounds and interpolated values for the well and barrier. Values that were not calculated or used are left blank.

Parameter	InAs	InSb	AlAs	AlSb	Well	Barrier
a_0 (Å)	6.0583	6.47937			6.0857	
C_{11} (10^{11} dynes/cm^2)	8.329	6.669			8.2211	
C_{12} (10^{11} dynes/cm^2)	4.526	3.645			4.469	
a (eV)	-6.0[a]	-7.7[a]			-5.9	
b (eV)	-1.8[a]	-2.0[a]			-1.8	
m_e (m$_0$)	0.0239	0.01359	0.15	0.259	0.0232	0.044
m_{hhz} (m$_0$)	0.35	0.34	0.409	0.336	0.35	0.36
m_{lhz} (m$_0$)	0.026	0.0158	0.153	0.123	0.025	0.044
m_{hhx} (m$_0$)	0.35	0.42			0.35	
m_{lhx} (m$_0$)	0.026	0.0158			0.025	
n_r	3.714[b]	4.418[b]	2.875[c]	3.182	3.760	3.730
$\varepsilon(0)$	15.15	16.8			15.2	

All values are from Madelung, 1991, except
a) Blacha, 1984
b) Aspnes, 1983
c) Fern, 1971

where x is the antimony mole fraction, T is in Kelvin, and E_g is in eV. The spontaneous emission spectrum calculated using an energy gap predicted by this relation showed that the gap was to large for this sample as shown in Figure 20.

Major Michael Marciniak studied several InAs$_{1-x}$Sb$_x$ samples with varying x and found smaller energy gaps for his samples (Marciniak, 1995). His samples were bulk samples grown by MIT/LL using Molecular Beam Epitaxy on GaSb substrates. Marciniak fit the temperature dependence of the energy gap for his samples using the Varshni relation (Equation 6). Using his data from the samples with $x = 0.059$ and $x = 0.071$, I

interpolated point by point to find the temperature dependence for the sample I studied (x = 0.065). The interpolated data was fit to the Varshni relation to find $E_g(0)$, α, and β for wafer B and resulted in

$$E_g(T) = 0.327 - \frac{3.79 \times 10^{-4}\, T^2}{346 + T} \tag{53}$$

for $x = 0.065$ and E_g in eV. Figure 20 shows a comparison between a time integrated spectrum of the sample and the spectra calculated with Equations (52) and (53) for $T = 77$ K. Equation (53) was used to calculate the well energy gap since it matched the experimental data from the sample better. Marciniak found inconclusive evidence of phase separation in his samples (Marciniak, 1995: 7-47 - 7-48). Since wafer B was grown by the same researchers using the same technique it may suffer from the same problems as Marciniak's samples.

The split-off energy band separation, Δ_{so}, was calculated with

$$\Delta_{so}(x) = 1.17x^2 - 0.75x + 0.39 \tag{54}$$

for $x = 0.065$ and Δ_{so} in eV (Rogalski, 1989: 37). This relation is used in Equation (39) to calculate $|M|^2$ for the well material.

Table 2 lists the calculated parameters for the system under strain at $T = 77$ K. The unstrained well energy gap was found using Equation (53). The strain and energy band shifts were calculated with Equations (7) and (8). The spin-orbit splitting and $|M|^2$ were calculated as described in the last paragraph.
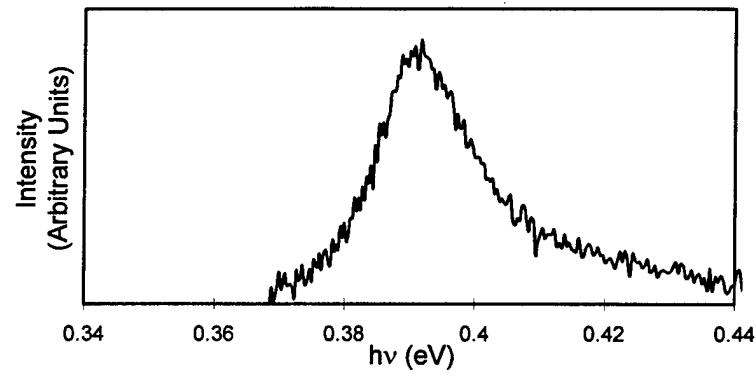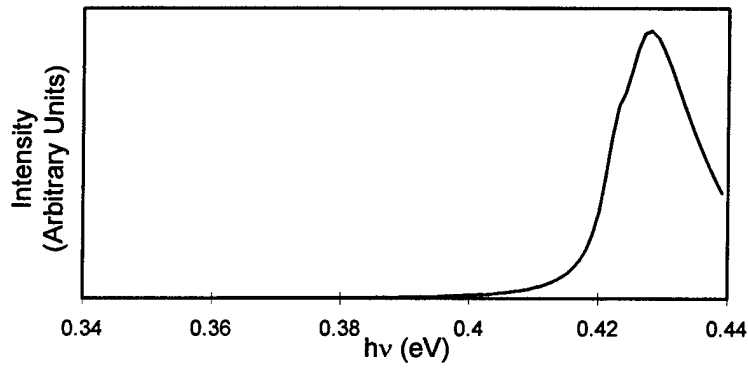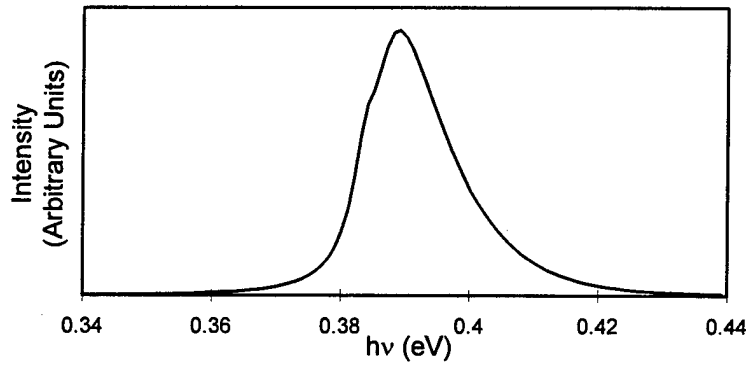
Figure 20: Comparison of a measured time integrated spectrum with calculated spectra.
(a) Measured time integrated spectrum. (b) Spectrum calculated using Equation (52).
(c) Spectrum calculated using Equation (53) which was derived from Marciniak's data.
$N = 3 \times 10^{16}$ for (b) and (c).

Table 2: Calculated well parameters. Values are in meV unless stated otherwise.	
ε_s (percent)	0.450
Well E_g	334
ΔE_{hh}	11.7
ΔE_{lh}	41.3
hh-lh separation	29.6
Δ_{so}	346
$|M|^2$ (2 eV/m_0)	16.9

The barrier material is a quarternary of the form $In_{1-y}Al_yAs_{1-x}Sb_x$. Values for most

of the barrier parameters A (except α and β) were interpolated with

$$A = (1-x)A(\text{InSb}) + (1-x)(1-y)A(\text{InAs}) + xyA(\text{AlSb}) + x(1-y)A(\text{AlAs}) \qquad (55)$$

using the values for InAs, InSb, AlAs, and AlSb, where x is the mole fraction of antimony

and y is the mole fraction of aluminum (Madelung, 1991: 156). Table 1 lists the values

for the binaries used to interpolate the values for the barrier.

The energy gap for the barrier was calculated at a given temperature by calculating

the gap for each of the four binary compounds using Equation (6). The Varshni

parameters used are listed in Table 3 along with the resulting energy gaps calculated for T

= 77 K. These four energy gaps were then interpolated using Equation (55) to find the

barrier band gap listed in the table. The fit parameters α and β were not calculated for the

barrier because these parameters are derived from the fit to the Varshni relation. Their

values are not related to the mole fractions and so cannot be interpolated (Marciniak,

1995:6-42 to 6-45 discusses this).

Table 3: Barrier energy gap calculation. The Varshni parameters were used to find the energy gap at T = 77 K for each binary compound. These energy gaps were interpolated using Equation (55) to find the barrier gap.

Varshni Parameter	InAs[a]	InSb[a]	AlAs[b]	AlSb[c]	Barrier
α (10^{-4} eV/K)	2.76	2.7	15.35	4.68	
β (K)	83	106	1018	190	
E_g(0 K) (eV)	0.415	0.235	3.133	2.384	
E_g(77 K) (meV)	405	226	3125	2374	641

a) Fang, 1990
b) from fit of data in figure from Monemar, 1973
c) from fit of data in figure from Joullie, 1982

Spectral Width Calculation

The first step in a calculation of the spectral widths is to calculate the energy levels in the quantum well. The depths of the wells were found using Equations (9) with the values in Table 2 and Table 3 and the conduction band offset listed on page 36. These well depths, listed in Table 4, were used in Equation (5) to calculate the energy levels for the conduction, heavy hole, and light hole bands (E_{cn}, E_{hhn}, and E_{lhn}) numerically. The energy levels are listed in Table 5 and plotted with the wells in Figure 21. The Mathematica code used in this calculation is listed in Appendix A.

Table 4: Well depths in meV at T = 77 K.	
V_{cb}	231
V_{hh}	76.8
V_{lh}	47.2

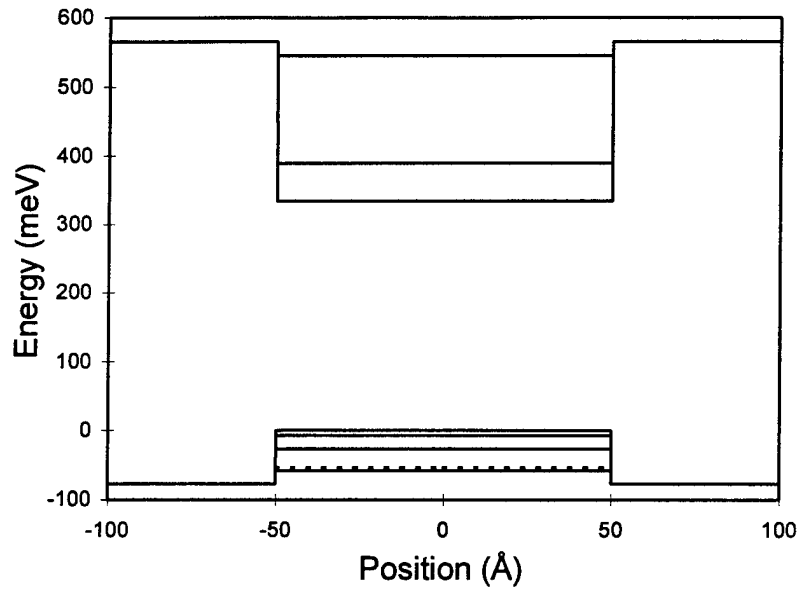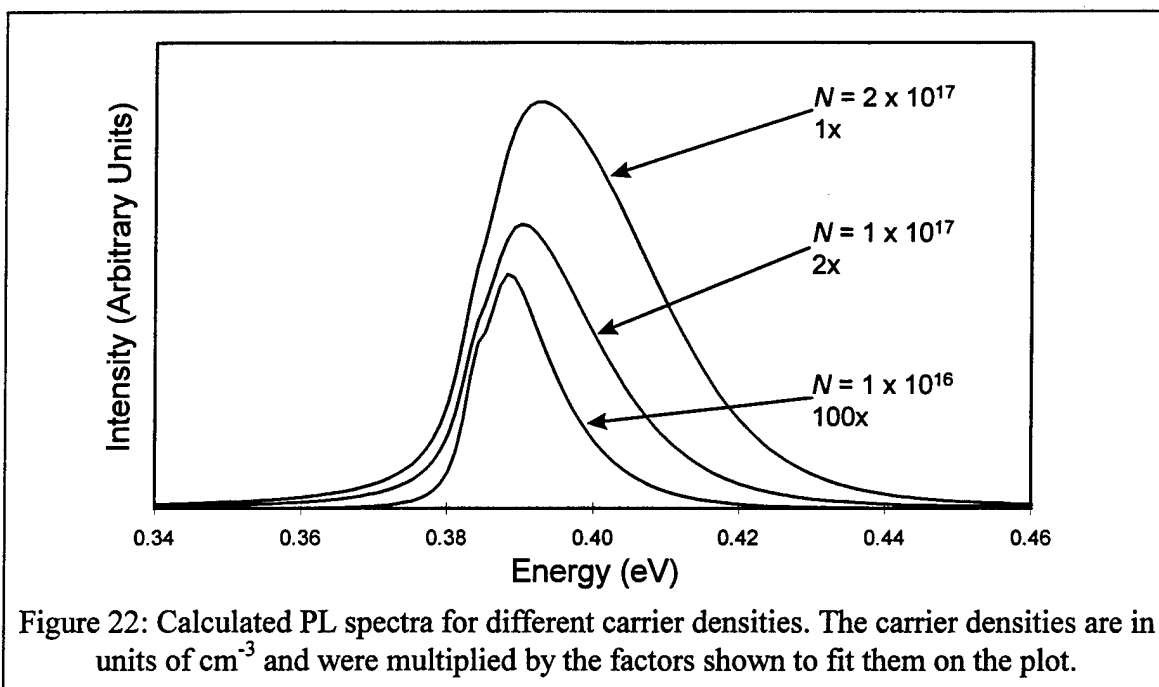| Table 5: Energy levels in meV at T = 77 K.	
CB Level 1	55.1
CB Level 2	210.7
HH Level 1	7.0
HH Level 2	27.2
HH Level 3	58.2
LH Level 1	54.0

Figure 21: Energy levels in the quantum well. The light hole level is dashed.

The unconvolved spontaneous emission spectrum is calculated next. The well

energies are used to define where the steps in the density of states occur (see Figure 9 on

page 17). The quasi-Fermi levels E_{Fc} and E_{Fv} were found by solving Equation (31)

numerically for the conduction band and the valence band for a given carrier density. The

well energies, quasi-Fermi levels, and $|M|^2$ were then used to calculate the spontaneous

emission spectrum for a given temperature and total carrier density with Equation (43).

The spectra were convolved using Equation (44), which finishes the computation of the

calculated spectra. The MatLab files used to calculate the spectra are listed in Appendix

B. They are based on code written by Chia-Fu Hsu, a Ph.D. student of Peter Zory at the

University of Florida. Figure 22 shows a plot of some calculated spectra for different

carrier densities.

The widths of the spectra were calculated using the Mathematica code in

Appendix C. One hundred spectra were calculated with carrier densities ranging from 1 x

43

Figure 22: Calculated PL spectra for different carrier densities. The carrier densities are in units of cm^{-3} and were multiplied by the factors shown to fit them on the plot.

10^{16} cm^{-3} to 1 x 10^{18} cm^{-3}. Each calculated spectrum is composed of 625 discrete points. The energy spacing (along the x axis) between these points is 1 meV. Decreasing this spacing increased calculation time dramatically, so the FWHM of the spectra was found by linearly interpolating between the two points nearest to the half maximum value at each side of the peak in order to gain more resolution. Each of these 100 spectra were calculated for a total carrier density, so the FWHM of these emission spectra can be plotted vs. carrier density.

Convolution With Upconversion Pump Beam

As described in Chapter 3, the upconversion process occurs when the second leg of the pump beam mixes with the PL from the sample in the KTA crystal. The resulting upconversion spectrum is broadened due to the convolution of the two electromagnetic waves. In order to compare the widths of the calculated spectra with the widths of the measured spectra, this effect must be taken into account. This is done by convolving the

calculated spectra with the measured spectrum of the pump beam. The code used to perform the convolutions is listed in Appendix C.

The first step was to measure the spectrum of the Ti:Sapphire pump beam while it was mode locked. Rick Patton, a technician with the Engineering Physics Department, performed this measurement by routing the beam into an EG&G model 1471 optical multichannel analyzer using an EG&G model 1453 silicon photodiode detector. The spectrum was converted from wavelength to energy and is shown in Figure 23. The FWHM of the peak is 15.39 meV. The spectrum was fit with a 30th order polynomial so that the spectrum could be regenerated with the same energy spacing as the calculated PL spectra.

Convolution is represented by $\otimes$ and $h = f \otimes g$ is defined as (Jansson, 1984: 6)

$$h(x) = \int_{\infty}^{-\infty} f(x - x')g(x')dx' \ . \tag{56}$$

Figure 23: Spectrum of Ti: Sapphire pump laser.
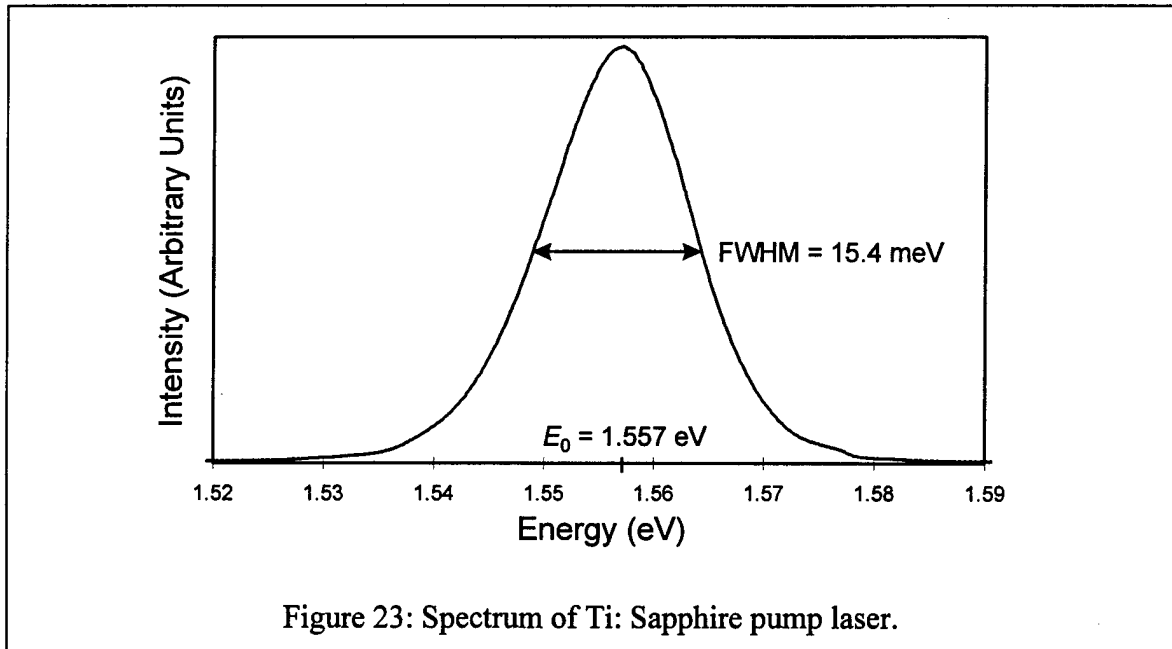
It is well known that the product of the Fourier Transform of two functions, f and g, is the Fourier Transform of the convolution of f and g:

$$\Im(f)\,\Im(g) = \Im(f \otimes g) = \Im(h) \tag{57}$$

where

$$\Im(f(\omega)) = \frac{1}{\sqrt{2\pi}} \int_{-\infty}^{\infty} f(\omega)e^{i\omega t}\,d\omega = f(t) \tag{58}$$

is the Fourier transform of $f(\omega)$ (Jansson, 1991: 11). The convolution, h, can be found by taking the inverse Fourier transform of the right hand side of Equation (57).

The convolution was performed using two methods. The first method used Fourier transforms with Equation (57). The high energy end of the calculated PL spectra was dropped to make the list of data 512 elements long. The values of the dropped elements were essentially zero and would have no effect on the convolution. The pump spectrum was regenerated with an energy spacing of 1 meV and zeros were added to each end of the list to make it 512 elements long (an equal number of points was required to use Mathematica's "Fourier" function). The transforms of the pump and calculated PL spectra were multiplied together and the inverse transform of the product taken with Mathematica's "InverseFourier" function. The widths were determined as described in the previous section on page 44.

The second method used Equation (56) to compute the convolution. The PL spectra were not truncated and no extra zeros were added to the pump spectrum. The pump spectrum data list was reversed and lined up with the left side of the calculated PL spectrum. Since the energy spacing of the two spectra is the same, the sum of the energy values (x coordinate) of each pair of lined up data points will be the same. This sum of

46

the energy values is the energy (x coordinate) for the first point in the convolved spectra. Each intensity data point (y coordinate) from the reversed pump spectrum was multiplied with the intensity data point (y coordinate) from the PL spectrum that was lined up with it. These products were summed and this was the value of the intensity (y coordinate) of the first data point of the convolved spectrum. The reversed pump was moved one element to the right and the process repeated until the end of the PL spectrum was reached. The end result is the convolved spectrum which corresponds to the upconversion spectra. The widths were determined as described in the previous section on page 44.

Both methods of convolution yielded the same widths for the convolved spectra. Since each of the PL spectra were calculated with a specific carrier density, these new convolved calculated widths can be plotted as a function of the carrier density of the PL spectrum used in the convolution. The calculated widths and convolved calculated widths are plotted as a function of carrier density in Figure 24. The effect of the convolution is
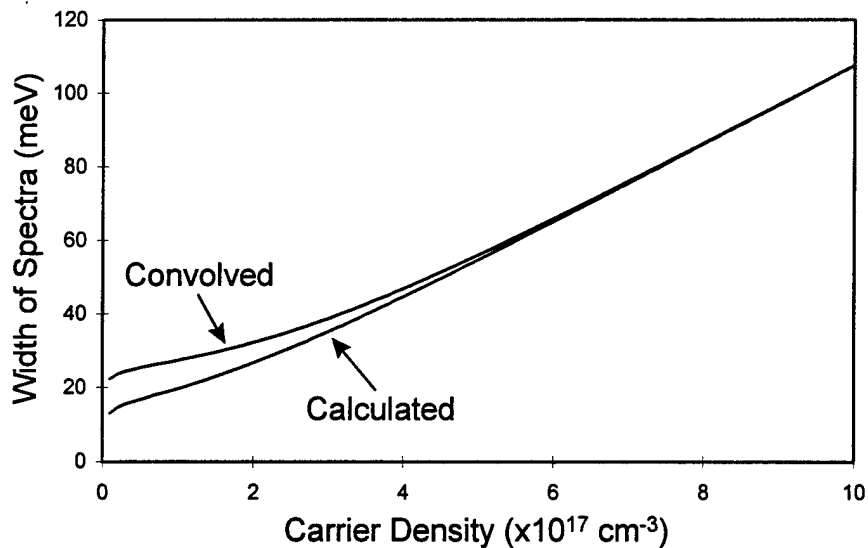

Figure 24: Calculated widths and convolved calculated widths as a function of carrier density.

greatest when the PL widths are smaller. As the PL widths widen, the pump beam width becomes narrower in comparison and broadens the PL less.

Carrier Density as a Function of Time

Since the convolved calculated widths were determined for specific carrier densities and the measured widths for specific times it should be possible to map the carrier densities to time. Each point in Figure 18 was measured at a specific time. The width measured at that time can be compared with the convolved widths calculated in Figure 24. Each of these convolved widths was calculated with a specific carrier density, so the a plot of carrier density as a function of time can be created. This plot is shown in Figure 25 and the code used to calculate the data is in Appendix D.

Capt Cooley calculated the carrier density as a function of time using a different method (Cooley, 1996: 5-1 to 5-7). He measured the luminescence from the sample at one wavelength for different delay times and then plotted the luminescence as a function
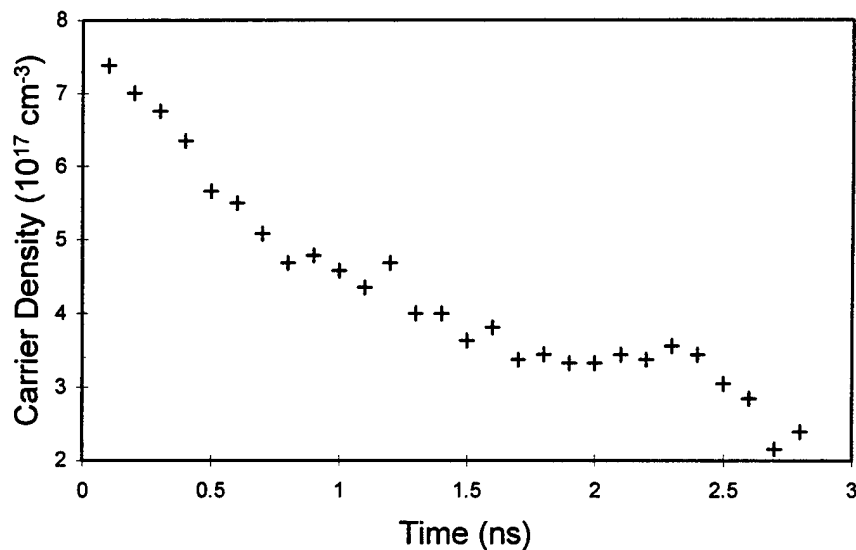

Figure 25: Carrier density as a function of time

of time. Using the absorption of the material, he calculated the two dimensional carrier density created by different pump beam powers. He measured the luminescence over a range of times for each of these pump power levels and associated the first data point at each power with his calculated value of two dimensional carrier density. This gave him the luminescence as a function of carrier density. He connected the carrier density to the times through the luminescence and converted from a two dimensional carrier density to a three dimensional carrier density using

$$n_{3D} = \frac{n_{2D}}{N L_z} \qquad (59)$$

where N is the number of quantum wells and L_z is the thickness of a quantum well. This relationship assumes that the carriers are confined to the well regions.

A comparison of Cooley's results and the results from this thesis are shown in Figure 26. The data is close at lower carrier densities but does not agree with Cooley's results at higher carrier densities. This discrepancy could be due to a slight change in the

Figure 26: Comparison of carrier density vs. time results with Cooley's results
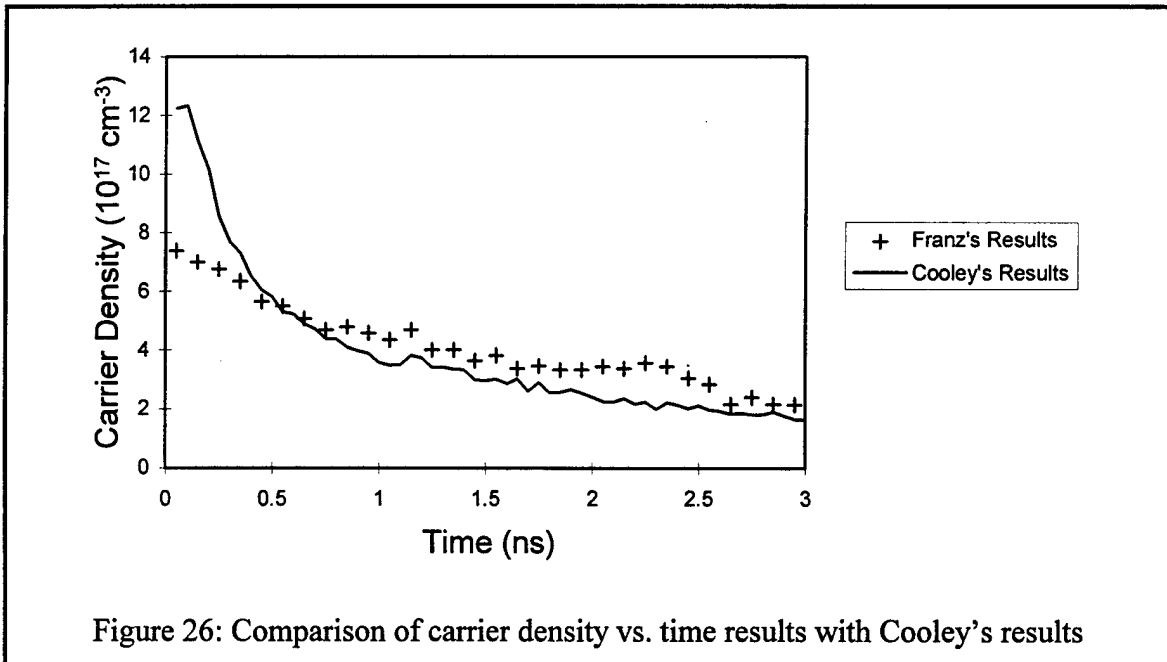
experimental conditions. For example, the spot size of the pump beam on the sample could have changed slightly between the times the measurements were taken. This will affect the number of carriers created and Cooley's absorption calculation. Also the model I used to calculate the PL spectra assumes parabolic bands. This assumption is good near the band edge and becomes less accurate the farther the carriers are from the edge. At higher carrier densities higher levels of the band will be occupied and the applicability of the parabolic band assumption is reduced.

5. Conclusion

Summary

The objective of this research is to study the temporal behavior of the carrier density in a mid-IR quantum well laser. This will help researchers make more efficient lasers that emit at these wavelengths. PL spectra can be calculated for a given carrier density and measured at different times. The calculated spectra can be compared with the measured spectra to associate a specific carrier density with a specific time. The width of the PL spectra was the parameter chosen to compare spectra.

The quasi-Fermi levels in a semiconductor can be related to the carrier density. As the carrier density increases the PL spectrum will become wider and shift slightly toward higher energies as the higher energy levels become more populated. The energy levels were calculated for an $InAs_{0.935}Sb_{0.065}/In_{0.85}Al_{0.15}As_{0.9}Sb_{0.1}$ multiple quantum well sample at a temperature of 77 K assuming parabolic bands. Using these energy levels 100 spectra were calculated for different carrier densities.

The UMIPS can measure spectra with a time resolution of the width of the pump pulse by measuring the upconversion spectra at different delay times. The PL spectrum of the sample was measured at 30 times using this technique. Because the pulse width of the pump is narrow, its spectrum is wide and the upconversion spectrum will be a convolution of the pump and the PL. The calculated spectra were convolved with the measured upconversion pump beam spectrum. The widths of these convolved calculated spectra were compared to the measured spectral widths to find the carrier density as function of time. These results agree with Cooley's results at low carrier densities and

disagree at higher carrier densities. This discrepancy could be due to changing experimental conditions or the break down of the parabolic band model at higher carrier densities.

Future Research

Two things can be done to improve the results of this research. The first would be to calculate the band structure of the material more accurately by using, for example, the k•p method. This would increase the accuracy of the spontaneous emission spectra calculation and provide a better relation between width and carrier density. This would also help determine the carrier densities at which the parabolic band approximation is applicable.

A second improvement would be to slave the rotation stage of the KTA crystal to the spectrometer controller. As the spectrometer is scanned the stage would rotate so the optimum phase matching angle was used for each wavelength. This would allow a complete spectrum over wavelength to be taken at once which would provide more data in each time slice. This would improve the accuracy of the fits and provide a better relation between the measured widths and time. If the improvements are significant it could allow entire spectra to be compared instead of just the widths of the spectra. These improvements would allow better estimates of the carrier density as a function of time to be made.

Appendices

Appendix A: Energy Level Calculation

Last Modified: 3 Oct 97

This file calculates the energy levels in a quantum well. The method follows the MatLab code written by Chia-Fu Hsu, a Ph.D. student of Peter Zory at the University of Florida. This code uses Newton's Method instead of the Bisection Method to numerically solve for the eigenenergies. The equations used are equations 68a and 68b on p. 60 of "Quantum Well Lasers", edited by Peter Zory. This model assumes parabolic bands with a single, finite square well.

The first part of the code is used to define the material parameters for the well and barrier materials. The conduction band offset is used to determine the well depths. The second part calculates the energies for a given well width. The well width is listed two places so make sure the appropriate value is current in the Kernel. The third part displays the results.

```
Off[General::"spell1"]
```

■ Parameters

```
T = 77; (* temperature of solid in K *)
```

Universal constants

```
m0 = 9.109 10^-31; (* electron mass in kg *)
c = 2.998 10^8; (* speed of light in m/s *)
h = 6.626 10^-34; (* Planck's constant in J·s *)
```

$$\hbar = \frac{h}{2\pi};$$

```
kb = 1.381 10^-23; (* Boltzmann's Constant in J/K *)
e = 1.602 10^-19; (* charge of electron *)
ε0 = 8.854 10^-12; (* permitivity of free space *)
```

Varshni formula and quarternary alloy interpolation formula

$$\varepsilon gT[\alpha\_, \beta\_, \varepsilon g0\_, T\_] := \varepsilon g0 - \frac{\alpha T^2}{T + \beta};$$

```
int[AlAs_, AlSb_, InAs_, InSb_, y_, x_] :=
  (1 - x) y InSb + (1 - x) (1 - y) InAs + x y AlSb + x (1 - y) AlAs;
```

ε stands for energy in this notebook.

■ Well Parameters

The well width is also listed below in the code to make calculations easier.

```
lz = 100 10^-10; (* well width in m *)
```

■ Material: InAs$_{1-x}$Sb$_x$

The well in composed of InAs$_{1-x}$Sb$_x$ on an InAs substrate. Laser B has an Antimony concentration of 6.5%.

```
x = 0.065; (* Antimony concentration fraction *)

(* Weider, Clawson heavy hole energy bandgap in eV *)
```
$$(*\epsilon gxT[x\_,t\_] = 0.411 - \frac{3.4\ 10^{-4}\ t^2}{t + 210} - 0.876\ x + 0.70\ x^2 + 3.4\ 10^{-4}\ t\ x\ (1-x);$$
```
egNoStrain = egxT[x,T];*)
(* energy gap from Marciniak's data *)
```
$$\epsilon gNoStrain = 0.327479 - \frac{3.79476\ 10^{-4}\ T^2}{T + 346.193};$$
```
(* lattice parameter in Angstroms *)
a0InAs = 6.0583; a0InSb = 6.47937;
a0 = x a0InSb + (1 - x) a0InAs;
(* substrate lattice parameter in Angstroms *)
a0s = a0InAs;
(* elastic stiffness coefficients in 10^11 dyne/cm^2 *)
c11InAs = 8.329; c11InSb = 6.669;
c11 = x c11InSb + (1 - x) c11InAs;
c12InAs = 4.526; c12InSb = 3.645;
c12 = x c12InSb + (1 - x) c12InAs;
(* hydrostatic deformation potential in eV *)
aInAs = -5.8; aInSb = -7.7; a = x aInSb + (1 - x) aInAs;
(* shear deformation potential in eV *)
bInAs = -1.8; bInSb = -2.0; b = x bInSb + (1 - x) bInAs;
(* strain, positive for compression *)
es = (a0 - a0s) / a0;
(* change in heavy hole energy gap *)
```
$$\Delta\epsilon hh = -2\ a\ es\ \frac{c11 - c12}{c11} + b\ es\ \frac{c11 + c12}{c11};$$
```
(* change in light hole energy gap *)
```
$$\Delta\epsilon lh = -2\ a\ es\ \frac{c11 - c12}{c11} - b\ es\ \frac{c11 + 2\ c12}{c11};$$
```
eg = egNoStrain + Aehh;
(* hh - lh gap *)
s = Aelh - Aehh;
(* electron effective mass in kg *)
meInAs = 0.0239 m0; meInSb = 0.01359 m0;
me = x meInSb + (1 - x) meInAs;
(* growth direction heavy hole effective mass in kg *)
mhhzInAs = 0.35 m0; mhhzInSb = 0.34 m0;
mhhz = x mhhzInSb + (1 - x) mhhzInAs;
(* growth direction light hole effective mass in kg *)
mlhzInAs = 0.026 m0; mlhzInSb = 0.0158 m0;
mlhz = x mlhzInSb + (1 - x) mlhzInAs;
(* in plane direction heavy hole effective mass in kg *)
mhhxInAs = 0.35 m0; mhhxInSb = 0.42 m0;
mhhx = x mhhxInSb + (1 - x) mhhxInAs;
(* in plane direction light hole effective mass in kg *)
```

```
mlhxInAs = 0.026 m0; mlhxInSb = 0.0158 m0;
mlhx = x mlhxInSb + (1 - x) mlhxInAs;
(* index of refraction *)
nInAs = 3.714; nInSb = 4.418;
n = x nInSb + (1 - x) nInAs;
(* static dielectric coefficient *)
εInAs = 15.15; εInSb = 16.8;
ε = x εInSb + (1 - x) εInAs;
(* spin orbit splitting energy in eV *)
Δso = 1.17 x² - 0.75 x + 0.39;
(* transition matrix elements in eV *)
```

$$m2 = \left(\frac{m0}{me} - 1\right) \frac{\varepsilon g + \Delta so}{2\,(\varepsilon g + \Delta so\, 2\,/\,3)}\, m0\, \varepsilon g;$$

```
Print["For the well:"]
Print[" εg (no strain) = ", εgNoStrain]
Print[" strain corrections: εs = ", εs]
Print["  a0 for well = ", a0, " Å, a0 for substrate = ", a0s, " Å"]
Print["  εg = ", εg, " eV, s = ", s, " eV"]
Print[" me = ", me / m0, " m0"]
Print[" mhhz = ", mhhz / m0, " m0, mhhx = ", mhhx / m0, " m0"]
Print[" mlhz = ", mlhz / m0, " m0, mlhx = ", mlhx / m0, " m0"]
```

$$\text{Print}\left[\text{" n = "}, n, \text{", "}, \varepsilon = \text{", "}, \epsilon, \text{", "}, M^2 = \text{", "}, \frac{2}{m0}\, m2, \text{" m0/2"}\right]$$

```
For the well:

 εg (no strain) = 0.322162

 strain corrections: εs = 0.00449738

  a0 for well = 6.08567 Å, a0 for substrate = 6.0583 Å

  εg = 0.333895 eV, s = 0.0296039 eV

me = 0.0232299 m0

mhhz = 0.34935 m0, mhhx = 0.35455 m0

mlhz = 0.025337 m0, mlhx = 0.025337 m0

n = 3.75976, ε = 15.2572, M² = 16.9087 m0/2
```

■ Barrier Parameters

```
lzb = 200 10⁻¹⁰; (* barrier width in m *)
```

■ Material: $In_{1-y}Al_yAs_{1-x}Sb_x$

The concentrations are also listed in the well section to calculate the strain on the well.

```
xb = 0.1; (* Antimony concentration fraction *)
yb = 0.15; (* Aluminum concentration fraction *)
```

```
(* barrier lattice parameter in Angstroms *)
a0AlAs = 5.660; a0AlSb = 6.1355;
a0b = int[a0AlAs, a0AlSb, a0InAs, a0InSb, yb, xb]; (* heavy hole energy bandgap in eV *)
αInAs = 2.76 10⁻⁴; βInAs = 83; εg0InAs = 0.415;
εgInAs = εgT[αInAs, βInAs, εg0InAs, T];
αInSb = 2.70 10⁻⁴; βInSb = 106; εg0InSb = 0.235;
εgInSb = εgT[αInSb, βInSb, εg0InSb, T];
αAlAs = 15.347 10⁻⁴; βAlAs = 1018; εg0AlAs = 3.133;
εgAlAs = εgT[αAlAs, βAlAs, εg0AlAs, T];
αAlSb = 4.684 10⁻⁴; βAlSb = 190; εg0AlSb = 2.384;
εgAlSb = εgT[αAlSb, βAlSb, εg0AlSb, T];
εgb = int[εgAlAs, εgAlSb, εgInAs, εgInSb, yb, xb];
(* electron effective mass in kg *)
meAlSb = 0.259 m0; meAlAs = 0.15 m0; meInAs = 0.0239 m0; meInSb = 0.01359 m0;
meb = int[meAlAs, meAlSb, meInAs, meInSb, xb, yb];
(* heavy hole effective mass in kg *)
mhhzAlSb = 0.336 m0; mhhzAlAs = 0.409 m0; mhhzInAs = 0.35 m0; mhhzInSb = 0.34 m0;
mhhb = int[mhhzAlAs, mhhzAlSb, mhhzInAs, mhhzInSb, xb, yb];
(* light hole effective mass in kg *)
mlhzAlSb = 0.123 m0; mlhzAlAs = 0.153 m0; mlhzInAs = 0.026 m0; mlhzInSb = 0.0158 m0;
mlhb = int[mlhzAlAs, mlhzAlSb, mlhzInAs, mlhzInSb, xb, yb];
Print["For the barrier:"]
Print[" a0 = ", a0b, " A"]
Print[" εg = ", εgb, " eV"]
Print[" me = ", meb / m0, " m0, mhh = ", mhhb / m0, " m0, mlh = ", mlhb / m0, " m0"]

For the barrier:

 a0 = 6.08245 A

 εg = 0.641398 eV

 me = 0.0435737 m0, mhh = 0.356905 m0, mlh = 0.043733 m0
```

■ Depths of conduction band and valence band wells

```
εcOffset = 0.75; (* conduction band offset for materials *)

εch = εcOffset (εgb - εg);   (* conduction band well depth in eV *)
εvh = (1 - εcOffset) (εgb - εg);  (* valence band well height in eV *)
Print["conduction band well depth = ", εch, " eV"]
Print["valence band well height = ", εvh, " eV"]

conduction band well depth = 0.230627 eV

valence band well height = 0.0768755 eV
```

▪ List Parameters

```
Print["temperature = ", T, " K"]
Print["For the well:"]
Print[" εg (no strain) = ", εgNoStrain]
Print[" strain corrections: εs = ", εs]
Print["  a0 for well = ", a0, " A, a0 for substrate = ", a0s, " A"]
Print["  a0 for barrier = ", a0b, " A"]
Print["  εg = ", εg, " eV, s = ", s, " eV"]
Print[" me = ", me / m0, " m0"]
Print[" mhhz = ", mhhz / m0, " m0, mhhx = ", mhhx / m0, " m0"]
Print[" mlhz = ", mlhz / m0, " m0, mlhx = ", mlhx / m0, " m0"]

Print[" n = ", n, ",  ε = ", ε, ", M² = ", 2/m0 m2, " m0/2"]

Print["For the barrier:"]
Print[" εg = ", εgb, " eV"]
Print[" me = ", meb / m0, " m0, mhh = ", mhhb / m0, " m0, mlh = ", mlhb / m0, " m0"]
Print["conduction band well depth = ", εch, " eV"]
Print["valence band well height = ", εvh, " eV"]
```

```
temperature = 77 K

For the well:

 εg (no strain) = 0.322162

 strain corrections: εs = 0.00449738

  a0 for well = 6.08567 A, a0 for substrate = 6.0583 A

  a0 for barrier = 6.08245 A

  εg = 0.333895 eV, s = 0.0296039 eV

me = 0.0232299 m0

mhhz = 0.34935 m0, mhhx = 0.35455 m0

mlhz = 0.025337 m0, mlhx = 0.025337 m0

 n = 3.75976, ε = 15.2572, M² = 16.9087 m0/2

For the barrier:

 εg = 0.641398 eV

 me = 0.0435737 m0, mhh = 0.356905 m0, mlh = 0.043733 m0

conduction band well depth = 0.230627 eV

valence band well height = 0.0768755 eV
```

▪ Energy Levels of a single quantum well

For ease of recomputing the well width is listed here so it can be changed.

```
lz = 100 10⁻¹⁰;  (* well width in m *)
```

Set up equations 68a and 68b for electrons, heavy holes, and light holes. The equations come from solving Schrödinger's equation and applying boundary conditions. The energy, ε, is in meV. The strain separation, s, for the light hole solutions is corrected for in the kzlh expression. The energies used by the light hole equations are really ε+s from s to the valence band height. This accounts for the compressive strain that pushes the light holes away from the gap.
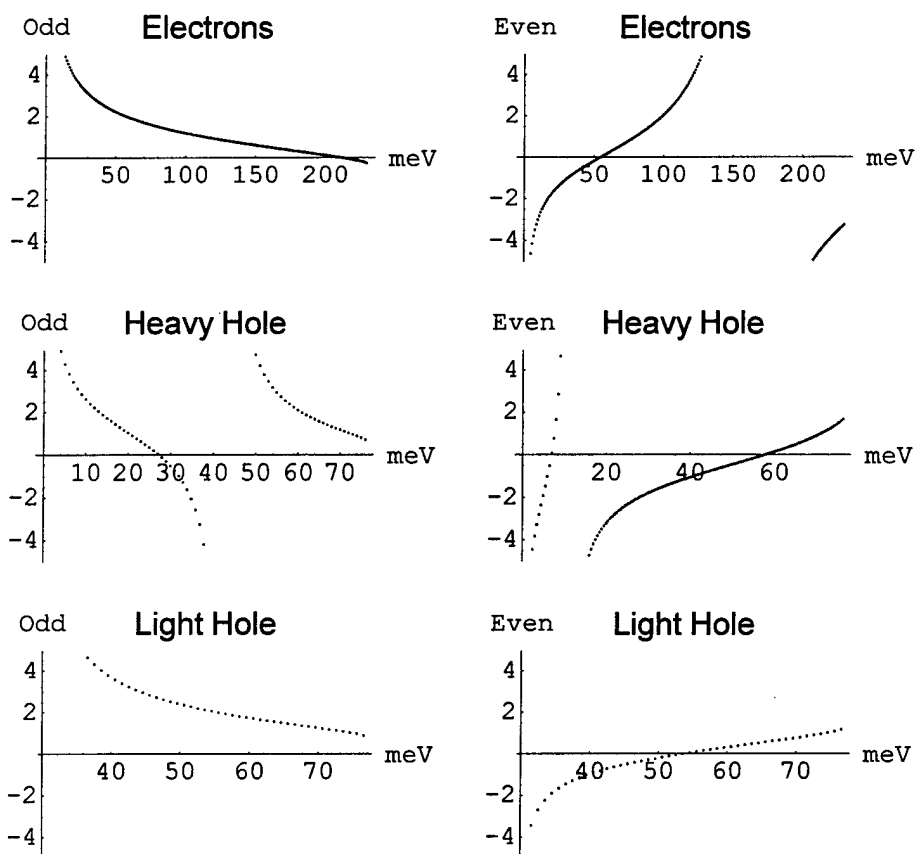
```
Clear[ε]
```

$$kze = \sqrt{\frac{2\,me}{\hbar^2}\,\frac{\varepsilon}{1000}}\ e\ ;\quad aze = \sqrt{\frac{2\,meb}{\hbar^2}\left(\varepsilon ch - \frac{\varepsilon}{1000}\right)}\ e\ ;$$

$$evene = Tan\left[kze\ \frac{lz}{2}\right] - \frac{me\ aze}{meb\ kze}\ ;\quad odde = Cot\left[kze\ \frac{lz}{2}\right] + \frac{me\ aze}{meb\ kze}\ ;$$

$$kzhh = \sqrt{\frac{2\,mhhz}{\hbar^2}\,\frac{\varepsilon}{1000}}\ e\ ;\quad azhh = \sqrt{\frac{2\,mhhb}{\hbar^2}\left(\varepsilon vh - \frac{\varepsilon}{1000}\right)}\ e\ ;$$

$$evenhh = Tan\left[kzhh\ \frac{lz}{2}\right] - \frac{mhhz\ azhh}{mhhb\ kzhh}\ ;\quad oddhh = Cot\left[kzhh\ \frac{lz}{2}\right] + \frac{mhhz\ azhh}{mhhb\ kzhh}\ ;$$

$$kzlh = \sqrt{\frac{2\,mlhz}{\hbar^2}\left(\frac{\varepsilon}{1000} - s\right)}\ e\ ;\quad azlh = \sqrt{\frac{2\,mlhb}{\hbar^2}\left(\varepsilon vh - \frac{\varepsilon}{1000}\right)}\ e\ ;$$

$$evenlh = Tan\left[kzlh\ \frac{lz}{2}\right] - \frac{mlhz\ azlh}{mlhb\ kzlh}\ ;\quad oddlh = Cot\left[kzlh\ \frac{lz}{2}\right] + \frac{mlhz\ azlh}{mlhb\ kzlh}\ ;$$

Plot the even and odd solutions to find guesses for the root finding. If the plots have too few points to make a good guess, increment the appropriate PlotData table to calculate more points. This is especially helpful for the heavy hole plots. It is easier to see if a plot crosses the axis if the plots are temporarily made larger by draging the frame. The plotrange can also be varied so the plots will show more points in the lines. The xxPlotData tables are used to plot the functions with discrete points. This avoids having intersections with the energy axis at the assymptotes of the trigonometric functions. The lower limit for the light holes is s meV + 1 meV to prevent kzlh = $\sqrt{0}$. This occurs when ε = s.

```
plotrange = 5;
Clear[evenePlotData, oddePlotData,
  evenhhPlotData, oddhhPlotData, evenlhPlotData, oddlhPlotData]
evenePlotData = Table[{ε, evene}, {ε, 1, 1000 εch}];
oddePlotData = Table[{ε, odde}, {ε, 1, 1000 εch}];
evenhhPlotData = Table[{ε, evenhh}, {ε, 1, 1000 εvh, 0.5}];
oddhhPlotData = Table[{ε, oddhh}, {ε, 1, 1000 εvh}];
evenlhPlotData = Table[{ε, evenlh}, {ε, 1000 s + 1, 1000 εvh}];
oddlhPlotData = Table[{ε, oddlh}, {ε, 1000 s + 1, 1000 εvh}];
oddePlot = ListPlot[oddePlotData,
  PlotRange → {-plotrange, plotrange}, AxesLabel → {"meV", "Odd"},
  PlotLabel → FontForm["Electrons", {"Arial", 12}], DisplayFunction → Identity];
evenePlot = ListPlot[evenePlotData,
  PlotRange → {-plotrange, plotrange}, AxesLabel → {"meV", "Even"},
  PlotLabel → FontForm["Electrons", {"Arial", 12}], DisplayFunction → Identity];
oddhhPlot = ListPlot[oddhhPlotData,
  PlotRange → {-plotrange, plotrange}, AxesLabel → {"meV", "Odd"},
  PlotLabel → FontForm["Heavy Hole", {"Arial", 12}], DisplayFunction → Identity];
evenhhPlot = ListPlot[evenhhPlotData,
  PlotRange → {-plotrange, plotrange}, AxesLabel → {"meV", "Even"},
  PlotLabel → FontForm["Heavy Hole", {"Arial", 12}], DisplayFunction → Identity];
oddlhPlot = ListPlot[oddlhPlotData,
  PlotRange → {-plotrange, plotrange}, AxesLabel → {"meV", "Odd"},
  PlotLabel → FontForm["Light Hole", {"Arial", 12}], DisplayFunction → Identity];
evenlhPlot = ListPlot[evenlhPlotData,
  PlotRange → {-plotrange, plotrange}, AxesLabel → {"meV", "Even"},
  PlotLabel → FontForm["Light Hole", {"Arial", 12}], DisplayFunction → Identity];
Print["Well Width = ", lz / 10^-10, " A, T = ", T, " K"]
Show[GraphicsArray[
  {{oddePlot, evenePlot}, {oddhhPlot, evenhhPlot}, {oddlhPlot, evenlhPlot}}],
  DisplayFunction → $DisplayFunction]

Well Width = 100 A, T = 77 K
```

Odd **Electrons**

Even **Electrons**

4
2
-2
-4
50 100 150 200 meV

4
2
-2
-4
50 100 150 200 meV

Odd **Heavy Hole**

Even **Heavy Hole**

4
2
-2
-4
10 20 30 40 50 60 70 meV

4
2
-2
-4
20 40 60 meV

Odd **Light Hole**

Even **Light Hole**

4
2
-2
-4
40 50 60 70 meV

4
2
-2
-4
40 50 60 70 meV

```
- GraphicsArray -
```

The equations are solved when ε equals the values of the x-intercepts. Plug the guesses from the plots into the respective lists below. Surround the values with curly brackets { } and separate multiple guesses with a comma. If there is no solution set the value equal to {}.

```
oddeGuess = {210}; eveneGuess = {60}; oddhhGuess = {27}; evenhhGuess = {7, 60};
oddlhGuess = {}; evenlhGuess = {57};
```

The eigenvalues are found using Newton's Method for each guess.

```
maxOddE = Length[oddeGuess]; maxEvenE = Length[eveneGuess];
maxOddHH = Length[oddhhGuess]; maxEvenHH = Length[evenhhGuess];
maxOddLH = Length[oddlhGuess]; maxEvenLH = Length[evenlhGuess];
oddeε = {}; eveneε = {}; oddhhε = {}; evenhhε = {}; oddlhε = {}; evenlhε = {};
Do[solution = FindRoot[odde == 0, {ε, oddeGuess[[i]]}];
 ε = ε /. solution; AppendTo[oddeε, ε], {i, 1, maxOddE}];
Do[solution = FindRoot[evene == 0, {ε, eveneGuess[[i]]}];
 ε = ε /. solution; AppendTo[eveneε, ε], {i, 1, maxEvenE}];
Do[solution = FindRoot[oddhh == 0, {ε, oddhhGuess[[i]]}];
 ε = ε /. solution; AppendTo[oddhhε, ε], {i, 1, maxOddHH}];
Do[solution = FindRoot[evenhh == 0, {ε, evenhhGuess[[i]]}];
 ε = ε /. solution; AppendTo[evenhhε, ε], {i, 1, maxEvenHH}];
Do[solution = FindRoot[oddlh == 0, {ε, oddlhGuess[[i]]}];
 ε = ε /. solution; AppendTo[oddlhε, ε], {i, 1, maxOddLH}];
Do[solution = FindRoot[evenlh == 0, {ε, evenlhGuess[[i]]}];
 ε = ε /. solution; AppendTo[evenlhε, ε], {i, 1, maxEvenLH}];
eε = Sort[Join[oddeε, eveneε]];
hhε = Sort[Join[oddhhε, evenhhε]]; lhε = Sort[Join[oddlhε, evenlhε]];
Print["Electron Energies: ", eε]
Print["Heavy Hole Energies: ", hhε]
Print["Light Hole Energies: ", lhε]

Electron Energies: {55.0927, 210.669}

Heavy Hole Energies: {6.95165, 27.2429, 58.2015}

Light Hole Energies: {53.9502}
```

■ Display Results

This displays the results.

```
Print["Well Width = ", lz/10^-10, " A, T = ", T, " K"]
Show[GraphicsArray[
  {{oddePlot, evenePlot}, {oddhhPlot, evenhhPlot}, {oddlhPlot, evenlhPlot}}],
 DisplayFunction -> $DisplayFunction];
Print["Electron Energy Guesses: ", Sort[Join[oddeGuess, eveneGuess]]]
Print["Heavy Hole Energy Guesses: ", Sort[Join[oddhhGuess, evenhhGuess]]]
Print["Light Hole Energy Guesses: ", Sort[Join[oddlhGuess, evenlhGuess]]]
Print["Electron Energies: ", eε]
Print["Heavy Hole Energies: ", hhε]
Print["Light Hole Energies: ", lhε]
```

Well Width = 100 A, T = 77 K
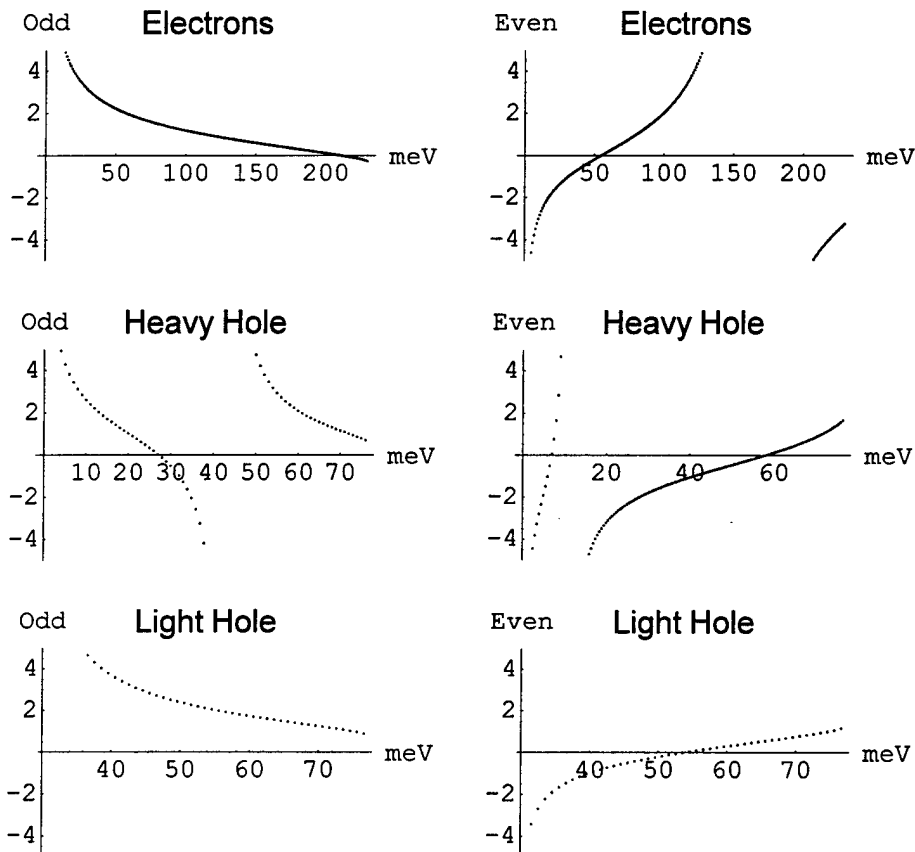
Electron Energy Guesses: {60, 210}

Heavy Hole Energy Guesses: {7, 27, 60}

Light Hole Energy Guesses: {57}

Electron Energies: {55.0927, 210.669}

Heavy Hole Energies: {6.95165, 27.2429, 58.2015}

Light Hole Energies: {53.9502}
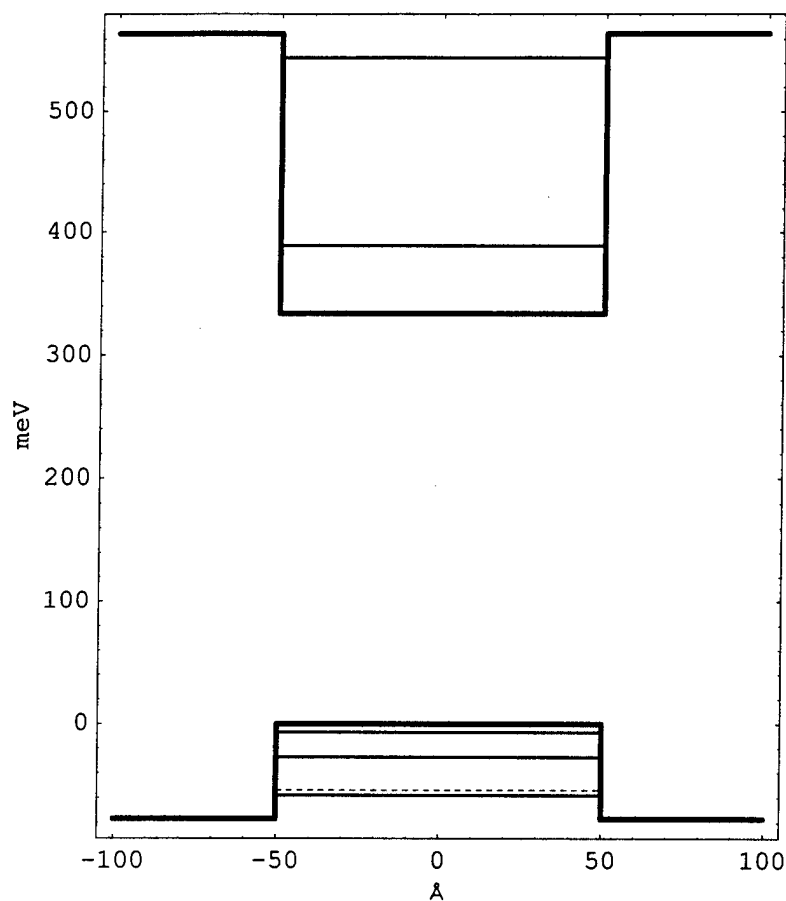
■ Well Plot

■ Energy Levels

This plots a diagram of the well and the energy levels.

```
Needs["Graphics`MultipleListPlot`"]

cBand1 = {{-100, 1000 (εch + εg)}, {-49.9, 1000 (εch + εg)}};
cBand2 = Table[{-50 + 100 i, 1000 εg}, {i, 0, 1}];
cBand3 = Table[{50.1 + 49.9 i, 1000 (εch + εg)}, {i, 0, 1}];
conductionBand = Join[cBand1, cBand2, cBand3];
vBand1 = Table[{-100 + 49.9 i, -1000 εvh}, {i, 0, 1}];
vBand2 = Table[{-50 + 100 i, 0}, {i, 0, 1}];
vBand3 = Table[{50.1 + 49.9 i, -1000 εvh}, {i, 0, 1}];
valenceBand = Join[vBand1, vBand2, vBand3];
cbLevel1 = Table[{-50 + 100 i, eε[[1]] + 1000 εg}, {i, 0, 1}];
cbLevel2 = Table[{-50 + 100 i, eε[[2]] + 1000 εg}, {i, 0, 1}];
hhLevel1 = Table[{-50 + 100 i, -hhε[[1]]}, {i, 0, 1}];
hhLevel2 = Table[{-50 + 100 i, -hhε[[2]]}, {i, 0, 1}];
hhLevel3 = Table[{-50 + 100 i, -hhε[[3]]}, {i, 0, 1}];
lhLevel1 = Table[{-50 + 100 i, -lhε[[1]]}, {i, 0, 1}];

Print["temperature = ", T, " K"]
MultipleListPlot[
 conductionBand, valenceBand, cbLevel1, cbLevel2, hhLevel1, hhLevel2, hhLevel3,
 lhLevel1, PlotJoined → True, PlotStyle → {AbsoluteThickness[2], AbsoluteThickness[2],
   AbsoluteThickness[1], AbsoluteThickness[1], AbsoluteThickness[1],
   AbsoluteThickness[1], AbsoluteThickness[1], AbsoluteDashing[{2, 2}]},
 SymbolShape → None, AspectRatio → 1.2,
 Axes → False, Frame → True, FrameLabel → {"A", "meV", "", ""}];
Print["well εg = ", εg, " eV, barrier εg = ", εgb, " eV"]
Print["conduction band well depth = ", εch, " eV"]
Print["valence band well height = ", εvh, " eV"]
Print["Electron Energies: ", eε, " meV"]
Print["Heavy Hole Energies: ", hhε, " meV"]
Print["Light Hole Energies: ", lhε, " meV"]

temperature = 77 K
```

```
well εg = 0.333895 eV, barrier εg = 0.641398 eV

conduction band well depth = 0.230627 eV

valence band well height = 0.0768755 eV

Electron Energies: {55.0927, 210.669} meV

Heavy Hole Energies: {6.95165, 27.2429, 58.2015} meV

Light Hole Energies: {53.9502} meV
```

■ Wavefunctions

This calculates the k=0 wavefunctions for the single quantum well. Define a function for k.

$$k[m\_, \varepsilon\_, v\_] := \sqrt{\frac{2\,m}{\hbar^2}\,\frac{(\varepsilon - v)}{1000}}\;e$$

Calculate wavefunctions and load them into tables. The factor of 50 enlarges the scale of the wavefunctions.

```
cb1ψ1 = Table[{d = -100 + i, 50 (Cos[k[me, eε[[1]], 0] (-50 10^-10)])/2

    (Exp[-i k[meb, eε[[1]], 1000 εch] d 10^-10])/(Exp[-i k[meb, eε[[1]], 1000 εch] (-50 10^-10)]) + 1000 εg + eε[[1]]}, {i, 0, 50, 1}];

cb1ψ2 =

    Table[{d = -50 + i, 50 (Cos[k[me, eε[[1]], 0] d 10^-10])/2 + 1000 εg + eε[[1]]}, {i, 0, 100, 1}];

cb1ψ3 = Table[{d = 50 + i, 50 (Cos[k[me, eε[[1]], 0] 50 10^-10])/2

    (Exp[i k[meb, eε[[1]], 1000 εch] d 10^-10])/(Exp[i k[meb, eε[[1]], 1000 εch] 50 10^-10]) + 1000 εg + eε[[1]]}, {i, 0, 50, 1}];

cb2ψ1 = Table[{d = -100 + i, 50 (Sin[k[me, eε[[2]], 0] (-50 10^-10)])/2

    (Exp[-i k[meb, eε[[2]], 1000 εch] d 10^-10])/(Exp[-i k[meb, eε[[2]], 1000 εch] (-50 10^-10)]) + 1000 εg + eε[[2]]}, {i, 0, 50, 1}];

cb2ψ2 =

    Table[{d = -50 + i, 50 (Sin[k[me, eε[[2]], 0] d 10^-10])/2 + 1000 εg + eε[[2]]}, {i, 0, 100, 1}];

cb2ψ3 = Table[{d = 50 + i, 50 (Sin[k[me, eε[[2]], 0] 50 10^-10])/2

    (Exp[i k[meb, eε[[2]], 1000 εch] d 10^-10])/(Exp[i k[meb, eε[[2]], 1000 εch] 50 10^-10]) + 1000 εg + eε[[2]]}, {i, 0, 50, 1}];

hh1ψ1 = Table[{d = -100 + i, 50 (Cos[k[mhhz, hhε[[1]], 0] (-50 10^-10)])/2

    (Exp[-i k[mhhb, hhε[[1]], 1000 εvh] d 10^-10])/(Exp[-i k[mhhb, hhε[[1]], 1000 εvh] (-50 10^-10)]) - hhε[[1]]}, {i, 0, 50, 1}];

hh1ψ2 =

    Table[{d = -50 + i, 50 (Cos[k[mhhz, hhε[[1]], 0] d 10^-10])/2 - hhε[[1]]}, {i, 0, 100, 1}];

hh1ψ3 = Table[{d = 50 + i, 50 (Cos[k[mhhz, hhε[[1]], 0] 50 10^-10])/2

    (Exp[i k[mhhb, hhε[[1]], 1000 εvh] d 10^-10])/(Exp[i k[mhhb, hhε[[1]], 1000 εvh] 50 10^-10]) - hhε[[1]]}, {i, 0, 50, 1}];

hh2ψ1 = Table[{d = -100 + i, 50 (Sin[k[mhhz, hhε[[2]], 0] (-50 10^-10)])/2

    (Exp[-i k[mhhb, hhε[[2]], 1000 εvh] d 10^-10])/(Exp[-i k[mhhb, hhε[[2]], 1000 εvh] (-50 10^-10)]) - hhε[[2]]}, {i, 0, 50, 1}];

hh2ψ2 =

    Table[{d = -50 + i, 50 (Sin[k[mhhz, hhε[[2]], 0] d 10^-10])/2 - hhε[[2]]}, {i, 0, 100, 1}];

hh2ψ3 = Table[{d = 50 + i, 50 (Sin[k[mhhz, hhε[[2]], 0] 50 10^-10])/2

    (Exp[i k[mhhb, hhε[[2]], 1000 εvh] d 10^-10])/(Exp[i k[mhhb, hhε[[2]], 1000 εvh] 50 10^-10]) - hhε[[2]]}, {i, 0, 50, 1}];

hh3ψ1 = Table[{d = -100 + i, 50 (Cos[k[mhhz, hhε[[3]], 0] (-50 10^-10)])/2
```

$$\frac{\text{Exp}[-\mathbf{i}\; \text{k[mhhb, hh}\varepsilon[[3]], \; 1000\; \varepsilon \text{vh}]\; d\; 10^{-10}]}{\text{Exp}[-\mathbf{i}\; \text{k[mhhb, hh}\varepsilon[[3]], \; 1000\; \varepsilon \text{vh}]\; (-50\; 10^{-10})]} - \text{hh}\varepsilon[[3]]\Big\}, \; \{i, \; 0, \; 50, \; 1\}\Big];$$

hh3ψ2 =

$$\text{Table}\Big[\Big\{d = -50 + i, \; 50\; \frac{\text{Cos[k[mhhz, hh}\varepsilon[[3]], \; 0]\; d\; 10^{-10}]}{2} - \text{hh}\varepsilon[[3]]\Big\}, \; \{i, \; 0, \; 100, \; 1\}\Big];$$

hh3ψ3 = Table$\Big[\Big\{d = 50 + i, \; 50\; \dfrac{\text{Cos[k[mhhz, hh}\varepsilon[[3]], \; 0]\; 50\; 10^{-10}]}{2}$

$$\frac{\text{Exp}[\mathbf{i}\; \text{k[mhhb, hh}\varepsilon[[3]], \; 1000\; \varepsilon \text{vh}]\; d\; 10^{-10}]}{\text{Exp}[\mathbf{i}\; \text{k[mhhb, hh}\varepsilon[[3]], \; 1000\; \varepsilon \text{vh}]\; 50\; 10^{-10}]} - \text{hh}\varepsilon[[3]]\Big\}, \; \{i, \; 0, \; 50, \; 1\}\Big];$$

lh1ψ1 = Table$\Big[\Big\{d = -100 + i, \; 50\; \dfrac{\text{Cos[k[mlhz, lh}\varepsilon[[1]], \; 0]\; (-50\; 10^{-10})]}{2}$

$$\frac{\text{Exp}[-\mathbf{i}\; \text{k[mlhb, lh}\varepsilon[[1]], \; 1000\; \varepsilon \text{vh}]\; d\; 10^{-10}]}{\text{Exp}[-\mathbf{i}\; \text{k[mlhb, lh}\varepsilon[[1]], \; 1000\; \varepsilon \text{vh}]\; (-50\; 10^{-10})]} - \text{lh}\varepsilon[[1]]\Big\}, \; \{i, \; 0, \; 50, \; 1\}\Big];$$

lh1ψ2 =

$$\text{Table}\Big[\Big\{d = -50 + i, \; 50\; \frac{\text{Cos[k[mlhz, lh}\varepsilon[[1]], \; 0]\; d\; 10^{-10}]}{2} - \text{lh}\varepsilon[[1]]\Big\}, \; \{i, \; 0, \; 100, \; 1\}\Big];$$

lh1ψ3 = Table$\Big[\Big\{d = 50 + i, \; 50\; \dfrac{\text{Cos[k[mlhz, lh}\varepsilon[[1]], \; 0]\; 50\; 10^{-10}]}{2}$

$$\frac{\text{Exp}[\mathbf{i}\; \text{k[mlhb, lh}\varepsilon[[1]], \; 1000\; \varepsilon \text{vh}]\; d\; 10^{-10}]}{\text{Exp}[\mathbf{i}\; \text{k[mlhb, lh}\varepsilon[[1]], \; 1000\; \varepsilon \text{vh}]\; 50\; 10^{-10}]} - \text{lh}\varepsilon[[1]]\Big\}, \; \{i, \; 0, \; 50, \; 1\}\Big];$$

cb1ψ = Join[cb1ψ1, cb1ψ2, cb1ψ3];
cb2ψ = Join[cb2ψ1, cb2ψ2, cb2ψ3]; hh1ψ = Join[hh1ψ1, hh1ψ2, hh1ψ3];
hh2ψ = Join[hh2ψ1, hh2ψ2, hh2ψ3]; hh3ψ = Join[hh3ψ1, hh3ψ2, hh3ψ3];
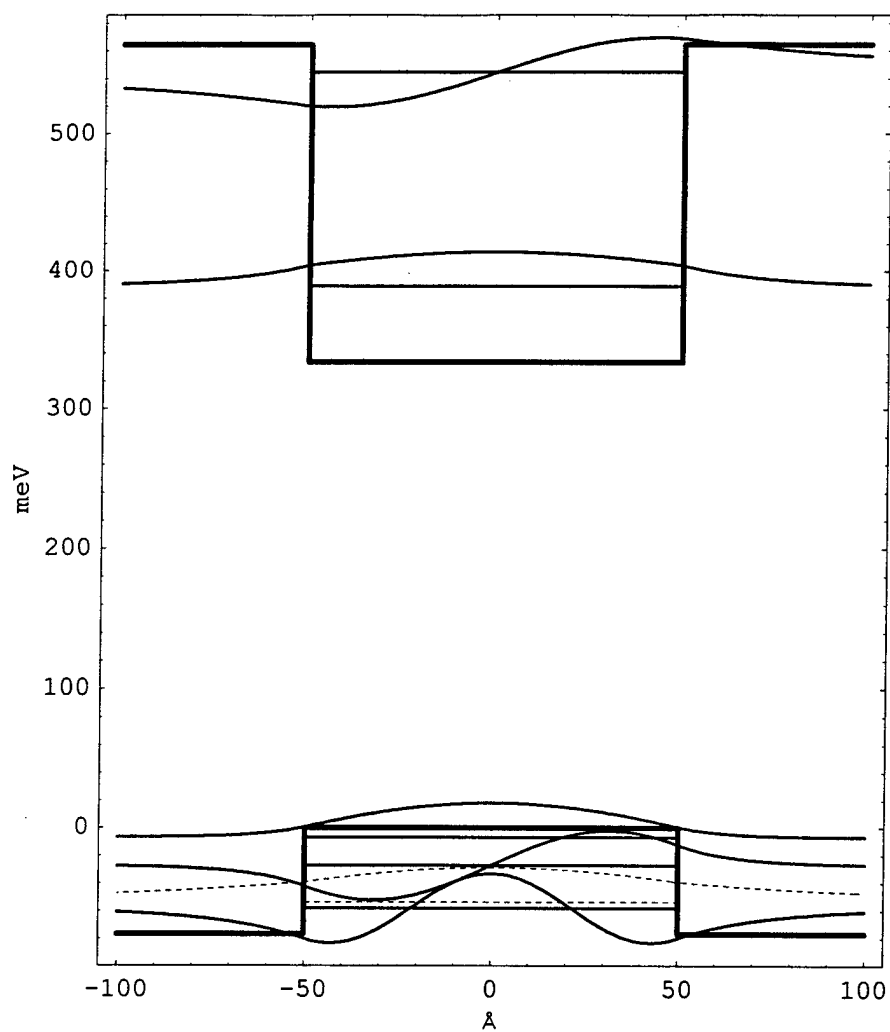lh1ψ = Join[lh1ψ1, lh1ψ2, lh1ψ3];

Plot wavefunctions.

```
Print["temperature = ", T, " K"]
MultipleListPlot[conductionBand, valenceBand, cbLevel1, cbLevel2, hhLevel1, hhLevel2,
  hhLevel3, lhLevel1, cb1ψ, cb2ψ, hh1ψ, hh2ψ, hh3ψ, lh1ψ, PlotJoined → True,
  PlotStyle → {AbsoluteThickness[2], AbsoluteThickness[2], AbsoluteThickness[1],
    AbsoluteThickness[1], AbsoluteThickness[1], AbsoluteThickness[1],
    AbsoluteThickness[1], AbsoluteDashing[{2, 2}], AbsoluteThickness[1],
    AbsoluteThickness[1], AbsoluteThickness[1], AbsoluteThickness[1],
    AbsoluteThickness[1], AbsoluteDashing[{2, 2}]}, SymbolShape → None,
  AspectRatio → 1.2, Axes → False, Frame → True, FrameLabel → {"A", "meV", "", ""}]
Print["well εg = ", εg, " eV, barrier εg = ", εgb, " eV"]
Print["conduction band well depth = ", εch, " eV"]
Print["valence band well height = ", εvh, " eV"]
Print["Electron Energies: ", eε, " meV"]
Print["Heavy Hole Energies: ", hhε, " meV"]
Print["Light Hole Energies: ", lhε, " meV"]

temperature = 77 K
```

- Graphics -

well εg = 0.333895 eV, barrier εg = 0.641398 eV

conduction band well depth = 0.230627 eV

valence band well height = 0.0768755 eV

Electron Energies: {55.0927, 210.669} meV

Heavy Hole Energies: {6.95165, 27.2429, 58.2015} meV

Light Hole Energies: {53.9502} meV

Appendix B: Spontaneous Emission Spectra Calculation

Sponlasb.m is the main program used to calculate the spectra. It calls P_InAsSb.m and P_BarB.m to input the material parameters for the well and the barrier. It also calls efc.m and efv.m to help with the quasi-Fermi level calculations.

SponlasB.m

```
%This program is to calculate gain and spontaneous emission
%spectrum for a QW laser structure.
%
% assumptions:(1) parabolic band model (finite well)
%            (2) large strain regime in-plane effective mass
(ansiotropic mass) (???)
%               (3) non-Lorentzian line-shape function (Ch2,
QWL)
%
%
%      written by by C.F. Hsu    08/05/96
%      modified for Laser B      08/01/97 by Anthony Franz
%      last modified         08/26/97
%
%      1.   specify well/barrier materials for p_<material>.m
%      2.   specify mole fractions of the materials
%      3.   specify Gamma, alpha
%      4.   choose QB=1 for QW, QB=2 for bulk
%      5.   temperature T in K
%      6.   conduction band offset ratio, Ec_off, in percent
%      7.   Run Mathematica code to find energy levels
%      9.   specify Ni(initial carrier density) & Nf(final
carrier density)
%      10.  specify tau(scattering time)

clear


% universal constant

c =2.998*10^8;
h =6.626*10^(-34);
h_=h/2/pi;
k =1.381*10^(-23);
m0=9.109*10^(-31);
e =1.602*10^(-19);
e0=8.854*10^(-12);                    % permittivity
```

```
% condition parameters

T=input('Enter temperature (K) --- ');  % enter temperature
in K
x=0.065;    % Sb concentration in well
xb=0.1;     % Sb concentration in barrier
yb=0.15;    % Al concentration in barrier

%   material parameter (call function pr_    .m)

mp=p_inassb(T,x); % active layer region

Eg_a=mp(1);                % Energy band gap (eV)
Nr_a=mp(2);                % refractive index
r1_a=mp(3);                % gamma1
r2_a=mp(4);                % gamma2
r3_a=mp(5);                % gamma3
Me_a=mp(6);                % electron effective mass (m0)
Mhz_a=mp(7);            % z-direction HH effective mass (m0)
Mlz_a=mp(8);            % z-direction LH effective mass (m0)
Mhx_a=mp(9);            % in-plane HH effective mass (m0)
Mlx_a=mp(10);           % in-plane LH effective mass (m0)
S=mp(11);             % splitting energy Eg(LH)-Eg(HH) (eV)
M_2=mp(12);           % transition coefficient M^2
ee=mp(13);            % static dielectric constant (e0)


mp=p_barB(T,xb,yb);    % barrier layer region
Eg_b=mp(1);                % Energy band gap (eV)
Nr_b=mp(2);                % refractive index
r1_b=mp(3);                % gama1
r2_b=mp(4);                % gama2
r3_b=mp(5);                % gama3
Me_b=mp(6);                % effective mass of e
Mh_b=mp(7);                %            of hh
Ml_b=mp(8);                %            of lh



% device parameters, kept from Jeff Hsu's code
```

```
MT=M_2;                     % basis function momentum matrix
element M^2
Gama=0.01;                  % confinement factor, from Choi et
al, Apl.Phys.Lett.68,2936,(1996)
alfa=1.7;           % internal loss 1/cm
eta_i=0.67;                 % injection efficiency


% potential profile, offset from Bill's thesis

Ec_off=0.75;                % conduction band offset
dEc=Ec_off*(Eg_b-Eg_a);
dEv=(1-Ec_off)*(Eg_b-Eg_a);


% variable limits

hv_i=0.001;         % initial Eeh-Eg
hv_f=0.8;           % final Eeh-Eg
hv_step=0.001;      % step in photon energy
dhv=hv_i:hv_step:hv_f;    % photon energy vector
dhv1=-1*hv_f:hv_step:2*hv_f;   % photon energy vector


% Data files generated at the very end of the code are named
% after the carrier density so update these as well
%%%%%%%%%%%%%%%%%%%%%

Ni=201*10^15;  % initial carrier density (cm^-3)

Nf=250*10^15;  % final carier density (cm^-3)

N_step=1*10^15;      % step (cm^-3)

%%%%%%%%%%%%%%%%%%%%%

% Entering quantum well width in A for Laser B

da=100;   % QW thickness in A

% Entering conduction band and valence band for
eigenenergies at kt=0

Ecm=input('Enter C subband energies (meV) --- ')/1000;
Ehm=input('Enter HH subband energies (meV) --- ')/1000;
Elm=input('Enter LH subband energies (mev) --- ')/1000;
```

```
N_C=length(Ecm);      % N_C: # of conduction subbands
N_HH=length(Ehm);     % N_HH: # of HH subbands
N_LH=length(Elm);     % N_LH: # of LH subbands

Eh1=Ehm(1);
in_ch=min(N_C,N_HH); % # of C-HH transitions, k selection
rule
in_cl=min(N_C,N_LH); % # of C-LH transitions, k selection
rule


% material parameter

dz=da;                % QW thickness
Me=Me_a;              % electron effective mass
Mhz=Mhz_a;            % z-direction HH effective mass
Mlz=Mlz_a;            % z-direction LH effective mass
Mhx=Mhx_a;            % in-plane HH effective mass
Mlx=Mlx_a;            % in-plane LH effective mass
Mrh=Me*Mhx/(Me+Mhx);% in-plane reduced C-HH effective mass
Mrl=Me*Mlx/(Me+Mlx);% in-plane reduced C-LH effective mass
Mrhz=Me*Mhz/(Me+Mhz)% z-direction reduced C-HH effective
mass
Mrlz=Me*Mlz/(Me+Mlz);% z-direction reduced C-LH effective
mass
nr=Nr_a;              % refractive index
Ro=(nr-1)^2/(nr+1)^2;% facet reflectivity
Rb=Ro;                % facet reflectivity
ee=ee*e0;             % static dielectric constant
ee1=nr^2*e0;          % optical dielectric constant

Eg=Eg_a;

% initial conditions

iN=0;

% start of N loops

for N=Ni:N_step:Nf
  iN=iN+1
```

```
  Eyc=0.15;% initial guess of electron fermi level Eyc=Efc-
Ec
  Eyv=-0.01;% initial guess of hole fermi level Eyv=Ev-Efv
  P=N;
  Nm(iN)=N;


% find fermi level Fc,Fv
  dE=0.00001;      % differential Energy (eV)
  tol=0.00001;     % tolerance


% using Newton method to find the solution of fermi level
  Fcc=1;                  % assumed former initial guess


  while abs(Eyc-Fcc) > tol
     % if the difference between two consequent initial
guesses is greater than tolerance
     yfc=efc(N,Eyc,Me,T,dz,Ecm);      % initial guess as input
     yfc_=(efc(N,Eyc+dE,Me,T,dz,Ecm)-yfc)/dE; % slope
     Fcc=Eyc;                  % initial guess becomes
former inital guess
     Eyc=Eyc-yfc/yfc_;                  % new initial guess
  end


  Fcm(iN)=Fcc;                  % Efc-Ec


  Fvv=1;        % assumed former initial guess


  while abs(Eyv-Fvv) > tol
     yfc=efv(P,Eyv,Mhx,Mlx,T,dz,Ehm,Elm);          % N in cm
     yfc_=(efv(N,Eyv+dE,Mhx,Mlx,T,dz,Ehm,Elm)-yfc)/dE;
     Fvv=Eyv;
     Eyv=Eyv-yfc/yfc_;
  end


  Fvm(iN)=Fvv;                  % Ev-Efv


  Phm=Mhx*m0*k*T/(pi*h_^2*dz*10^(-10))*log(1+exp(e*(Fvv-
Ehm)/(k*T)));
  Plm=Mlx*m0*k*T/(pi*h_^2*dz*10^(-10))*log(1+exp(e*(Fvv-
Elm)/(k*T)));



  gc=MT*e^2*h/2/(e0*nr*c*m0^2);     % B(hv)/hv/MT2
```

```
   rdh=Mrh*m0/2/pi/h_^2/(dz*10^(-10));    % reduce density of
states for C-HH transition
   rdl=Mrl*m0/2/pi/h_^2/(dz*10^(-10));    % reduce density of
states for C-LH transition

   rc=(4*pi*e^2*nr)/(e0*h^2*c^3*m0^2)*MT;% eq.44, p.43 of QWL

   gE_sum=dhv.*0;
   gM_sum=dhv.*0;
   rh_sum=dhv.*0;
   rl_sum=dhv.*0;

   for ii=1:1:in_ch  % C_ii to HH_ii transition

      fch1=(dhv-Ecm(ii)-Ehm(ii)).*e*Mrh/Me;           % Ee-Ecnz
in eq.29,p.34 QWL
      fch2=(Ecm(ii)-Fcc)*e;                      % Ecnz-Efc
      fch=1./(1+exp((fch1+fch2)./k/T));          % eq.28,
Fermi-Dirac distribution
      fvh1=(dhv-Ecm(ii)-Ehm(ii)).*e*Mrh/Mhx;           % Ehnz-Eh
      fvh2=(Ehm(ii)-Fvv)*e;                      % Efv-Ehnz
      fvh=1./(1+exp((fvh1+fvh2)./k/T));          % (1-fv)
eq.28,p.34 QWL
      iic=0;
      for ii1=hv_i:hv_step:hv_f
        iic=iic+1;
        if fch1(iic) < 0
           gnh(iic)=0;                           % normalization
factor=0 when hv<Eg+Ecnz+Ehnz
        elseif fch1(iic) == 0
           gnh(iic)=1;
        else
           gnh(iic)=1;
        end
      end


      cos2=(Ecm(ii)+Ehm(ii))*(Mrhz/Mrh)./((dhv-Ecm(ii)-
Ehm(ii))+(Ecm(ii)+Ehm(ii))*Mrhz/Mrh);    % cos^2(Theta_nz)

      sh_TE=0.5*(1+cos2);                        % transition
strength S_TE for HH, p.22 Kenny's thesis
```

73

```
    sh_TM=1-cos2;                         % transition strength
S_TM for HH, p.22 Kenny's thesis


    gh_TE(ii,:)=((((dhv+Eg).*e).\(gc*rdh)).*sh_TE).*(fch -
(1-fvh))*0.01;
    gE_sum=gE_sum+gh_TE(ii,:).*gnh;        % C-HH TE gain



    gh_TM(ii,:)=((((dhv+Eg).*e).\(gc*rdh)).*sh_TM).*(fch -
(1-fvh))*0.01;
    gM_sum=gM_sum+gh_TM(ii,:).*gnh;        % C-HH TM gain



    sh_avg=(2*sh_TE+1*sh_TM)/3;            % e average for
C-HH



    rh=((((dhv+Eg).*e*rc).*sh_avg).*rdh).*(fch.*fvh); % C-HH
e average spontaneous
    rh_sum=rh_sum+rh.*gnh;                 % C-HH e average
spontaneous

  end


  for ii=1:1:in_cl   % C_ii to LH_ii transition

    fcl1=(dhv-Ecm(ii)-Elm(ii)).*e*Mrl/Me;    % Ee-Ec in
eq.29,p.34 QWL
    fcl2=(Ecm(ii)-Fcc)*e;                    % Ec-Efc
    fcl=1./(1+exp((fcl1+fcl2)./k/T));        % eq.28, Fermi-
Dirac distribution

    fvl1=(dhv-Ecm(ii)-Elm(ii)).*e*Mrl/Mlx;   % Ev-Eh
    fvl2=(Elm(ii)-Fvv)*e;                    % Efv-Ev
    fvl=1./(1+exp((fvl1+fvl2)./k/T));        % (1-fv)
eq.28,p.34 QWL


    iic=0;

    for ii1=hv_i:hv_step:hv_f
      iic=iic+1;
```

```
        if fcl1(iic) < 0                      % normalization
factor=0 when hv<Eg+Ecnz+Elnz
            gnl(iic)=0;
        elseif fcl1(iic) == 0
            gnl(iic)=1;
        else
            gnl(iic)=1;
        end

    end


    cos2=(Ecm(ii)+Elm(ii))*(Mrlz/Mrl)./((dhv-Ecm(ii)-
Elm(ii))+(Ecm(ii)+Elm(ii))*Mrlz/Mrl);    % cos^2(Theta_nz)

    sl_TE=1/6*(5-3*cos2);                     % transition
strength S_TE for LH
    sl_TM=1/3+cos2;                           % transition strength
S_TM for LH


    gl_TE(ii,:)=((((dhv+Eg).*e).\(gc*rdl)).*sl_TE).*(fcl -
(1-fvl))*0.01;
    gE_sum=gE_sum+gl_TE(ii,:).*gnl;           % + C-LH TE
gain


    gl_TM(ii,:)=((((dhv+Eg).*e).\(gc*rdl)).*sl_TM).*(fcl -
(1-fvl))*0.01;
    gM_sum=gM_sum+gl_TM(ii,:).*gnl;           % + C-LH TM
gain


    sl_avg=(2*sl_TE+1*sl_TM)/3;               % e average for
C-LH


    rl=((((dhv+Eg).*e*rc).*sl_avg).*rdl).*(fcl.*fvl);
    rl_sum=rl_sum+rl.*gnl;                     % + C-LH e average
spontaneous
```

```
    end


% parameters used in the non-Lorentzian lineshape function

  % Broadening factors

  BFv=12+0.3*(N-1.5*10^18)/(0.2*10^18); % broadening factor
(meV)
  BFc=8+0.3*(N-1.5*10^18)/(0.2*10^18);  % broadening factor
(meV)
  BFFv(iN)=BFv;
  BFFc(iN)=BFc;

  tau_v=h_*1000/BFv/e;                  % intraband scattering
time
  tau_c=h_*1000/BFc/e;                  % intraband scattering
time
  t_v(iN)=tau_v;
  t_c(iN)=tau_c;


  % effective well widths, modified eq.38, p.112, QWL

  Lc=[1:1:N_C]*pi*h_./sqrt(2*Me*m0*Ecm*e);   % effective
well width for e, eq.38, p.112, QWL
  Lh=[1:1:N_HH]*pi*h_./sqrt(2*Mhz*m0*Ehm*e); % effective
well width for HH, eq.38, p.112, QWL
  Ll=[1:1:N_LH]*pi*h_./sqrt(2*Mlz*m0*Elm*e); % effective
well width for LH, eq.38, p.112, QWL

  % equivalent z component wavevectors, eq.38, p.112, QWL

  kv1t=pi/Lh(1);    % equivalent z component wavevector,
kv1_perpendicular, eq.38, p.112, QWL
  kc1t=pi/Lc(1);    % equivalent z component wavevector,
kc1_perpendicular, eq.38, p.112, QWL

  % minimum of the effective well widths, in eq.41, p.113,
QWL

  Leh=Lh(1);
```

```
Lec=Lc(1);

% inverse screeing length

a_c=Me*m0*1./(1+exp((Ecm-Fcc)*e/k/T))./Lc; % mcfc(Ecj)/Lcj
a_h=Mhx*m0*1./(1+exp((Ehm-Fvv)*e/k/T))./Lh;      %
mvfv(Evj)/Lvj for HH
a_l=Mlx*m0*1./(1+exp((Elm-Fvv)*e/k/T))./Ll;      %
    for LH
a_L=e^2/pi/h_^2/ee*(sum([a_c a_h a_l]));   % eq.39, p.112,
QWL

% T(0,kv1t,kv1t), in eq.64, p.124, QWL

T_1v=2/a_L+1/(a_L+4*kv1t^2);
T_2v=2/Leh/sqrt(a_L)*(1-exp(-Leh*sqrt(a_L)));
T_3v=1/a_L-(a_L+8*kv1t^2)/(a_L+4*kv1t^2)^2;
T_4v=Leh*kv1t*(Leh*kv1t-pi)*(a_L-
4*kv1t^2)/4/(a_L+4*kv1t^2)^2/(exp(Leh*sqrt(a_L))-1);

T_Lv=(T_1v-T_2v*(T_3v+T_4v))^2;  % eq.42, p.113, QWL

% T(0,kc1t,kc1t), in eq.64, p.124, QWL

T_1c=2/a_L+1/(a_L+4*kc1t^2);
T_2c=2/Lec/sqrt(a_L)*(1-exp(-Lec*sqrt(a_L)));
T_3c=1/a_L-(a_L+8*kc1t^2)/(a_L+4*kc1t^2)^2;
T_4c=Lec*kc1t*(Lec*kc1t-pi)*(a_L-
4*kc1t^2)/4/(a_L+4*kc1t^2)^2/(exp(Lec*sqrt(a_L))-1);

T_Lc=(T_1c-T_2c*(T_3c+T_4c))^2;  % eq.42, p.113, QWL

% big K, eq.64, p.124, QWL

k_v=e^4/(48*pi*ee^2*h_*Lh(1)^2)*(2*Mhx*m0/h_^2)^2*k*T;
    % eq.64, p.124, constant in the front
k_c=e^4/(48*pi*ee^2*h_*Lc(1)^2)*(2*Me*m0/h_^2)^2*k*T;
    % eq.64, p.124, constant in the front
Kv=k_v*tau_v*T_Lv/(1+exp(-Fvv*e/k/T));            %
eq.64, p.124, QWL
Kc=k_c*tau_c*T_Lv/(1+exp(-Fcc*e/k/T));            %
eq.64, p.124, QWL
```

```matlab
% BGR

N_2D=N*10^6*(dz*10^(-10));                          % n2D 1/m^2
d_L=0*(-1)*e^2/4/ee/Lh(1)*sqrt(T_Lv)*(N_2D);     %
delta_v1, eq.63, p.123, QWL

% lineshape normalization factor

G_vf=h_/2/tau_v*(1+exp((Eg-(Eg+dhv1)-
Fvv).*e/k/T))./(1+exp(-Fvv*e/k/T));
G_v1=G_vf.*exp((-Kv*e*abs(Eg-(Eg+dhv1)))./k/T);       %
G_v1k11(E), eq.62, p.123, QWL
G_cf=h_/2/tau_c*(1+exp((Eg-(Eg+dhv1)-
Fcc).*e/k/T))./(1+exp(-Fcc*e/k/T));
G_c1=G_cf.*exp((-Kc*e*abs(Eg-(Eg+dhv1)))./k/T);       %
G_c1k11(E), eq.62, p.123, QWL

Ln=e*1/pi*(G_v1+G_c1)./(((Eg-(Eg+dhv1)).*e-
d_L).^2+(G_v1+G_c1).^2).*(1-i*((dhv1+Eg-
Eg)+d_L/e)./(G_v1+G_c1)*e);

sum_L=sum(real(real(Ln)))*hv_step;           % normalization
factor

ic=0;

chv=Eg-0.08*hv_f:hv_step:Eg+0.7*hv_f;

for oj=1:length(chv)

ic=ic+1;

% non-Lorentzian lineshape

G_vf=h_/2/tau_v*(1+exp((chv(oj)-(Eg+dhv)-
Fvv).*e/k/T))./(1+exp(-Fvv*e/k/T));
G_v1=G_vf.*exp((-Kv*e*abs(chv(oj)-(Eg+dhv)))./k/T);
% G_v1k11(E), eq.62, p.123, QWL

G_cf=h_/2/tau_c*(1+exp((chv(oj)-(Eg+dhv)-
Fcc).*e/k/T))./(1+exp(-Fcc*e/k/T));
G_c1=G_cf.*exp((-Kc*e*abs(chv(oj)-(Eg+dhv)))./k/T);
% G_c1k11(E), eq.62, p.123, QWL
```

```
    G_L=G_v1+G_c1;

    L=e*1/pi*G_L./(((chv(oj)-(Eg+dhv)).*e-
d_L).^2+G_L.^2).*(1-i*((dhv+Eg-chv(oj))+d_L/e)./G_L*e);

    L=L/sum_L;

    gEc(iN,ic)=sum(L.*gE_sum)*hv_step;

    rch_sum(iN,ic)=sum(L.*rh_sum)*hv_step;

    rcl_sum(iN,ic)=sum(L.*rl_sum)*hv_step;

  end     % end of ic



  gEu(iN,:)=gE_sum;         % unconvolved gain spectra

  Rspu(iN,:)=rh_sum+rl_sum;    % unconvolved spontaneous
emission

  [gc_max(iN) iMAX(iN)]=max(real(gEc(iN,:)));

  L_cav(iN)=0.5*log(1/(Ro*Rb))/(Gama*gc_max(iN)-alfa); %
cavity length

  hv_lasing(iN)=chv(iMAX(iN));                % lasing
energy

  lamda_lasing(iN)=h*c/e/hv_lasing(iN);        %
wavelength

  Rspc(iN,:)=rch_sum(iN,:)+rcl_sum(iN,:);       %
convolved spontaneous emission

  jrad(iN)=real(sum(Rspc(iN,:))*(hv_step*e)*e/10^4*dz*10^(-
10)); % Jrad in A/(cm^2)

end  % end of N loops
```

```
jth=jrad/eta_i; % Jth in A/cm^2


% plot unconvolved TE gain

%figure(1)

%plot(dhv+Eg,gEu)



% plot convolved TE gain

%figure(2)

%plot(chv,real(gEc))



% plot unconvolved spontaneous emission

%figure(3)

%plot(dhv+Eg,Rspu)



% plot convolved spontaneous emission

%figure(4)

%plot(chv,real(Rspc))

% plots I added

%figure(5)
%plot(dhv+Eg,Rspu(1,:),chv,real(Rspc(1,:)))
%xlabel('Energy (eV)')
%title(['Spontanoeus Emission, N=',num2str(Ni)])

%figure(6)
%plot(dhv+Eg,Rspu(2,:),chv,real(Rspc(2,:)))
```

```
%xlabel('Energy (eV)')
%title(['Spontanoeus Emission, N=',num2str(Ni+N_step)])

%figure(7)
%plot(dhv+Eg,Rspu(3,:),chv,real(Rspc(3,:)))
%xlabel('Energy (eV)')
%title(['Spontanoeus Emission, N=',num2str(Nf)])

%figure(8)
%plot(dhv+Eg,gEu(1,:),chv,real(gEc(1,:)))
%xlabel('Energy (eV)')
%ylabel('cm^-1')
%title(['TE Gain, N=',num2str(Ni)])

%figure(9)
%plot(dhv+Eg,gEu(2,:),chv,real(gEc(2,:)))
%xlabel('Energy (eV)')
%ylabel('cm^-1')
%title(['TE Gain, N=',num2str(Ni+N_step)])

%figure(10)
%plot(dhv+Eg,gEu(3,:),chv,real(gEc(3,:)))
%xlabel('Energy (eV)')
%ylabel('cm^-1')
%title(['TE Gain, N=',num2str(Nf)])


%save 150testx.txt chv -ascii; % me##x.txt: x data for 10^##
%export=real(Rspc(1,:));
%save 150test1.txt export -ascii; % m#e##.txt: y data for #
x 10^##
%export=real(Rspc(2,:));
%save 150test2.txt export -ascii;
%export=real(Rspc(3,:));
%save 150test3.txt export -ascii;

save all2x17x.txt chv -ascii;
export=real(Rspc)/10^49;
save all2x17.txt export -ascii;
```

P_InAsSb.m

```
function mt=p_inassb(T,x)
```

```
% last modified by Anthony Franz on 7 Aug 97
% well material for laser B
% material parameters for InAs(1-x)Sb(x) at temp T K
% output mt=[Eg Nr gama1 gama2 gama3 Me Mhz Mlz Mhx Mlx S M2 ee]

% strain effect on energy gap is included
% matrix elements approximated from k.p model

m0=9.109*10^(-31);
e =1.602*10^(-19);

% Luttinger parameters
 gama1InAs = 20.4; % LB, vol 22a, p 118
 gama1InSb = 36.13; % LB, vol 22a, p 126
gama1 = x*gama1InSb + (1 - x)*gama1InAs;
 gama2InAs = 8.3; % LB, vol 22a, p 118
 gama2InSb = 16.24; % LB, vol 22a, p 126
gama2 = x*gama2InSb + (1 - x)*gama2InAs;
 gama3InAs = 9.1; % LB, vol 22a, p 118
 gama3InSb = 17.34; % LB, vol 22a, p 126
gama3 = x*gama3InSb + (1 - x)*gama3InAs;

% energy gap with no strain, from Rogalski, Infrared Phys., vol 29, no
1, p 35, 1989

%egNoStrain=0.411-(3.4*10^(-4)*T^2)/(T+210)-0.876*x+0.7*x^2+(3.4*10^(-
4)*T*x*(1-x));

% strain correction to energy gap

 a0InAs = 6.0583; % LB1991, p 136
 a0InSb = 6.47937; % LB1991, p 144
a0 = x*a0InSb + (1 - x)*a0InAs; % well lattice parameter in Angstroms
a0s = a0InAs; % substrate lattice parameter
 c11InAs = 8.329; % LB1991, p 137
 c11InSb = 6.669; % LB1991, p 147
c11 = x*c11InSb + (1 - x)*c11InAs; % elastic stiffness coefficients in
10^11 dyne/cm^2
 c12InAs = 4.526; % LB1991, p 137
 c12InSb = 3.645; % LB1991, p 147
c12 = x*c12InSb + (1 - x)*c12InAs;
 aInAs = -6.0; % Blacha, Phys Stat Sol b, vol126, p 11, table 2
 aInSb = -7.7; % Blacha, Phys Stat Sol b, vol126, p 11, table 2
a = x*aInSb + (1 - x)*aInAs; % hydrostatic deformation potential in eV
 bInAs = -1.8; % Blacha, Phys Stat Sol b, vol126, p 11, table 3
 bInSb = -2.0; % Blacha, Phys Stat Sol b, vol126, p 11, table 3
b = x*bInSb + (1 - x)*bInAs; % shear deformation potential in eV
es = (a0 - a0s)/a0; % compressive strain (positive) from eq 9, p. 377 of
Zory, QWL
delehh = -2*a*es*(c11 - c12)/c11 + b*es*(c11 + c12)/c11; % change in hh
position relative to cb, eq7,p377,QWL
```

```
delelh = -2*a*es*(c11 - c12)/c11 - b*es*(c11 + 2*c12)/c11; % change in
hh position relative to cb, eq8,p377,QWL
egNoStrain = 0.327479 - (3.79476*10^(-4)*T^2)/(T + 346.193);
Eg = egNoStrain + delehh; % strain corrected energy gap in eV
S = delelh - delehh; % strain induced hh-lh gap in eV

% effective masses

 meInAs = 0.0239; % LB1991, p 134
 meInSb = 0.01359; % LB1991, p 142
Me = x*meInSb + (1 - x)*meInAs; % electron effective mass
 mhhzInAs = 0.35; % LB1991, p 134
 mhhzInSb = 0.34; % LB1991, p 142
Mhz = x*mhhzInSb + (1 - x)*mhhzInAs; % z-direction hh effective mass
 mlhzInAs = 0.026; % LB1991, p 134
 mlhzInSb = 0.0158; % LB1991, p 142
Mlz = x*mlhzInSb + (1 - x)*mlhzInAs; % z-direction lh effective mass
 mhhxInAs = 0.35; % LB1991, p 134
 mhhxInSb = 0.42; % LB1991, p 142
Mhx = x*mhhxInSb + (1 - x)*mhhxInAs; % in-plane hh effective mass
 mlhxInAs = 0.026; % LB1991, p 134
 mlhxInSb = 0.0158; % LB1991, p 142
Mlx = x*mlhxInSb + (1 - x)*mlhxInAs; % in-plane lh effective mass

 nInAs = 3.714; % LB1991, p 138
 nInSb = 4.418; % LB1991, p 148
Nr = x*nInSb + (1 - x)*nInAs; % index of refraction

 eInAs = 15.15; % LB1991, p 138
 eInSb = 16.8; % LB1991, p 147
ee = x*eInSb + (1 - x)*eInAs; % static dielectric constant coefficient

 delso = 1.17*x^2 - 0.75*x + 0.39; % spin-orbit splitting in eV, from
Rogalski, 1989
M2 = (1/Me - 1)*((Eg + delso)/(2*(Eg + delso*(2/3))))*Eg*m0*e; %
momentum matrix elements, eq54,p49,QWL

mt=[Eg Nr gama1 gama2 gama3 Me Mhz Mlz Mhx Mlx S M2 ee];
```

P_BarB.m

```
function mt=p_barB(T,x,y)

% last modified by Anthony Franz on 7 Aug 97
% barrier material for laser B
% material parameter for In(1-y)Al(y)As(1-x)Sb(x) at temp T K
% output mt=[Eg Nr gama1 gama2 gama3 Me Mh Ml]

m0=9.109*10^(-31);
e =1.602*10^(-19);
```

```
% final values are interpolated using formula from LB, vol 22a, p 151
% strain in the barrier layer has not been considered

% Luttinger parameters

  gama1InAs = 20.4; % LB, vol 22a, p 118
  gama1InSb = 36.13; % LB, vol 22a, p 126
  gama1AlAs = 4.04; % P. Lawaetz, Phys Rev B, vol 4, p 3460
  gama1AlSb = 4.15; % Lawaetz
gama1 = (1-x)*y*gama1InSb + (1-x)*(1-y)*gama1InAs + x*y*gama1AlSb +
x*(1-y)*gama1AlAs;
  gama2InAs = 8.3; % LB, vol 22a, p 118
  gama2InSb = 16.24; % LB, vol 22a, p 126
  gama2AlAs = 0.78; % Lawaetz
  gama2AlSb = 1.01; % Lawaetz
gama2 = (1-x)*y*gama2InSb + (1-x)*(1-y)*gama2InAs + x*y*gama2AlSb +
x*(1-y)*gama2AlAs;
  gama3InAs = 9.1; % LB, vol 22a, p 118
  gama3InSb = 17.34; % LB, vol 22a, p 126
  gama3AlAs = 1.57; % Lawaetz
  gama3AlSb = 1.75; % Lawaetz
gama3 = (1-x)*y*gama3InSb + (1-x)*(1-y)*gama3InAs + x*y*gama3AlSb +
x*(1-y)*gama3AlAs;

% energy gaps in eV from Varshni's relation (Physica, vol 34, p 149,
1967)

  alphaInAs = 2.76*10^(-4);
  betaInAs = 83;
  eg0InAs = 0.415; % parameters from Fang, J Appl Phys, vol 67, p 7034,
1990
 egInAs = eg0InAs - alphaInAs*T^2/(T+betaInAs);
  alphaInSb = 2.7*10^(-4);
  betaInSb = 106;
  eg0InSb = 0.235; % parameters from Fang, J Appl Phys, vol 67, p 7034,
1990
 egInSb = eg0InSb - alphaInSb*T^2/(T+betaInSb);
  alphaAlAs = 15.35*10^(-4); % calculated from data from:
  betaAlAs = 1018;           %  Monemar, Phys Rev B, vol 8, p 5711, 1973
  eg0AlAs = 3.133;           %  LB vol 22a, p 63
 egAlAs = eg0AlAs - alphaAlAs*T^2/(T+betaAlAs);
  alphaAlSb = 4.68*10^(-4); % calculated from data from:
  betaAlSb = 190;            %  Joullie, Phys Rev B, vol 25, p 7830, 1982
  eg0AlSb = 2.384;           %  LB vol 22a, p 67
 egAlSb = eg0AlSb - alphaAlSb*T^2/(T+betaAlSb);
Eg = (1-x)*y*egInSb + (1-x)*(1-y)*egInAs + x*y*egAlSb + x*(1-y)*egAlAs;

% barrier lattice parameter in case I need to add in strain later
% a0InAs = 6.0583; % LB1991, p 136
% a0InSb = 6.47937; % LB1991, p 144
% a0AlAs = 5.660; % LB1991, p
```

```
% a0AlSb = 6.1355; % LB1991, p
%a0b = (1-x)*y*a0InSb + (1-x)*(1-y)*a0InAs + x*y*a0AlSb + x*(1-
y)*a0AlAs;

% effective masses

 meAlSb = 0.259;
 meAlAs = 0.15;
 meInAs = 0.0239; % LB1991, p 134
 meInSb = 0.01359; % LB1991, p 142
Me = (1-x)*y*meInSb + (1-x)*(1-y)*meInAs + x*y*meAlSb + x*(1-y)*meAlAs;
 mhhzAlSb = 0.336;
 mhhzAlAs = 0.409;
 mhhzInAs = 0.35; %, LB1991, p 134
 mhhzInSb = 0.34; % LB1991, p 142
Mh = (1-x)*y*mhhzInSb + (1-x)*(1-y)*mhhzInAs + x*y*mhhzAlSb + x*(1-
y)*mhhzAlAs;
 mlhzAlSb = 0.123;
 mlhzAlAs = 0.153;
 mlhzInAs = 0.026; % LB1991, p 134
 mlhzInSb = 0.0158; % LB1991, p 134
Ml = (1-x)*y*mlhzInSb + (1-x)*(1-y)*mlhzInAs + x*y*mlhzAlSb + x*(1-
y)*mlhzAlAs;

% index of refraction

 nInAs = 3.714; % LB1991, p 138
 nInSb = 4.418; % LB1991, p 148
 nAlAs = 2.875; % RE Fern, A Onton, J Appl Phys, vol 42, p.3499, 1971
 nAlSb = 3.182; % LB1991, p 85
Nr = (1-x)*y*nInSb + (1-x)*(1-y)*nInAs + x*y*nAlSb + x*(1-y)*nAlAs;

mt=[Eg Nr gama1 gama2 gama3 Me Mh Ml];
```

efc.m

```
function yf=Efc(N,E,Me,T,d,Ecm)
%
% _____

% This subroutine is to calculate the Fermi level of conduction band
% N = carrier density (1/cm^3)
% Me= conduction band effective mass
% T = temperature (K)
% d = active layer thickness (A)
% Ecm= eigenvalue of Ec1,Ec2..
%
% _____
% universal constants
c =2.998*10^8;
h =6.626*10^(-34);
h_=h/2/pi;
```

```matlab
k =1.381*10^(-23);
m0=9.109*10^(-31);
e =1.602*10^(-19);
%
c1=Me*m0*k*T/(pi*h_^2*d*10^(-10));
%
 ym=c1*log(1+exp( e/k/T* (E-Ecm) ));
 yf=sum(ym);        % sum of N(subbands)
 yf=yf-N*10^6;      % [sum of N(subbands)]-[N(given)]. if yf=0, we get the
solution
```

efv.m

```matlab
function yf=Efv(N,E,Mh,Ml,T,d,Ehm,Elm)
%
% _____
% This subroutine is to calculate the Fermi level of conduction band
% N = carrier density (1/cm^3)
% Mh= heavy hole effective mass
% Ml= light hole effective mass
% T = temperature (K)
% d = active layer thickness (A)
%
% _____
% universal constant
%
c =2.998*10^8;
h =6.626*10^(-34);
h_=h/2/pi;
k =1.381*10^(-23);
m0=9.109*10^(-31);
e =1.602*10^(-19);
%
ch=Mh*m0*k*T/(pi*h_^2*d*10^(-10));
cl=Ml*m0*k*T/(pi*h_^2*d*10^(-10));
%
yhm=ch*log(1+exp( e/k/T* (E-Ehm) ));
ylm=cl*log(1+exp( e/k/T* (E-Elm) ));
yf=sum(yhm)+sum(ylm);
yf=yf-N*10^6;
```

Appendix C: Width Calculations and Convolution of Calculated Spectra

This files convolves the calculated spontaneous emission spectra with the measured pump spectra and creates a file of the results.

```
Off[General::"spell1"]
```

This module calculates the FWHM of a set of x,y data. The x-data should be in one list and the y-data in another list.

```
fwhm[x_, y_] := Module[{max, i, count, xlow, xhigh}, max = Max[y];
  For[i = 1; count = 1, y[[i]] <= 0.5 max, count = i; i = i + 1];
  xlow = ((x[[count + 1]] - x[[count]]) (0.5 max - y[[count]]))/(y[[count + 1]] - y[[count]]) + x[[count]];
  For[i = Flatten[Position[y, max]][[1]]; count = 1, y[[i]] >= 0.5 max, count = i; i = i + 1];
  xhigh = ((x[[count + 1]] - x[[count]]) (0.5 max - y[[count]]))/(y[[count + 1]] - y[[count]]) + x[[count]];
  xhigh - xlow]
```

Read in calculated spectra. Check the file names. The magnitudes have been divided by 10^{49}.

```
xData = ReadList["c:\Tony\Thesis\Calculations\SpectralData\unconvx.txt", Number];
yData = ReadList["c:\Tony\Thesis\Calculations\SpectralData\unconv.txt",
  Number, RecordLists -> True];

Length[yData]
Length[yData[[1]]]

100

625
```

```
testPlotData = Transpose[{xData, yData[[1]]}];
testPlotData2 = Transpose[{xData, yData[[100]]}];
ListPlot[testPlotData, PlotRange -> All]
ListPlot[testPlotData2, PlotRange -> All]
```
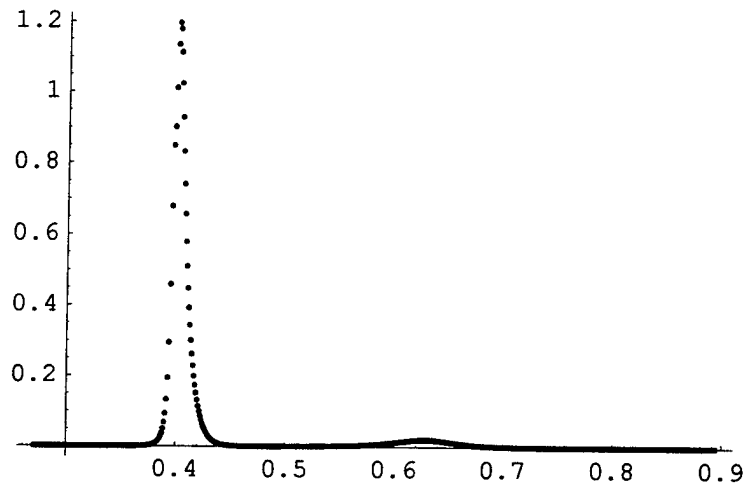

- Graphics -
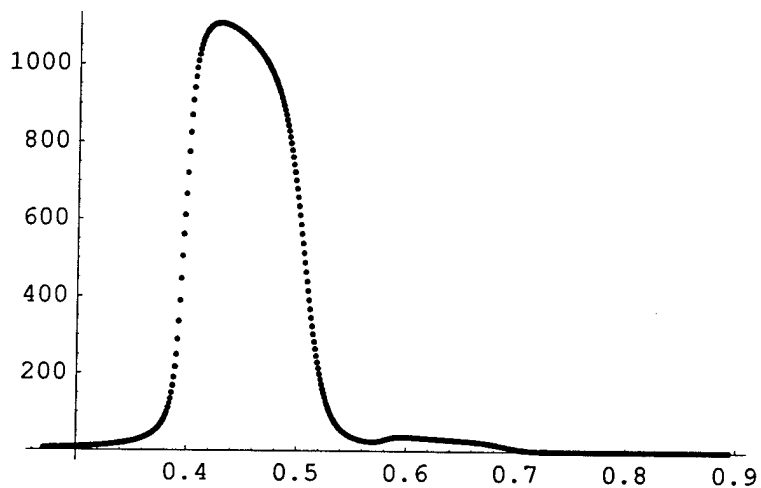
- Graphics -

List of the carrier densities associated with each spectrum.

```
density = Table[i 10^16, {i, 100}];
```

Find the widths before convolution.

```
calcwidth = {};
Do[dataPoint = fwhm[xData, yData[[i]]];
   AppendTo[calcwidth, dataPoint],
 {i, 1, Length[yData]}]
```
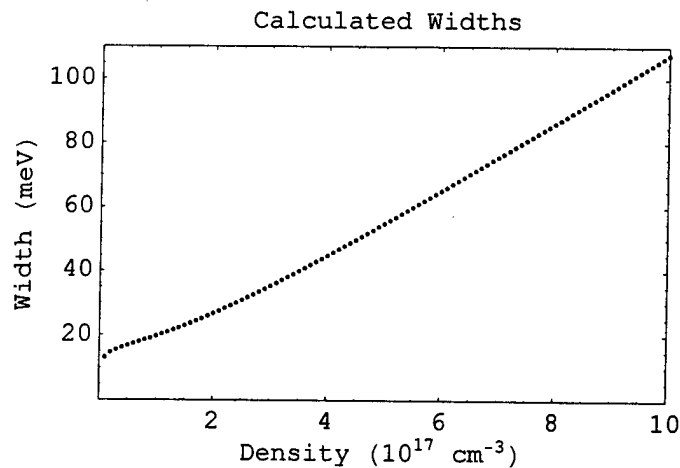
```
Length[calcwidth]

100

plotData = Transpose[{N[density 10^-17], N[1000 calcwidth]}];

calcPlot =
 ListPlot[plotData, PlotRange -> {{0, 10}, {0, 110}}, Axes -> False, Frame -> True,
  FrameLabel -> {"Density (10^17 cm^-3)", "Width (meV)", "Calculated Widths", ""}]
```


Calculated Widths

```
- Graphics -
```

Writes a tab delimited file of width vs. n data called "CalculatvedWidthVsDensity.txt"

```
outputA = OpenWrite["CalculatedWidthVsDensity.txt"]

OutputStream[CalculatedWidthVsDensity.txt, 5]

Do[WriteString[outputA, ToString[plotData[[i, 1]]],
  "\t", ToString[plotData[[i, 2]]], "\n"], {i, 1, Length[plotData]}];
Close[outputA];
```

Load the measured pump spectrum. Subtract the background and normalize it before fitting. The fit is with a 30th order polynomial.

```
Needs["NumericalMath`PolynomialFit`"]
```

```
pumpData =
 ReadList["c:\Tony\Thesis\Calculations\DensityVsTime\pumpdata.txt", {Number, Number}];
xpumpData = Table[pumpData[[i, 1]], {i, 1, Length[pumpData]}];
ypumpDataBG = Table[pumpData[[i, 2]], {i, 1, Length[pumpData]}];
ypumpDataBG2 = Table[ypumpDataBG[[i]] - 4000, {i, 1, Length[xpumpData]}];
ypumpData =
 Table[If[ypumpDataBG2[[i]] < 0, 0, ypumpDataBG2[[i]]], {i, 1, Length[xpumpData]}];
pumpNormalization = Sum[ypumpData[[i]], {i, 1, Length[ypumpData]}];
ypumpData = Table[ypumpData[[i]] / pumpNormalization, {i, 1, Length[xpumpData]}];
pumpFitData = Table[{xpumpData[[i]], ypumpData[[i]]}, {i, 1, Length[xpumpData]}];
Clear[e];
pumpFit = PolynomialFit[pumpFitData, 30];
Length[xpumpData]

1021


xpumpData[[1]]
xpumpData[[-1]]

1.48904

1.60857


dataPlot = ListPlot[pumpFitData, DisplayFunction -> Identity];
fitPlot = Plot[pumpFit[e], {e, 1.489, 1.609}, DisplayFunction -> Identity];
Show[dataPlot, fitPlot, DisplayFunction -> $DisplayFunction, PlotRange -> {0, 0.0005}]
```
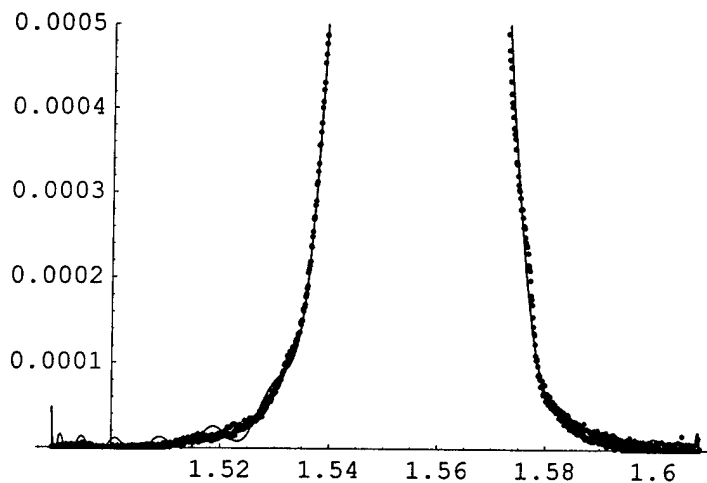


```
- Graphics -
```

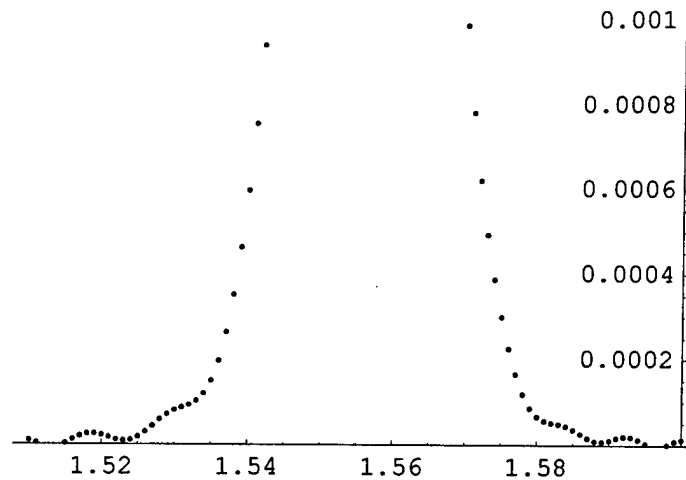Data for pump with same x spacing as the spectra (1 meV).

```
xPump = Table[1.51 + i, {i, 0, 1.6 - 1.51, 0.001}];
yPump = Table[pumpFit[xPump[[i]]], {i, 1, Length[xPump]}];
pumpPlotData = Transpose[{xPump, yPump}];
Length[pumpPlotData]

91
```

```
ListPlot[pumpPlotData, PlotRange -> {0, 0.001}]
```



```
- Graphics -
```

Set up pump with 512 data points for Fourier transform.

```
buffer = Table[0, {i, (512 - Length[xPump] - 1) / 2}];
largeYPump = Flatten[Prepend[yPump, buffer]];
largeYPump = Flatten[Prepend[largeYPump, {0}]];
largeYPump = Flatten[Append[largeYPump, buffer]];
Length[largeYPump]

512
```

Drop end elements of the spectra so they are 512 elements long.

```
shortYData = Table[Drop[yData[[i]], -(Length[xData] - 512)], {i, Length[yData]}];
Length[shortYData]
Length[shortYData[[1]]]

100

512
```

Set up an x data list with the same spacing between points as the other lists (1 meV).

```
xConv = Table[0 + 0.001 i, {i, 1, Length[xData]}];
```

Convolve using Fourier transforms.

```
conv = Table[RotateRight[InverseFourier[Fourier[RotateLeft[shortYData[[i]], 256]]
        Fourier[RotateLeft[largeYPump, 256]]], 256],
    {i, 1, Length[yData]}];
```

```
ListPlot[Abs[conv[[10]]], PlotRange -> All]
```



```
- Graphics -
```
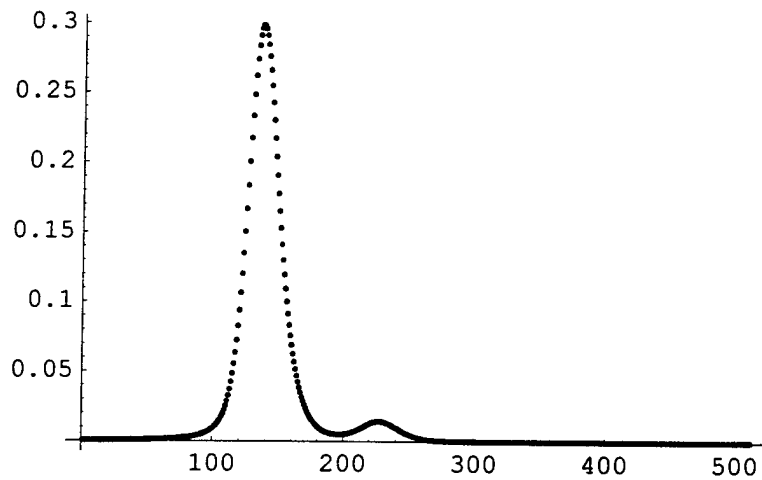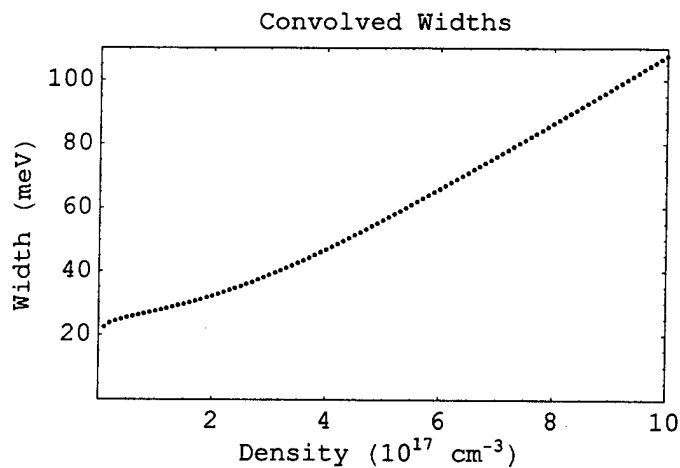
Find the widths of the convolved spectra.

```
convwidth = {};
Do[dataPoint = fwhm[xConv, Abs[conv[[i]]]];
    AppendTo[convwidth, dataPoint],
 {i, 1, Length[yData]}]
Length[convwidth]

100

plotConvData = Transpose[{N[density 10^-17], 1000 convwidth}];
plotConvData[[-1]]

{10., 107.592}
```

```
convPlot =
  ListPlot[plotConvData, PlotRange -> {{0, 10}, {0, 110}}, Axes -> False, Frame -> True,
    FrameLabel -> {"Density (10^17 cm^-3)", "Width (meV)", "Convolved Widths", ""}]
```


Convolved Widths

- Graphics -

Compare the widths of the calculated spectra with the corresponding convolved spectra.

```
Show[calcPlot, convPlot, Graphics[Text["Convolved", {0.1, 40}, {-1, -0.1}]],
  Graphics[Text["Calculated", {2, 20}, {-1, 0}]],
  FrameLabel -> {"Density (10^17 cm^-3)", "Width (meV)", "Comparison", ""}]
```


Comparison
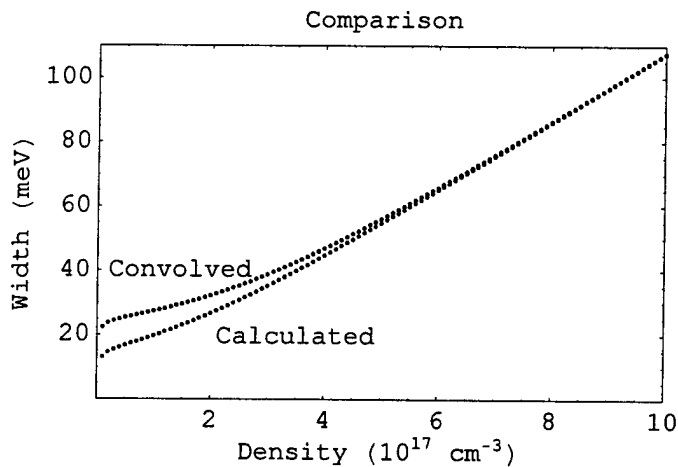
- Graphics -

```
diff = Table[ convwidth[[i]] - calcwidth[[i]], {i, 1, Length[density]}];
plotDiffData = Transpose[{density 10^-17, 1000 diff}];
```

```
ListPlot[plotDiffData, Axes -> False, Frame -> True,
  FrameLabel -> {"Density (10^17 cm^-3)", "(meV)", "Convolved - Calculated", ""}]
```


Convolved - Calculated
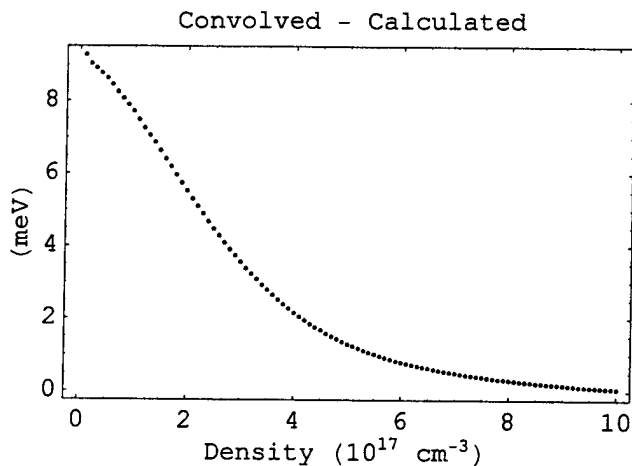
- Graphics -

Writes a tab delimited file of width vs. n data called "Fourier512WidthVsDensity.txt"

```
outputB = OpenWrite["Fourier512WidthVsDensity.txt"]

OutputStream[Fourier512WidthVsDensity.txt, 40]

Do[WriteString[outputB, ToString[plotConvData[[i, 1]]],
  "\t", ToString[plotConvData[[i, 2]]], "\n"], {i, 1, Length[yData]}];
Close[outputB];
```
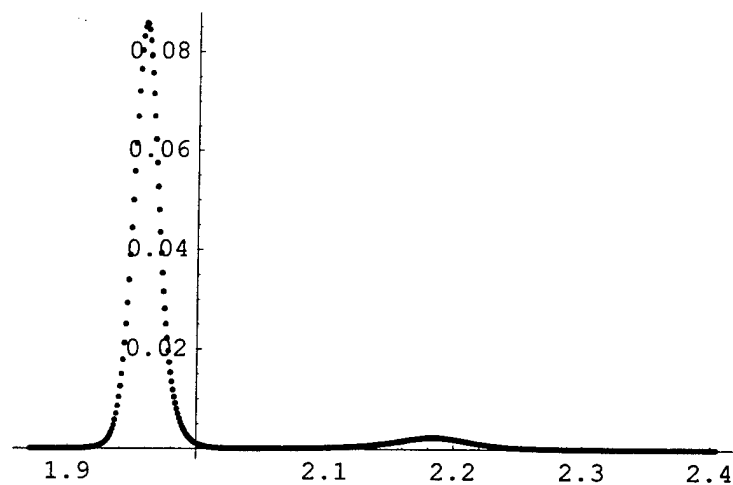
Convolve by summation.

```
pumpLength = Length[xPump];
plLength = Length[xData];
xConv = Table[xPump[[-1]] + xData[[j]], {j, 1, plLength - pumpLength + 1}];
                   pumpLength
yConv = Table[Table[  ∑      (yPump[[-i]] yData[[k, j + i - 1]]),
                   i=1
  {j, 1, plLength - pumpLength + 1}], {k, 1, Length[yData]}];
Length[yConv]

100

Length[yConv[[1]]]

535
```

```
testData = Transpose[{xConv, yConv[[1]]}];
ListPlot[testData, PlotRange -> All]
```


- Graphics -
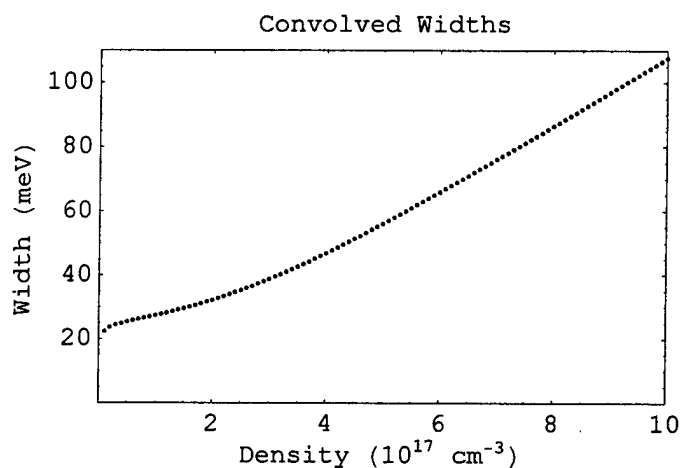
Find the widths of the convolved spectra.

```
convSumWidth = {};
Do[dataPoint = fwhm[xConv, yConv[[i]]];
   AppendTo[convSumWidth, dataPoint],
 {i, 1, Length[yConv]}]
Length[convSumWidth]

100

plotConvSumData = Transpose[{N[density 10^-17], 1000 convSumWidth}];
plotConvSumData[[-1]]

{10., 107.592}
```
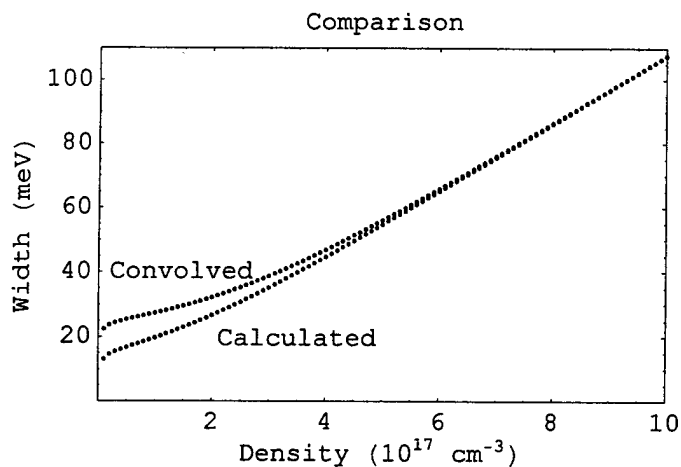
```
convSumPlot =
  ListPlot[plotConvSumData, PlotRange -> {{0, 10}, {0, 110}}, Axes -> False, Frame -> True,
    FrameLabel -> {"Density (10^17 cm^-3)", "Width (meV)", "Convolved Widths", ""}]
```

Convolved Widths

- Graphics -

Compare the widths of the calculated spectra with the corresponding convolved spectra.

```
Show[calcPlot, convSumPlot, Graphics[Text["Convolved", {0.1, 40}, {-1, -0.1}]],
  Graphics[Text["Calculated", {2, 20}, {-1, 0}]],
  FrameLabel -> {"Density (10^17 cm^-3)", "Width (meV)", "Comparison", ""}]
```

Comparison

- Graphics -

```
diff = Table[ convSumWidth[[i]] - calcwidth[[i]], {i, 1, Length[density]}];
plotDiffSumData = Transpose[{density 10^-17, 1000 diff}];
```

```
ListPlot[plotDiffSumData, Axes -> False, Frame -> True,
  FrameLabel -> {"Density (10^17 cm^-3)", "(meV)", "Convolved - Calculated", ""}]
```


Convolved - Calculated
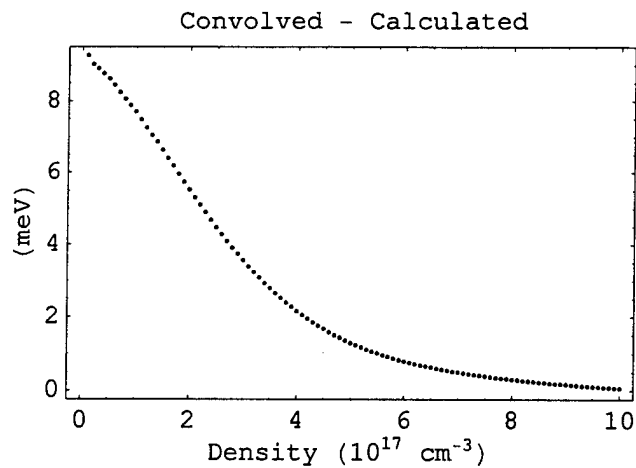
- Graphics -

Writes a tab delimited file of width vs. n data called "ConvolvedWidthVsDensity.txt"

```
outputB = OpenWrite["ConvolvedWidthVsDensity.txt"]
```

```
OutputStream[ConvolvedWidthVsDensity.txt, 39]
```

```
Do[WriteString[outputB, ToString[plotConvSumData[[i, 1]]],
  "\t", ToString[plotConvSumData[[i, 2]]], "\n"], {i, 1, Length[yData]}];
Close[outputB];
```

Appendix D: Carrier Density as a Function of Time

This file maps the carrier density to the delay time using the convolved calculated widths and the measured widths.

```
Off[General::"spell1"]

h = 6.626 10^-34; c = 2.998 10^8; e = 1.602 10^-19;
```

Read in the convolved calculated spectral widths. Check the file name. Format is {density, width} where densities are in units of 10^{17} / cm^3 and widths are in units of meV.

```
calc = ReadList["c:\Tony\Thesis\Calculations\
    DensityVsTime\ConvolvedWidthVsDensity.txt", {Number, Number}];
Length[calc]

100
```

Read in the measured spectral widths. Check the file name. Format is {time, low, high, FWHM} where time is in ps and everything else is in nm.

```
measnm = ReadList["c:\Tony\Thesis\Calculations\DensityVsTime\WidthVsTimenm.txt",
    {Number, Number, Number, Number}];
Length[measnm]

30
```

Convert measured widths to meV and times to ns.

```
mTomeV = 1000 h c / e;
meas = Table[{N[measnm[[i, 1]] / 1000],
         mTomeV                    mTomeV
    ───────────────────  -  ───────────────────}, {i, Length[measnm]}];
    measnm[[i, 2]] 10^-9     measnm[[i, 3]] 10^-9
Length[meas]

30
```

```
TableForm[meas, TableHeadings -> {{}, {"Time (ns)", "Width (meV)"}}]
```

Time (ns)	Width (meV)
0.1	81.0064
0.2	77.1179
0.3	74.534
0.4	70.3492
0.5	63.4071
0.6	61.811
0.7	57.7276
0.8	53.9536
0.9	54.9048
1.	52.9698
1.1	50.8694
1.2	53.9536
1.3	47.7102
1.4	47.7102
1.5	44.5611
1.6	46.0618
1.7	42.4294
1.8	43.0309
1.9	42.0887
2.	42.0887
2.1	42.9903
2.2	42.4294
2.3	43.9601
2.4	42.9903
2.5	39.8561
2.6	38.353
2.7	33.7234
2.8	35.2288
2.9	33.7234
3.	33.6704

```
ListPlot[meas, Axes -> False, Frame -> True,
  FrameLabel -> {"Time (ns)", "Width (meV)", "Measured", ""}]
```
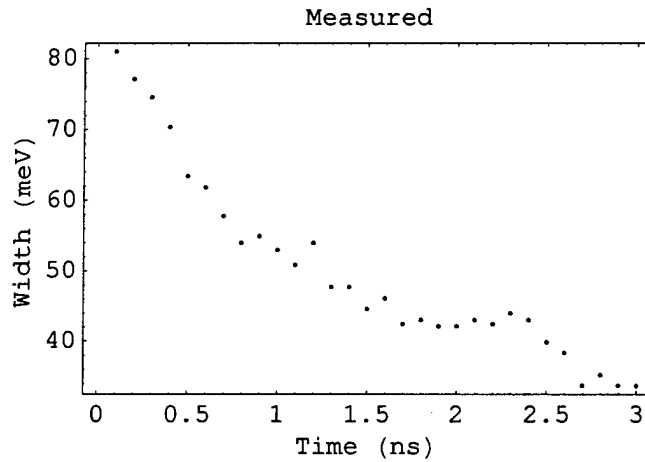

- Graphics -

This module finds an X value for a Y value equal to A using interpolation on the X,Y list of data.

$$int[a\_, x\_, y\_] := Module\Big[\{i, count, xa\},$$
$$\quad For[i = 1; count = 1, y[[i]] <= a, count = i; i = i + 1];$$
$$\quad xa = x[[count]] - \frac{(y[[count + 1]] - a)\ (x[[count + 1]] - x[[count]])}{y[[count + 1]] - y[[count]]}\Big]$$

Calculate a table of n vs. t.

```
xData = Table[calc[[i, 1]], {i, Length[calc]}];
yData = Table[calc[[i, 2]], {i, Length[calc]}];
nt = Table[{meas[[i, 1]], int[meas[[i, 2]], xData, yData]}, {i, Length[meas]}];
Length[nt]
```

30

```
TableForm[nt, TableHeadings -> {{}, {"Time (ns)", "n (10^17 cm^-3)"}}]
```

Time (ns)	n $(10^{17}$ cm$^{-3})$
0.1	7.38127
0.2	7.00538
0.3	6.75402
0.4	6.34424
0.5	5.65386
0.6	5.49289
0.7	5.07474
0.8	4.67895
0.9	4.77991
1.	4.57415
1.1	4.34777
1.2	4.67895
1.3	3.99695
1.4	3.99695
1.5	3.63213
1.6	3.8081
1.7	3.37363
1.8	3.44734
1.9	3.33156
2.	3.33156
2.1	3.44238
2.2	3.37363
2.3	3.56022
2.4	3.44238
2.5	3.04655
2.6	2.84505
2.7	2.15773
2.8	2.39615
2.9	2.15773
3.	2.1492

```
ListPlot[nt, Axes -> False, Frame -> True,
  FrameLabel -> {"Time (ns)", "n (10^17 cm^-3)", "n vs. t", ""}]
```



```
- Graphics -
```
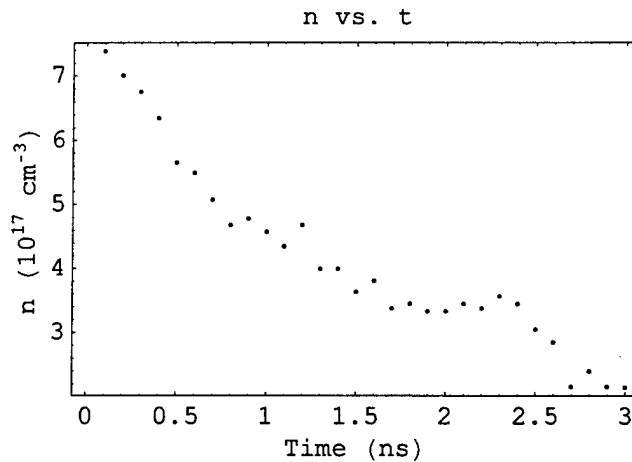
Writes a tab delimited file of carrier density vs. time called "DensityVs.Time.txt"

```
outputA = OpenWrite["DensityVsTime.txt"]

OutputStream[DensityVsTime.txt, 5]

Do[WriteString[outputA,
  ToString[nt[[i, 1]]], "\t", ToString[nt[[i, 2]]], "\n"], {i, 1, Length[nt]}];
Close[outputA];
```

Writes a tab delimited file of meassured width vs. time called "WidthVsTimemeV.txt"

```
outputB = OpenWrite["WidthVsTimemeV.txt"]

OutputStream[WidthVsTimemeV.txt, 6]

Do[WriteString[outputB, ToString[meas[[i, 1]]],
  "\t", ToString[meas[[i, 2]]], "\n"], {i, 1, Length[meas]}];
Close[outputB];
```

Bibliography

Agrawal, G.P. and N.K. Dutta. *Semiconductor Lasers*, 2nd ed. New York: Van Nostrand Reinhold, (1993).

Asada, M. "Intraband Relaxation Effect on Optical Spectra," in *Quantum Well Lasers*, ed. P.S. Zory. San Diego: Academic, (1993).

Aspnes, D.E., and A.A. Studna. *Phys. Rev. B* **27**, 985, (1983).

Blacha, A., H. Presting, and M. Cardona. *Phys. Status Solidi B* **126**, 11, (1984).

Bransden, B.H. and C.J. Joachain. *Physics of Atoms and Molecules*. Essex, England: Longman Scientific & Technical, (1983).

Choi, H.K., G.W. Turner, M.J. Manfra, and M.K. Connors. *Appl. Phys. Lett.* **68**, 2936, (1996).

Cohen-Tannoudji, C., B. Diu, and F. Laloë. *Quantum Mechanics*. New York: Wiley, (1977).

Coleman, J.J. "Strained Layer Quantum Well Heterostructure Lasers," in *Quantum Well Lasers*, ed. P.S. Zory. San Diego: Academic, (1993).

Cooley, W.T., Private Communication, (1996).

Corzine, S.W., R.H. Yan, and L.A. Coldren. "Optical Gain in III-V Bulk and Quantum Well Semiconductors," in *Quantum Well Lasers*, ed. P.S. Zory. San Diego: Academic, (1993).

Dmitriev, V.G., G.G. Gurzadyan, and D.N. Nikogosyan. *Handbook of Nonlinear Optical Crystals*. Berlin: Springer-Verlag, (1991).

Fang, Z.M., K.Y. Ma, D.H. Jaw, R.M. Cohen, and G.B. Stringfellow. *J. Appl. Phys.* **67**, 7034, (1990).

Fern, R.E. and A. Onton. *J. Appl. Phys.* **42**, 3499, (1971).

Jansson, P.A. "Convolution and Related Concepts," in *Deconvolution with Applications in Spectroscopy*, ed. P.A. Jansson. Orlando: Academic, (1984).

Joullie, A., B. Girault, A.M. Joullie, A. Zien-Eddine. *Phys. Rev. B* **25**, 7830, (1982).

Kittel, C. and H. Kroemer. *Thermal Physics*, 2nd ed. New York: W.H. Freeman, (1980).

Liboff, R.L. *Introductory Quantum Mechanics*, 1st ed. Reading, MA: Addison-Wesley, (1989).

Madelung, O. *Semiconductors: Group IV Elements and III-V Compounds*. Berlin: Springer-Verlag, (1991).

Marciniak, M.A. *Optical Characterization of Indium Arsenide Antimonide Semiconductors Grown by Molecular Beam Epitaxy*. Dissertation. Air Force Institute of Technology (AU), Wright-Patterson AFB OH, AFIT/DS/ENP/95-03, (1995).

McKelvey, J.P. *Solid State Physics for Engineering and Materials Science*. Malabar, FL: Krieger, (1993).

Midwinter, J.E. and J. Warner. *Br. J. Appl. Phys.* **16**, 1135, (1965).

Monemar, B. *Phys. Rev. B* **8**, 5711, (1973).

O'Reilly, E.P. *Semicond. Sci. Technol.* **4**, 121, (1989).

Osbourn, G.C. *J. Vac. Sci. Technol. B* **2**, 176, (1984).

Rogalski, A. and K. Józwikowski. *Infrared Phys.* **29**, 35, (1989).

Shah, J. *IEEE J. Quantum Electron.* **24**, 276, (1988).

Stringfellow, G.B. and P.E. Greene. *J. Electrochem. Soc.* **118**, 805, (1971).

Turner, G.W., H.K. Choi, and H.Q. Le. *J. Vac. Sci. Technol. B* **13**, 699, (1995).

Varshni, Y.P. *Physica* **34**, 149, (1967).

Verdeyen, J.T. *Laser Electronics*, 3rd ed. Englewood Cliffs, NJ: Prentice-Hall, (1995).

Wieder, H.H. and A.R. Clawson. *Thin Solid Films* **15**, 217, (1973).

Woolley, J.C. and J. Warner. *Can. J. Phys.* **42**, 1879, (1964).

Yariv, A. and P. Yeh. *Optical Waves in Crystals*. New York: John Wiley & Sons, (1984).

Yen, M.Y., B.F. Levine, C.G. Bethea, H.K. Choi, and A.Y. Cho. *Appl. Phys. Lett.* **50**, 927, (1987).

Vita

Anthony L. Franz was born on 11 July 1970 in Morgantown, WV. He graduated from St. Francis High School in 1988. He studied Space Physics at the U.S. Air Force Academy and earned a Bachelor of Science degree in Physics in 1992. He was commissioned in the U.S. Air Force upon graduation. His first assignment was to the Air Force Technical Applications Center, Patrick AFB, FL, where he served as a Nuclear Systems Evaluator and later as the Advanced Nuclear Detection Program Manager. He was assigned to the Air Force Institute of Technology, Wright-Patterson AFB, OH, in 1996 and received a Master of Science degree in December, 1997. His next assignment was with the Air Force Information Warfare Center, Kelly AFB, TX.

Permanent Address: 913 Hawthorne Ave.
Morgantown, WV 26505

REPORT DOCUMENTATION PAGE

Form Approved
OMB No. 0704-0188

1. AGENCY USE ONLY *(Leave blank)*	2. REPORT DATE	3. REPORT TYPE AND DATES COVERED
	December 1997	Master's Thesis

4. TITLE AND SUBTITLE
TIME RESOLVED PHOTOLUMINESCENCE SPECTRA OF A MID-INFRARED MULTIPLE QUANTUM WELL SEMICONDUCTOR LASER

5. FUNDING NUMBERS

6. AUTHOR(S)
Anthony L. Franz, Captain, USAF

7. PERFORMING ORGANIZATION NAME(S) AND ADDRESS(ES)
Air Force Force Institute of Technology
2750 P Street
WPAFB, OH 45433-7765

8. PERFORMING ORGANIZATION REPORT NUMBER

AFIT/GAP/ENP/97D-04

9. SPONSORING/MONITORING AGENCY NAME(S) AND ADDRESS(ES)
PL/LIDA
3550 Aberdeen Ave SE
Bldg. 416
Kirtland AFB, NM 87117-5776

10. SPONSORING/MONITORING AGENCY REPORT NUMBER

11. SUPPLEMENTARY NOTES

12a. DISTRIBUTION AVAILABILITY STATEMENT
Approved for public release; distribution unlimited

12b. DISTRIBUTION CODE

13. ABSTRACT *(Maximum 200 words)*
Recombination mechanisms in mid-IR semiconductor lasers are strongly dependent on the carrier density of the active region. The objective of this research is to improve previous carrier density estimates through the incorporation of spectral information. One hundred photoluminescence (PL) spectra were calculated for a variety of carrier densities. Calculations were made for an InAsSb/InAlAsSb multiple quantum well laser sample assuming parabolic bands. The widths of the calculated spectral profiles were tabulated as a function of carrier density. Actual spectra were measured using the Ultrafast Mid-Infrared Photoluminescence System, which uses upconversion to measure the PL intensity in time steps smaller than 1 ps. PL spectra were obtained at 30 times, ranging from 100 ps to 3 ns. Spectral widths were measured and tabulated as a function of time. Combining the plot of calculated spectral width vs. carrier density with the plot of measured spectral width vs. time, we were able to describe the variation of carrier density with time. The carrier density vs. time plot thus generated agreed with earlier measurements by Cooley for low carrier densities. The discrepancy at higher carrier densities could be due to changing experimental conditions or the break down of the parabolic band approximation.

14. SUBJECT TERMS
Infrared Lasers, Semiconductor Lasers, Photoluminescence, Sum Frequency Generation, Carrier Density, Indium Arsenide Antimonide, InAsSb

15. NUMBER OF PAGES
118

16. PRICE CODE

17. SECURITY CLASSIFICATION OF REPORT	18. SECURITY CLASSIFICATION OF THIS PAGE	19. SECURITY CLASSIFICATION OF ABSTRACT	20. LIMITATION OF ABSTRACT
Unclassified	Unclassified	Unclassified	UL